이학박사 학위논문

Organo-compatible TiO_2 nanoparticle-based superhydrophobic layers to enhance device reliability of organic thin film transistors

이산화타이타늄 나노입자 기반의 초소수성 박막을 이용한 유기 트랜지스터의 소자 안정성 향상 연구

2020 년 1 월

서울대학교 대학원

물리·천문학부

유대경

Organo-compatible TiO_2 nanoparticle-based superhydrophobic layers to enhance device reliability of organic thin film transistors

이산화타이타늄 나노입자 기반의 초소수성 박막을 이용한 유기 트랜지스터의 소자 안정성 향상 연구

지도교수 이 탁 희

이 논문을 이학박사 학위논문으로 제출함

2020 년 1 월

서울대학교 대학원

물리·천문학부 물리학 전공

유대경

유대경의 이학박사 학위논문을 인준함

2020 년 1 월

위 원 장	김창영	(인)
부 위 원 장	이탁희	(인)
위 원	유재준	(인)
위 원	박윤	(인)
위 원	정승준	(인)

Abstract

Organo-compatible TiO_2 nanoparticle-based superhydrophobic layers to enhance device reliability of organic thin film transistors

Daekyoung Yoo
Department of Physics and Astronomy

Recently, organic materials have attracted tremendous attention for realizing flexible device applications due to their low-cost, non-vacuum, and large-area solution processability. To be utilized in practical applications, further easy-to-manage organic devices with acceptable device reliability is highly desirable. Specifically, because accumulated harmful dust or water-based threats can degrade the functions of organic electronic devices, demands for solutions to facilitate sustainable surface management against external threats have been increased. In this regard, it is desirable to introduce a superhydrophobic layer directly onto organic devices which can eliminate contaminants and water-based threats via excellent water repellency.

First, I report a facile method to deposit an organo-compatible superhydrophobic protection layer on organic semiconductors under ambient conditions. The protection layer exhibiting excellent water-repellency and self-cleaning abilities was deposited onto organic semiconductors directly by using a dip-coating process in a highly fluorinated solution with fluoroalkylsilane-coated titanium dioxide (TiO_2) nanoparticles. The proposed protection layer did not damage the underlying organic semiconductors and had excellent resistance against mechanical-, thermal-, light-stress and water-based threats. The protected organic

thin film transistors (OTFTs) exhibited more reliable electrical properties even exposed to corrosive solvents due to their superhydrophobicity.

Secondly, I studied transparent superhydrophobic layers for organic optoelectronic devices. The optimization of TiO_2 nanoparticle layer, such as surface roughness and thickness of film, enables to realize a transparent superhydrophobic layer, therefore it can be utilized in organic optoelectronics, especially in phototransistor applications based on organic semiconductors. The transparent superhydrophobic layer exhibited good water repellency without critical delamination issues even after or during bending and stretching tests. Flexible organic phototransistors with the transparent superhydrophobic layers showed enhanced device reliability against water droplets and harmful contaminants on surface due to their excellent water repellency and self-cleaning ability.

Keywords: Organic materials, Titanium oxide nanoparticles, Superhydrophobic, Transistor, Phototransistor, Fluorinated materials

Student Number: 2015-30093

List of Contents

List of Figures

Chapter 2.

coated TiO_2 nanoparticle layers on a pentacene layer. Adapted from Yoo et al.

Figure 2.21 (a) TEM image of a bare TIPS-pentacene layer. (b) TEM image of a bare TIPS-pentacene layer with the PFOTES-coated TiO_2 nanoparticle layers. (c) EDS profiles of the PFOTES-coated TiO_2 nanoparticle layers on the TIPS-pentacene layer. (d) TEM image of a bare P3HT layer. (e) TEM image of a bare P3HT layer with the PFOTES-coated TiO_2 nanoparticle layers. (f) EDS profiles of the PFOTES-coated TiO_2 nanoparticle layers on the P3HT layer. Adapted from Yoo et al.

Figure 2.22 (a) TEM image of a bare P(NDI2OD-T2) layer (the top layer is carbon coating). (b) TEM image of a bare P(NDI2OD-T2) layer with the PFOTES-coated TiO_2 nanoparticle layers. (c) EDS profiles of the PFOTES-coated TiO_2 nanoparticle layers on the P(NDI2OD-T2) layer. (d) SEM images of the surface of PFOTES-coated TiO_2 nanoparticle layers on a P(NDI2OD-T2) layer. (e) Optical image of the water contact angle on the protected P(NDI2OD-T2) layer with the PFOTES-coated TiO_2 nanoparticle layers. (d) TEM image of a bare P3HT layer. (e) TEM image of a bare P3HT layer with the PFOTES-coated TiO_2 nanoparticle layers. (f) EDS profiles of the PFOTES-coated TiO_2 nanoparticle layers on the P3HT layer. Adapted from Yoo et al.

Figure 2.23 (a) Water contact angles of the superhydrophobic layer after exposure to HCl (pH 1.0), CH_3COOH (pH 2.5), DI water (pH 6.7), NH_4OH (pH 11.7), and NaOH (pH 13.0) droplets for 1, 5, and 10 s. (b) Water contact angles of the PFOTES-coated TiO_2 nanoparticle layers after exposure to air for 1 year. Adapted from Yoo et al.

Figure 2.24 (a) Water contact angles of the PFOTES-coated TiO_2 nanoparticle layer after 20-times rolling with lateral pressure of 1 kPa depending on shearing speed. (b) Water contact angles of the layers after each rolling cycles with applying different lateral pressure 1, 5 and 25 kPa with shearing speed of 1 cm s^{-1}. (c-e) SEM images of (c) the layers before the rolling cycles, (d) the layers which lost its roughness partially showing a water contact angle ~135° after the rolling cycles, and (e) the layers which lost superhydrophobicity completely after the rolling over 100-cycles. Adapted from Yoo et al.

Figure 2.25 (a) Water contact angles of the superhydrophobic layer under vertical pressures for 1000 s. (b) SEM images of the PFOTES-coated TiO_2 nanoparticle layers after pressed at 50 N cm^{-2} for 1000 s. Adapted from Yoo et al.

Figure 2.26 Contact angle measurements of PFOTES-coated TiO_2 nanoparticle layers

*‘As deposited’ condition means that the electrical parameters were characterized as soon as the superhydrophobic protection layers were deposited on OTFTs.

†‘ΔThreshold voltage’ means that the threshold voltage difference after exposure to liquid-based substances compared to that measured at the ‘As deposited’ condition.

Table 2.3. Electrical parameters of the protected OTFTs before and after exposure to tap water. Adapted from Yoo et al.

Table 2.4. Extracted electrical parameters in average values of the protected and unprotected OTFTs before and after exposure to humid air (75% RH). *‘Δ Field effect mobility ($cm^2 V^{-1} s^{-1}$)’ indicates that the mobility difference after exposure to humid air (75% RH). The average initial mobility of unprotected and protected OTFTs were 0.13 $cm^2 V^{-1} s^{-1}$ and 0.29 $cm^2 V^{-1} s^{-1}$, respectively.

†‘Δ Threshold voltage’ indicates that the threshold voltage difference after exposure to humid air (75% RH), The average initial threshold voltage of unprotected and protected OTFTs were -18.4 V and -15.8 V, respectively. Adapted from Yoo et al.

Chapter 3.

Figure 3.1 Schematic images for fabricating the transparent superhydrophobic layers onto an organic phototransistor. Adapted from Yoo et al.

Figure 3.2 (a) Molecular structures of HFE-7500, TIPS-pentacene and PFOTES. (b) Optical image of a water contact angle on a TIPS-pentacene layer. (c) Optical image of a water contact angle on a transparent superhydrophobic layers on the TIPS-pentacene layer. Adapted from Yoo et al.

Figure 3.3 Optical images demonstrated that water droplets on the transparent superhydrophobic layers formed onto a) paper, b) PET and c) PDMS. Adapted from Yoo et al.

Figure 3.4 Optical images of water droplets on a) PFOTES-coated glass, b) PDMS, c) PET and d) Glass before and after depositing transparent superhydrophobic layers. Adapted from Yoo et al.

Figure 3.5 Optical image of a water droplet on the transparent superhydrophobic layers deposited onto the white paper. Adapted from Yoo et al.

Figure 3.6 AFM images of the transparent superhydrophobic layers on a) PFOTES-

nm and different light intensity from 15 μW cm^{-2} to 1500 μW cm^{-2} in ambient condition. e,f) Transfer curves on the semilogarithmic scale for the TIPS-pentacene phototransistor with and without transparent superhydrophobic layer before after exposure to DI water in ambient condition. Adapted from Yoo et al.

Figure 3.28 Threshold voltage shifts of TIPS-pentacene phototransistor with fixed wavelength of a) 450 nm, b) 520 nm and c) 635 nm while varying different light intensities from 10 to 1500 μW cm^{-2}. Adapted from Yoo et al.

Figure 3.29 a) Photoresponsivity, detectivity and EQE of TIPS-pentacene phototransistor with different wavelength (450, 520 and 635 nm), fixed light intensities 1500 μW cm^{-2}, source-drain voltage of – 60V and gate-source voltage of - 60V with and without transparent superhydrophobic layers. Adapted from Yoo et al.

Figure 3.30 Self-cleaning ability of a TIPS-pentacene phototransistor by applying the transparent superhydrophobic layers. a) Removing soils on a TIPS-pentacene phototransistor with transparent superhydrophobic layers by simply dropping water droplets. b,c) Transfer curves on the semilogarithmic scale for TIPS-pentacene organic phototransistors with transparent superhydrophobic layers b) before and c) after self-cleaning process under dark and light illumination with fixed wavelengths 450 nm and different light intensity from 15 μW cm^{-2} to 1500 μW cm^{-2}. Adapted from Yoo et al.

Chapter 1. Introduction

1.1. Brief introduction of organic electronic materials and their needs for effective protection layers

Organic electronic materials have been studied to realize ubiquitous and large-area flexible devices due to their low-cost and low temperature solution processabilities. [1-11] Also, they have been studied as various optoelectronic devices since their optoelectronic properties could be easily tuned by controlling their molecular structures. [12-14] However, it is widely known that they suffer from their environmental instability, which hinder their possibilities for commercial uses. Especially their weakness for water significantly degrade their optical and electrical properties.[15-18] Therefore, many studies to address these issues by encapsulating various materials have been reported, however, more efficient studies which preserve process benefits of organic electronic materials are highly desirable. In this regard, directly deposited organo-compatible protection layers which could introduce excellent water-repellency with a facile solution process is a promising approach to realize practical applications of organic electronic materials.

1.2. Superhydrophobic protection layers for organic electronics

For extreme water repellency of the superhydrophobic surfaces, there are two important factors of surface morphologies. One is a total area ratio of a solid surface to contact with liquid or air under unit projected area, which was connected to water contact angles of the surface. In order to reduce the contact area ratio between solid surface and

liquid, reported superhydrophobic layers generally have hierarchical structures with micro and nanoscale roughness.[19-21] The other factor for extreme water repellency is spacings between local maximum peaks of superhydrophobic surfaces. Since small water droplets might be pinned onto even superhydrophobic surfaces if the spacings between local maximum peaks within area contacting with water droplets were large enough.[22-24] With the surface morphologies described above, low surface tension is also essential part of the superhydrophobicity. Therefore, I need to fabricate the protection layer having well-controlled surface morphologies with low surface tensions without damaging underlying chemically weak organic materials for rendering superhydrophobicity to organic electronics

.

1.3. Brief introduction of organic optoelectronic devices and their needs for transparent superhydrophobic layers

As describe above, organic electronic materials have paved a promising route for realizing large-area flexible applications using low-cost solution processing, even for optoelectronic devices[1-14] and, protected organic electronic devices have shown possibilities to be utilized in practical applications.[25] To achieve better reliability in a perspective of devices, one of the key challenges is to integrate effective protection layers against external threats in daily conditions. In this thread, introducing transparent superhydrophobic layers onto organic optoelectronics have been regarded as an attractive solution because excellent water-repellency can remove harmful dusts or water-based treats efficiently from the self-cleaning ability.[19-21] However, the opaque superhydrophobic layers having a thickness over 10 μm could be a critical hurdle to be utilized in thin film

optoelectronic applications. As a solution to provide transparency to the protection layers, the optimization of their thickness and surface roughness is a most facile methodology that allow the enhanced transmittance via reduced light scattering.[26] Specifically, because the high surface roughness is a key parameter for maintaining the superhydrophobicity, the investigation on the optimized conditions for realizing transparent superhydrophobic layers is highly desirable as well as preserving organo-compatibility. In addition, environmental stabilities of superhydrophobic layers under mechanical deformation, thermal stress, and light-exposure are necessary to be integrated onto practical applications.

1.4. Outline of This Thesis

This thesis mainly focuses on enhancing reliabilities of OTFTs devices with applying superhydrophobic layers. In chapter 2, I discuss the enhanced reliabilities of OTFTs against moisture and waters by organo-compatible superhydrophobic protection layers. Analyses about organo-compatible superhydrophobic protections on mechanical stabilities and preserved electrical properties of protected OTFTs against moisture and waters are also discussed. In chapter 3, I discuss the electrical and optical characteristics of organic phototransistors with and without transparent superhydrophobic layers, and surface properties of the transparent superhydrophobic layers. Finally, chapter 4 summaries this thesis and suggests some future directions.

References

[1] Forrest, S. R. *Nature* **2004**, *428***,** 911-918.

[2] Sekitani, T.; Yokota, T.; Zschieschang, U.; Klauk, H.; Bauer, S.; Takeuchi, K.; Takamiya, M.; Sakurai, T.; Someya, T. *Science* **2009,** *326*, 1516-1519.

[3] Song, Y.; Jeong, H.; Jang, J.; Kim, T.-Y; Yoo, D.; Kim, Y.; Jeong, H.; Lee, T. *ACS Nano*, **2015**, *9*, 7697–7703.

[4] Zhou, Y.; Fuentes-Hernandez, C.; Shim, J.; Meyer, J.; Giordano, A. J.; Li, H.; Winget, P.; Papadopoulos, T.; Cheun, H.; Kim, J.; Fenoll, M.; Dindar, A.; Haske, W.; Najafabadi, E.; Khan, T. M.; Sojoudi, H.; Barlow, S.; Graham, S.; Brédas, J. -L ; Marder, S. R.; Kahn, A.; Kippelen, B. *Science* **2012**, *336*, 327-332.

[5] Sirringhaus, H. *Adv. Mater.* **2014**, *26*, 1319-1335.

[6] Klauk, H.; Zschieschang, U.; Pflaum, J.; Halik, M. *Nature* **2007**, *445*, 745-748.

[7] Diao, Y.; Tee, B. C-K.; Giri, G.; Xu, J.; Kim, D. H.; Becerril, H. A.; Stoltenberg, R. M.; Lee, T. H.; Xue, G.; Mannsfeld, S. C. B.; Bao, Z. *Nat. Mater.* **2013**, *12*, 665-671.

[8] Baeg, K. J.; Caironi, M.; Noh, Y. Y. *Adv. Mater.* **2013**, *25*, 4210-4244.

[9] Kang, H.; Kitsomboonloha, R.; Jang, J.; Subramanian, V. *Adv. Mater.* **2012,** *24*, 3065-3069.

[10] Chung, S.; Jang, M.; Ji, S. B.; Im, H.; Seong, N.; Ha, J.; Kwon, S.-K.; Kim, Y.-H.; Yang, H.; Hong, Y. *Adv. Mater.* **2013**, *25*, 4773-4777.

[11] Sonar, P.; Singh, S. P.; Li, Y.; Soh, M. S.; Dodabalapur, A. *Adv. Mater.* **2010**, *22*, 5409-5413.

[12] Lucas, B.; Trigaud, T.; Videlot-Ackermann, C. *Polym. Int.* **2012**, *61*, 374-389.

[13] Pierre, A.; Gaikwad, A.; Arias, A. C. *Nat. Photonics* **2017**, *11*, 193.

[14] Huang, J.; Du, J.; Cevher, Z.; Ren, Y.; Wu, X.; Chu, Y. *Adv. Funct. Mater.* **2017**, *27*, 1604163.

[15] Sirringhaus, H. *Adv. Mater*. **2009**, *21*, 3859-3873.

[16] Kaltenbrunner, M.; Sekitani, T.; Reeder, J.; Yokota, T.; Kuribara, K.; Tokuhara, T.; Drack, M.; Schwödiauer, R.; Graz, I.; Baier-Gogonea, S.; Bauer, S.; Someya, T. *Nature* **2013**, *499***,** 458.

[17] McCulloch, I.; Heeney, M.; Bailey, C.; Genevicius, K.; MacDonald, I.; Shkunov, M.; Sparrowe, D.; Tierney, S.; Wagner, R.; Zhang, W.; Chabinyc, M. L.; Kline, R. J.; McGehee, M. D.; Toney M. F.; *Nat. Mater*. **2006**, *5*, 328.

[18] Knopfmacher, O.; Hammock, M. L.; Appleton, A. L.; Schwartz, G.; Mei, J.; Lei, T.; Pei, J.; Bao, Z. *Nat. Commun.* **2014**, *5*, 2954.

[19] Lafuma, A.; Quéré, D. *Nat. Mater.* **2003**, *2*, 457.

[20] Feng, L.; Li, S.; Li, Y.; Li, H.; Zhang, L.; Zhai, J.; Song, Y.; Liu, B.; Jiang, L.; Zhu, D. *Adv. Mater.* **2002**, *14*, 1857-1860.

[21] Wang, S.; Jiang, L *Adv. Mater.* **2007**, *19*, 3423-3424.

[22] Extrand, C. W. *Langmuir* **2002**, *18*, 7991-7999.

[23] Nosonovsky, M. *Langmuir* **2007**, *23*, 3157-3161.

[24] Luo, C.; Xiang, M.; Liu, X.; Wang, H.; *Microfluid. Nanofluid.* **2011**, *10*, 831-842.

[25] Yoo, D.; Kim, Y.; Min, M.; Ahn, G. H.; Lien, D. H.; Jang, J.; Jeong, H.; Song, Y.; Chung, S.; Javey, A.; Lee, T. *ACS Nano* **2018**, *12*, 11062-11069.

[26] Rahmawan, Y.; Xu, L.; Yang, S. *J. Mater. Chem. A* **2013**, *1*, 2955-2969.

Chapter 2. Enhancing reliabilities of OTFTs by organo-compatible superhydrophobic layers

In this chapter, I will discuss about how organo-compatible superhydrophobic layers increased reliabilities of OTFTs. In addition, I investigated the organo-compatibilities of my process to deposit nanoparticle layers and their mechanical durability. With transmitted electron microscope (TEM) images, I could confirm that my process and materials were organo-compatible. Furthermore, my superhydrophobic layers showed stabilities against high temperature, vertical and later pressures and light. By fabricating durable and organo-compatible superhydrophobic layers onto OTFTs, their electrical properties were preserved against strong acid, base, Deionized (DI) water and moistures. This study will be helpful in applying OTFTs in more practical applications and will also give chances to realize other types of organic electronic devices to be used in open environments.

2.1. Introduction

Organic semiconductors have attracted significant interest for electronic device applications, low-cost, and low-temperature processabilities.[1-7] Also, they can be regarded as one of the promising candidates to be employed in additive manufacturing such as printing processes.[8-11] Nevertheless, it is widely reported that they suffer from environmental instability; in particular, they can be drastically degraded by water-based hindrances.[12-15] Although many efforts to address this issue by encapsulating organic electronics with various materials such as parylene, silicone, barrier-foil, or a superhydrophobic glass have been reported,[13,16-19] studies on organo-compatible materials and processing to introduce an effective protection layer which can be directly

deposited onto organic components are highly desirable. Superhydrophobic protection layers provide the attractive water-repellency, which could eliminate water-based hindrances from surfaces of organic semiconductors. Therefore, the introduction of a superhydrophobic protection layer onto organic semiconductors could be a promising approach to realize more reliable organic semiconductor applications, because the materials and processes for the superhydrophobic protection layer formation need to be organo-compatible, so that they do not damage physically or chemically when placed onto the organic layers, and thus their electrical characteristics would not be degraded by the protection layers. In addition, fast, facile, and low-cost approaches to implement the protection layer are desirable to bring the advantages of organic components.

In this study, I report that organo-compatible superhydrophobic protection layers which could be directly fabricated onto onto various organic semiconductors for highly reliable OTFTs. The protection layers could be deposited by dipping OTFTs into a highly fluorinated solvent with fluoroalkylsilane-coated TiO_2 nanoparticles. By optimizing the solvent system with a consideration of surface energy, the uniform protection layers could be deposited onto universal organic semiconductors without any observable damages. The surface roughness of TiO_2 nanoparticle-based protection layer allowed the excellent water repellency and self-cleaning abilities regardless of underlying organic semiconductors. The presented superhydrophobic protection layer provided much improved stability of OTFTs against water-based threats and ambient air while exhibiting good resistance against thermal- and mechanical- stresses. Therefore, this method can foster to realize more reliable organic electronics working in the outdoor environment.

2.2. Experiments

2.2.1. Organo-compatible superhydrophobic layer fabrication process

To prepare the superhydrophobic protection solution, I purchased 3-ethoxy-1,1,1,2,3,4,4,5,5,6,6,6-dodecafluoro-2-trifluoromethylhexane (HFE-7500) from 3M^{TM}, and titanium (IV) oxide in a mixture of rutile and anatase nanopowders having particle sizes below 100 nm (TiO_2 nanoparticles) and 1*H*,1*H*,2*H*,2*H*-perfluorooctyltriethoxysilane (PFOTES) from Sigma Aldrich. First, 0.5 g of PFOTES was placed into 29.8 ml of HFE-7500, and then it was mixed with 8.0 g of TiO_2 nanoparticles. By keeping the mixed solution in N_2 for 24 h, the PFOTES-coated TiO_2 nanoparticles in HFE-7500 were prepared. A heavily *p*-doped Si substrate with SiO_2 (270 nm thick, 1.5 cm × 1.5 cm) was cleaned by acetone, isopropanol, and DI water for 10 min at each step by ultrasonication. For the source-drain electrodes, 5 nm-thick Ti and 50 nm-thick Au were deposited sequentially on the SiO_2 dielectric layer using an electron-beam evaporator with a deposition rate of 0.5 Å s^{-1} at a pressure ~10^{-7} torr. Before depositing pentacene as the active channel layer, a surface treatment was conducted on SiO_2 using a PFOTES (0.5 g) solution in HFE-7200 (7 ml) to induce ordered crystals of organic semiconductors by providing enough hydrophobic surface for SiO_2.[20] The prepared PFOTES solution was spin-coated with a spin speed of 500 rpm for 30 s. After performing a drying process on a hot plate at 100 °C for 10 min, then a 120 nm-thick pentacene active layer was thermally evaporated using a shadow mask with a deposition rate of 0.2 Å s^{-1} at a pressure ~10^{-5} torr. The channel length and width were 60 μm and 300 μm, respectively.

On the bottom-contact field-effect transistor structure prepared by the same procedures, 0.5 wt% 6,13-Bis(triisopropylsilylethynyl)pentacene (TIPS-pentacene)

dissolved in toluene and 1.0 wt% Poly(3-hexylthiophene) (P3HT) dissolved in 1,2-Dichlorobenzene were drop-casted and spin-coated at 1500 rpm for 30 s, on the engineered surface, respectively. Then, the TIPS-pentacene and P3HT layers were dried in air and N_2 for 1 h and 6 h, respectively. P3HT was purchased from Rieke Metals, and all the other reagents were purchased from Sigma-Aldrich. All the reagents were used as received.

The fabricated organic thin film transistors (OTFTs) were dipped into the PFOTES-coated TiO_2 nanoparticle solution at room temperature. Figure S1 shows the procedure for the formation of the superhydrophobic protection layer on the pentacene layer by dipping the sample into the prepared solution. The PFOTES-coated TiO_2 nanoparticles covered the entire surface of OTFTs in a short time (~2 s) (Figure 2.1). The PFOTES-coated TiO_2 nanoparticle layers were dried with N_2 gas to remove any remaining solvent. Finally, the source-drain electrode pads were exposed by rubbing the PFOTES-coated TiO_2 nanoparticle layers with a methanol-soaked swab. Moreover, my strategy has a great strength to sensitive organic semiconductors compared to the previously reported fabrication methods for superhydrophobic layer.[21,22]

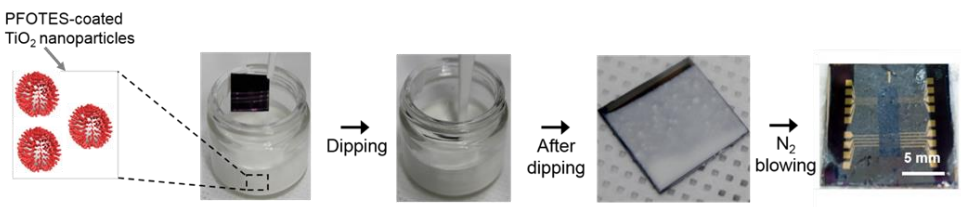

Figure 2.1 The procedure for forming the superhydrophobic protection layer on OTFTs.

Note that the PFOTES-coated TiO_2 nanoparticles highly dispersed in HFE-7500 (14.0 wt%) allow an excellent film formation universally on various organic semiconductors (pentacene, 6,13-bis(triisopropylsilylethynyl)pentacene (TIPS-pentacene), and poly(3-hexylthiophene) (P3HT) for thermally evaporated organic small-molecule, solution-deposited organic small-molecule, and solution-deposited polymer semiconductors, respectively) by simply dipping them into the prepared solution for a short time (~2 s) in ambient (see Figure 2.1)

2.2.2. Characterization

Cross-sectional images of the devices were obtained using scanning electron microscopy (SEM) (MERLIN, ZEISS) and analytical scanning transmission electron microscopy (STEM) (JEM-2100F, JEOL). To determine the surface moieties on the PFOTES-coated TiO_2 nanoparticle layers, XPS (Axis-HSI, Kratos Inc.) was conducted with an Al monochromator anode at a power of 18 mA and 12 kV. Roughness parameters were evaluated by using 3D laser profiler (VK-250K, KENENCE) and AFM (NX10, Park Systems Corp.). The contact angle, roll-off angle and contact angle hysteresis of the OTFTs with and without the superhydrophobic protection layer were measured by standard procedures (SmartDrop Lab HS, Femtofab) in ambient conditions. The electrical characteristics of the fabricated OTFTs were measured using a semiconductor parameter analyzer (Model 4200 SCS, Keithley) and a probe station (Model ST-500, JANIS).

2.3. Results and Discussions

2.3.1. Formation of superhydrophobic layers on the organic semiconductors

A solution process using 1*H*,1*H*,2*H*,2*H*-perfluorooctyltriethoxysilane (PFOTES) attached to TiO_2 nanoparticles (average diameter < 100 nm) dispersed in 3-ethoxy-1,1,1,2,3,4,4,5,5,6,6,6-dodecafluoro-2-trifluoromethylhexane (HFE-7500) was conducted to form the protection layer (Figure 2.2a). Highly fluorinated HFE-7500 is immiscible to most organic materials; thus, the solution-dipping process does not damage organic layer during the protection layer formation.[23] Moreover, PFOTES has been widely used to introduce superhydrophobic properties on the surface of TiO_2 nanoparticles by reacting with hydroxyl groups (Figure 2.2b).[21,22,24,25] Therefore, PFOTES-coated TiO_2 nanoparticle layers can deliver superhydrophobic properties to protect the underlying organic layer from water-based solutions without additional surface treatments, structures, or dedicated procedures (Figure 2.2c,d). Note that the PFOTES-coated TiO_2 nanoparticles highly dispersed in HFE-7500 (14.0 wt%) allow an excellent film formation universally on various organic semiconductors (pentacene, 6,13-bis(triisopropylsilylethynyl)pentacene (TIPS-pentacene), and poly(3-hexylthiophene) (P3HT) for thermally evaporated organic small-molecule, solution-deposited organic small-molecule, and solution-deposited polymer semiconductors, respectively) by simply dipping them into the prepared solution for a short time (~2 s) in ambient. As a result, the protection layers having similar morphologies were produced onto the all different organic semiconductors (Figure 2.2e-g). This was possible since the PFOTES-coated TiO_2 nanoparticle layers should be well-deposited using a simple dipping process without additional surface treatments or thermal treatments. The non-polar fluorinated solvent (HFE-7500) showed excellent wetting property with a contact angle near 0° not only on all of semiconductors used in this study (evaporated pentacene, solution-processed TIPS-pentacene, and solution-processed P3HT), but also on Au contacts and SiO_2 gate dielectric (Figure 2.3a-e). Due to the good wetting

property of HFE-7500, my solution composed of HFE-7500 and PFOTES-coated TiO_2 nanoparticles quickly spread out on the surfaces mentioned above after dropping the solution onto the substrates (Figure 2.3f-j). This good wetting property of the solution makes it possible for the PFOTES-coated TiO_2 nanoparticles to be deposited onto the surface by the simple dipping process.

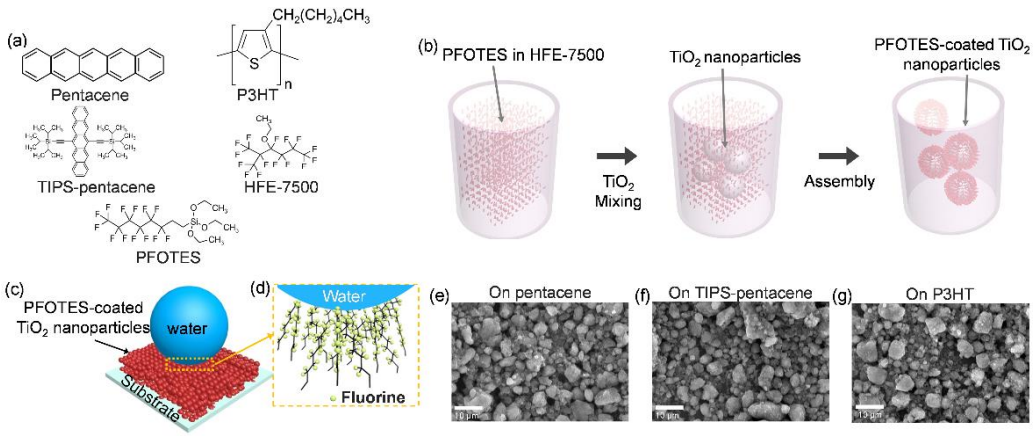

Figure 2.2 (a) Molecular structures of pentacene, TIPS-pentacene, P3HT, HFE-7500, and PFOTES. (b) Schematic for preparing the solution of PFOTES-coated TiO_2 nanoparticles. (c) Schematic of a water droplet contacting the PFOTES-coated TiO_2 nanoparticle layers on organic semiconducting layers. (d) Schematic for the interface between water and the fluorinated end-groups of PFOTES. (e-g) SEM images for the PFOTES-coated TiO_2 nanoparticles on (e) pentacene (f) TIPS-pentacene (g) P3HT layers

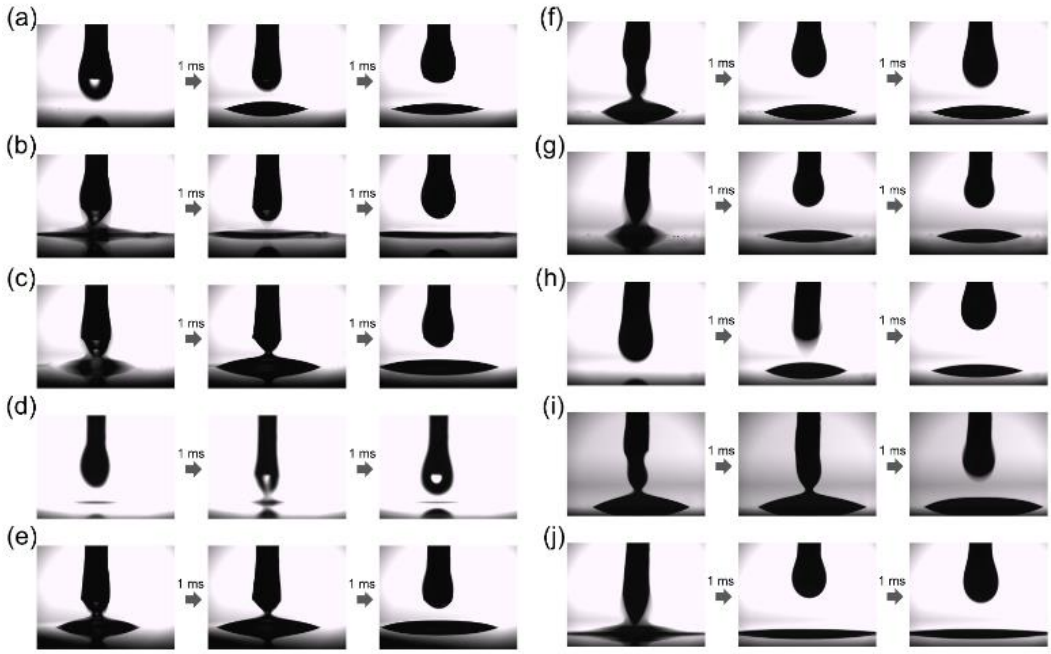

Figure 2.3 (a-e), After dropping HFE-7500 droplet onto (a) pentacene, (b) TIPS-pentacene, (c) P3HT, (d) Au, and (e) SiO_2 layer, the HFE-7500 was wetted on these layers in 3 ms. (f-j), After dropping the solution of HFE-7500 and PFOTES-coated TiO_2 nanoparticles onto (f) pentacene, (g) TIPS-pentacene, (h) P3HT, (i) Au, and (j) SiO_2 layer, the solution was wetted on these layers in 3 ms.

Also, to determine if HFE-7500 is a suitable solvent for dispersing PFOTES-coated TiO_2 nanoparticles used for superhydrophobicity, sedimentation of PFOTES-coated TiO_2 nanoparticles in HFE-7500 and ethanol (which was used for previously reported superhydrophobic solution as a solvent[21]) was compared since sedimentation speed of nanoparticles in the solution was one of the parameters which indicate the ability of a particle dispersion.[26] As shown in Figure 2.4, sedimentation of PFOTES-coated TiO_2 nanoparticles in ethanol was faster than the sedimentation in HFE-7500, which indicates that HFE-7500 had better dispersion stability for PFOTES-coated TiO_2 nanoparticles than ethanol. Furthermore, I verified cluster sizes of PFOTES-coated TiO_2 nanoparticles, which had been dispersed in HFE-7500 and ethanol, on SiO_2 layers by scanning electron

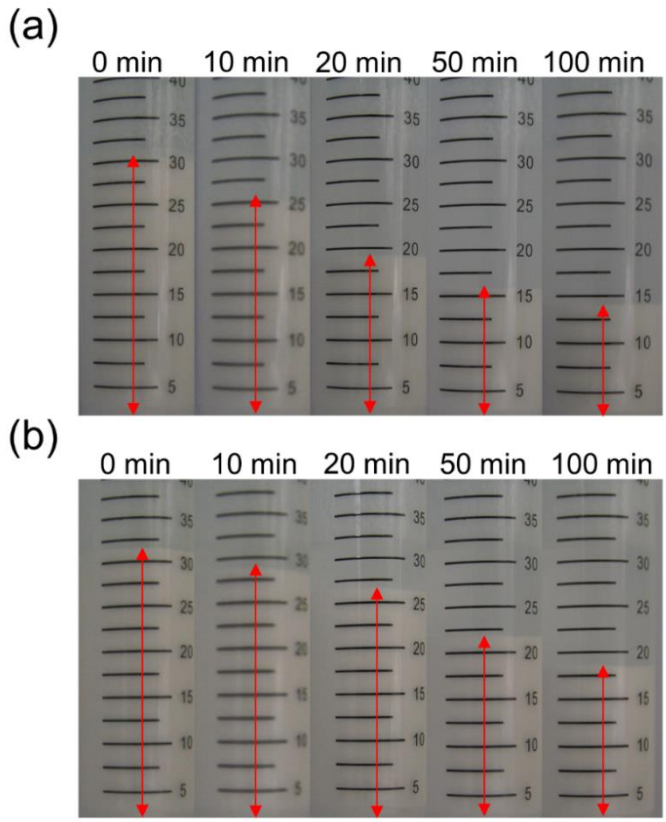

Figure 2.4 (a, b) Sedimentation of the PFOTES-coated TiO_2 nanoparticles in (a) ethanol and (b) HFE-7500

microscope (SEM) images after dipping processes, and the results showed that the PFOTES-coated TiO_2 nanoparticles dispersed at similar levels in both solutions (Figure 2.5). In addition, HFE-7500 also has various environmental merits. One of them is that HFE-7500 is not flammable since it does not have flash point and has high autoignition temperature. Moreover, it has low global warming potential and has low toxicity, and its octanol-water partition coefficient is high, even compared with other fluorinated solvents, which implies that it would be unmixed with organic materials.[23]

Also, the resultant surface densities of TiO_2 nanoparticle layers were investigated depending on different densities of PFOTES-coated TiO_2 nanoparticles: 4.0 g of TiO_2 and 0.25 g of PFOTES in HFE-7500 (4 wt% TiO_2), 8.0 g of TiO_2 and 0.5 g of PFOTES in HFE-7500 (14 wt% TiO_2 used in this study), and 16.0 g of TiO_2 and 1.0 g of PFOTES in HFE-7500 (24 wt% TiO_2). After depositing them onto SiO_2 layers, the TiO_2 nanoparticle layers with 4 wt% TiO_2 solution showed relatively lower surface density with many vacancies by SEM and optical images (Figure 2.6a,d). In contrast, the TiO_2 nanoparticle layers with 14 wt% and 24 wt% TiO_2 solution exhibited much improved surface coverage without clearly observed voids (Figure 2.6b,c,e,f). Note that from my experiments, TiO_2 density of 14 wt% was the critical ratio to realize tightly packed protection layers. Consequently, the protection properties of TiO_2 nanoparticle layers would be degraded due to water molecules and oxygen penetration via the uncovered area if solutions with a lower TiO_2 nanoparticle density less than ~14 wt% are used to deposit the protection layer.

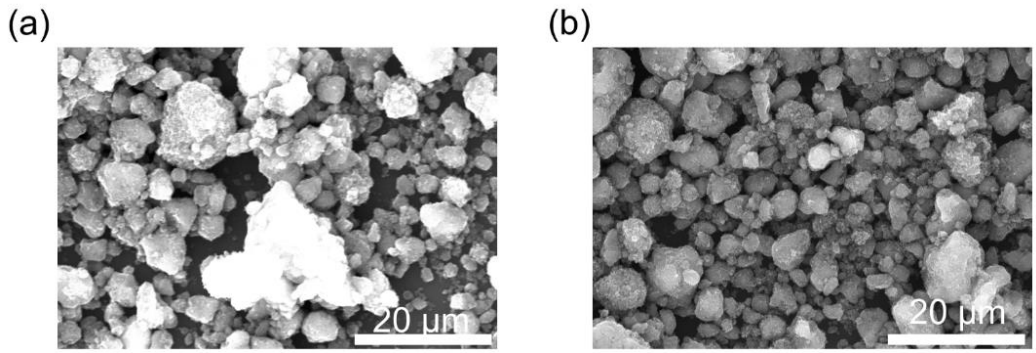

Figure 2.5 (a, b) SEM images for the PFOTES-coated TiO_2 nanoparticles on SiO_2 surfaces which had been dispersed in (a) ethanol and (b) HFE-7500.

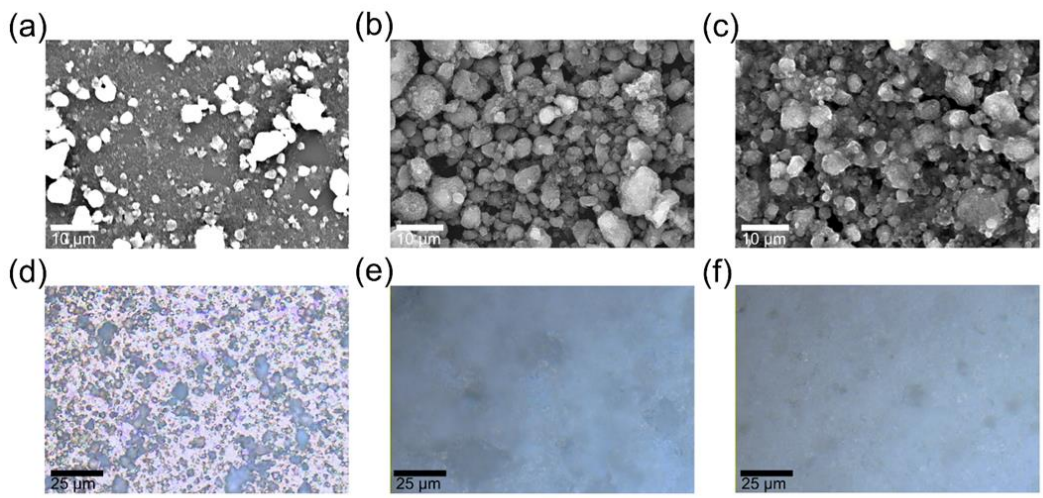

Figure 2.6 (a-c) SEM images for the PFOTES-coated TiO_2 nanoparticle layers on a SiO_2 layer with (a) 4 wt%, (b) 14 wt%, and (c) 24 wt% TiO_2 solutions. (d-f) Optical images for the PFOTES-coated TiO_2 nanoparticle layers on a SiO_2 layer by (d) 4 wt%, (e) 14 wt%, and (f) 24 wt% TiO_2 solutions.

I measured the surface roughness of PFOTES-coated TiO_2 nanoparticle layers by using a 3-dimensional (3D) laser profiler in a scanning size of 95.1 μm × 71.6 μm and the highest point to lowest point value was measured to be 24.7 μm and root-mean-square (RMS) value was measured to be 4.09 μm (Figure 2.7). I also measured the surface roughness in a smaller area of 5.0 μm × 5.0 μm using atomic for AFM. The highest point to lowest point and RMS value were measured to be 2.3 μm and 0.3 μm, respectively (Figure 2.8).

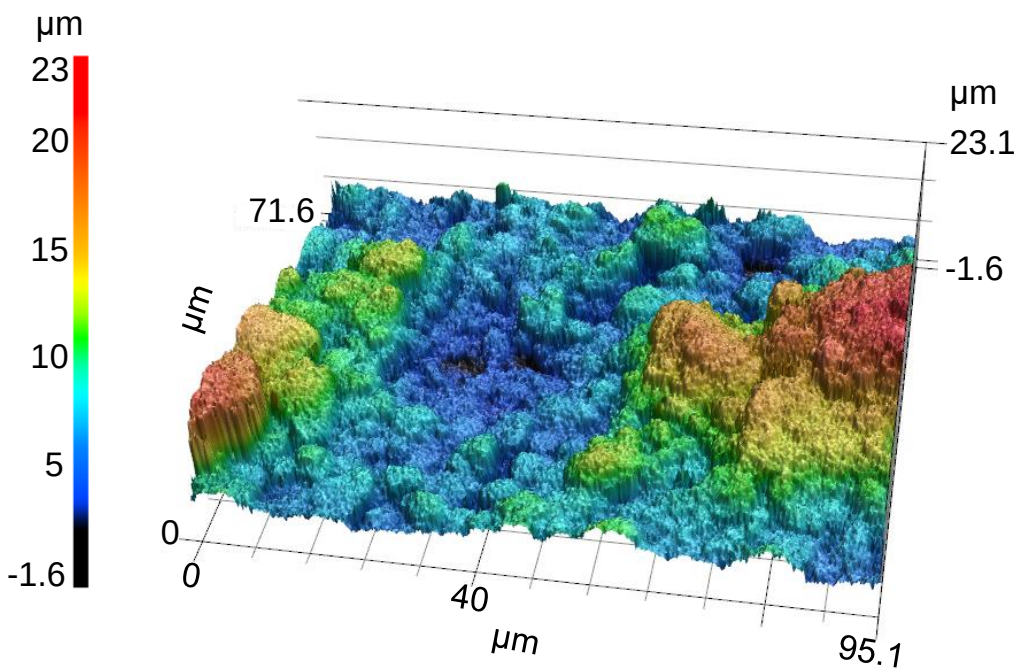

Figure 2.7 3D laser surface profile image of the PFOTES-coated TiO_2 nanoparticle layers on a SiO_2 layer (scan size of 95.1 μm × 71.6 μm).

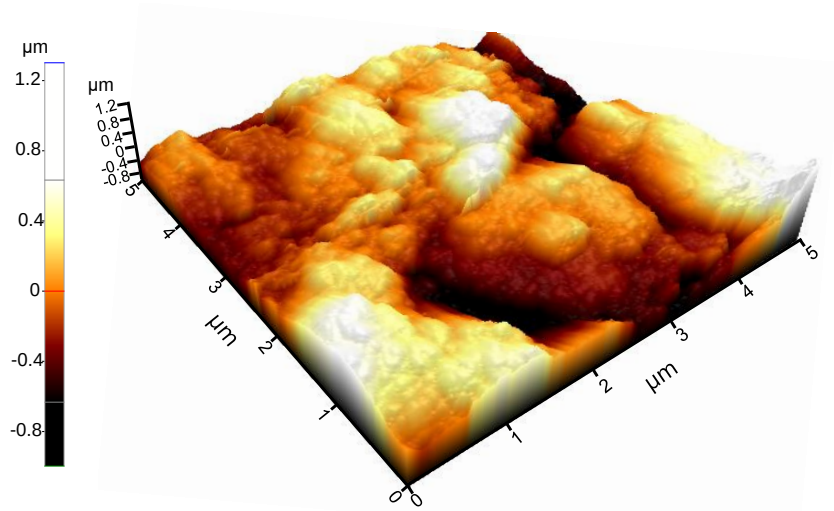

Figure 2.8 AFM image of the PFOTES-coated TiO_2 nanoparticle layers on a SiO_2 layer (scan size of 5.0 µm × 5.0 µm).

More detailed analysis for thickness, particle and cluster sizes of TiO_2 nanoparticles was also proceeded. At a certain area, the thickness of the superhydrophobic protection layers was generally about ~ 4 µm, and the average particle radius is about ~50 nm as received. (Figure 2.9a and b) In addition, largest cluster sizes from horizontal view is about 15 µm. (Figure 2.9c) Since fluorine is rarely detected by EDS data from TEM images as shown in Figure 2.10, roughness and thickness were mostly contributed to TiO_2 nanoparticles.

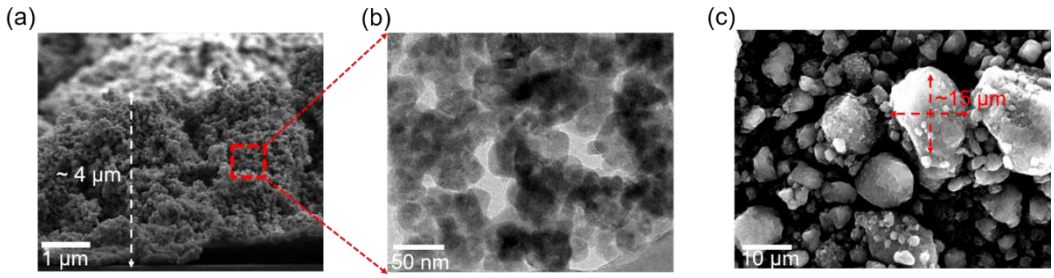

Figure 2.9 (a) SEM image of the PFOTES-coated TiO_2 nanoparticle layers on a pentacene layers with vertical view. (b) TEM image of the PFOTES-coated TiO_2 nanoparticle layers on a pentacene layers with vertical view. (c) SEM image of the PFOTES-coated nanoparticle layers on a pentacene layers with horizontal view.

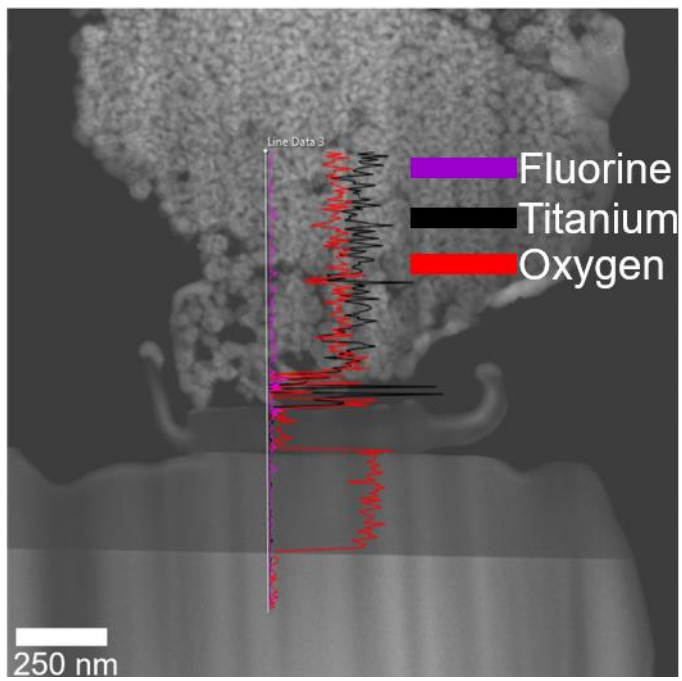

Figure 2.10 TEM image and EDS data of the PFOTES-coated TiO_2 nanoparticle layers on a pentacene layer with large scale as ~ 1.5 μm by 1.5 μm.

2.3.2. Water repellency of the presented superhydrophobic protection layers

The rough surface of TiO_2 nanoparticles and the low surface tension induced by the trifluoromethyl ($-CF_3$) groups of PFOTES make the superhydropobic surface,[21,22,25,27] which delivered a high contact angle > 150° regardless of the underlying organic semiconducting layers (Figure 2.11a), whereas the bare pentacene layer exhibited a water contact angle of 81° (Figure 2.11b).

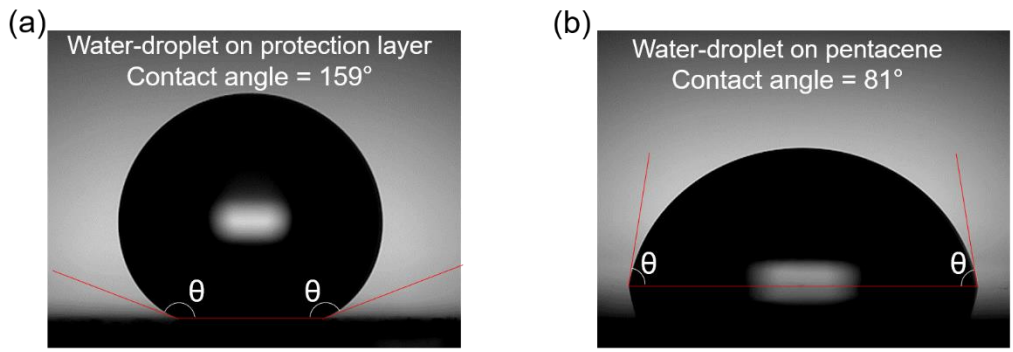

Figure 2.11 (a) Optical image of the water contact angle on a protected pentacene layer with the PFOTES-coated TiO_2 nanoparticles. (b) Optical image of the water contact angle on a bare pentacene layer.

To investigate the repellency of my superhydrophobic protection layer for liquid having a lower surface tension than water, solutions of water mixed with methanol at different weight ratios were prepared. Since liquid having low surface tension could be easily spread on a surface,[28] the contact angle may be different. And if their contact angles were below 150°, it meant that they could not be repelled by our deposited nanoparticle layers. Therefore, I confirmed how repellent my superhydrophobic protection is to liquid with low surface tension. Under my experimental conditions, Figure 2.12a illustrated surface tensions of the solutions mentioned above and I found that the measured surface tensions were similar to the previous reported results.[29] I placed each different

solutions having different surface tensions onto the nanoparticle-based superhydrophobic protection layer and measured their contact angles. As a result, my superhydrophobic protection layer had excellent repellency for the solutions having a surface tension, 34.5 mN m^{-1} (methanol 50 wt%) or higher, since they showed high contact angles >150° on my superhydrophobic surface (Figure 2.12b-d), which is comparable to water contact angles of the other reported superhydrophobic layers.[19,21,22,27] For more detailed study of water repellency of presented superhydrophobic protection layers, contact angle hysteresis was also measured for each solution by captive method through contact angle measurement equipment (SmartDrop Lab HS, Femtofab). As Figure S8a showed, liquid droplet having surface tension (> 44 mN m^{-1}) showed low contact angle hysteresis (< 5°) and these high contact angles and low contact angle hysteresis indicated superhydrophobic Cassie state, where contact areas between water and solid surfaces were decreased by air gaps in the rough surfaces (Figure 2.13).[28,29] For liquid having low surface tension (~ 34.5 mN m^{-1}), superhydrophobic Wenzel state, where liquid penetrated air gaps in rough surfaces to increase contact areas between solid and liquid became dominant on my superhydrophobic protection layers (Figure 2.13).[28,29] It is well-known that high contact angles and low contact angle hysteresis can be observed in micro/nanoscale hierarchical superhydrophobic surfaces because of air gaps in roughened surfaces, that play a critical role for water repellency of superhydrophobic surfaces.

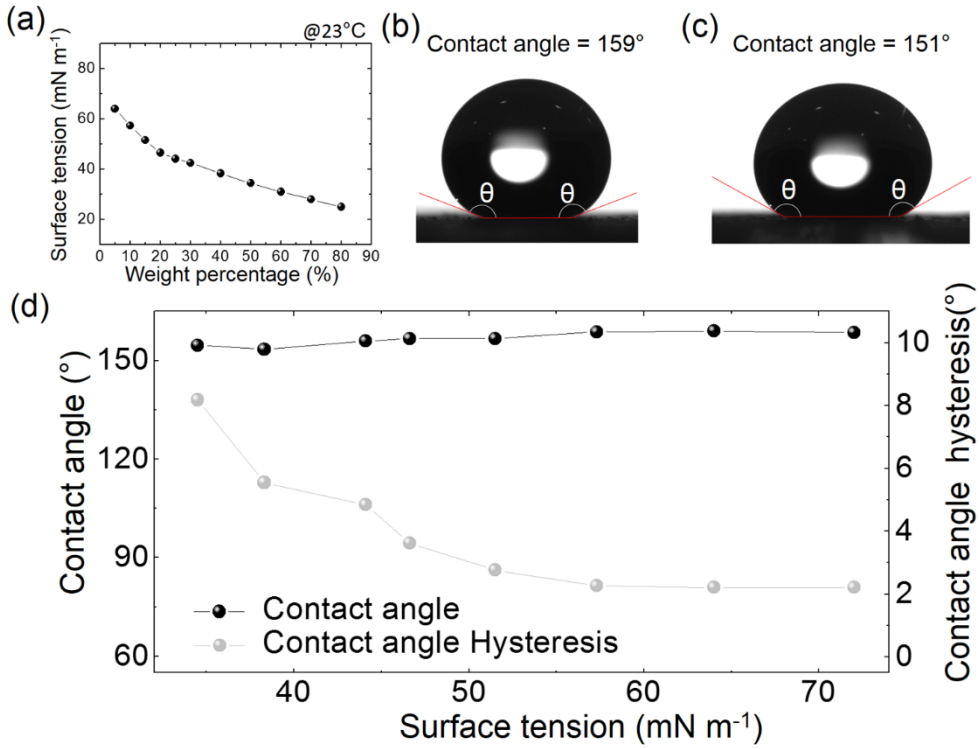

Figure 2.12 (a) Surface tensions for the water-based solution with different methanol weight percentages. (b, c) Optical contact angle image of the solutions having surface tensions of (b) 64.0 mN m^{-1} and (c) 34.5 mN m^{-1} on the PFOTES-coated TiO_2 nanoparticle layers. (d) Measured contact angles and contact angle hysteresis for the water-based solution with different surface tensions on PFOTES-coated TiO_2 nanoparticle layers.

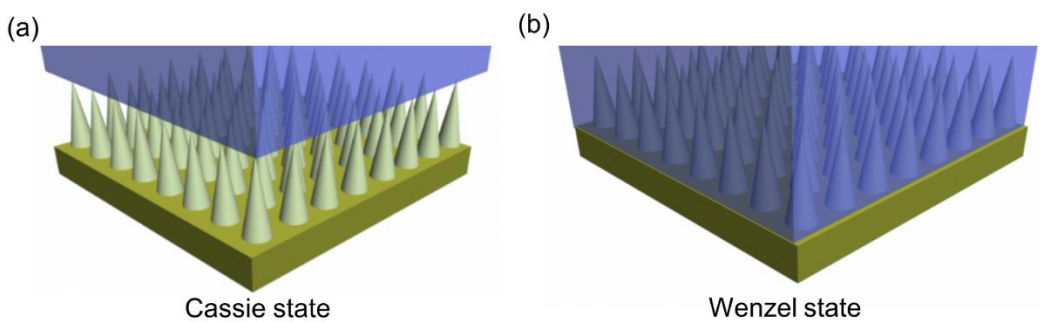

Figure 2.13 (a, b) Schematic images of (a) Cassie and (b) Wenzel state.

The surface morphology by PFOTES-coated TiO_2 nanoparticles created enough air gaps to allow extreme water repellency showing the ability of water-bouncing comparable to other reported superhydrophobic surfaces (Figure 2.14).

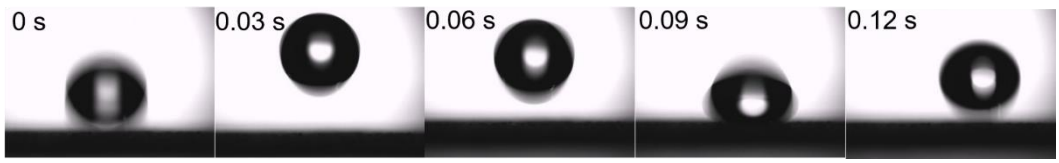

Figure 2.14 Time-resolved images for water droplet bouncing on the PFOTES-coated TiO_2 nanoparticle layers.

For a detailed analysis of a bouncing ability of my organo-compatible superhydrophobic protection layer, solutions of water mixed with methanol at different weight ratios were prepared and then these solutions were dropped as a droplet (~1 mm radius) onto the surface by different velocities (Table 2.1). Since liquid having low surface tension tends to be easily spread on a surface,[28] droplets having low surface tension may not be repelled from the superhydrophobic surface. Therefore, it is important to check bouncing properties of the superhydrophobic layer for a droplet having lower surface tension than water. It was confirmed that the droplets having surface tension (> 44 mN m^{-1}) could be bounced off from the superhydrophobic protection layer while the other droplets having relatively low surface tension (~ 42.6 mN m^{-1}) were pinned onto the surface (Table 2.1). Furthermore, the low-surface-tension-droplets impacted onto the surface at relatively faster velocities were scattered by small droplets (Figure 2.15 and Table 2.1), which also indicated superhydrophobicity.[30] For water droplet without methanol at different impact velocities, my superhydrophobic protection had good bouncing ability, which is comparable to other published superhydrophobic surface (Table 2.1).[31]

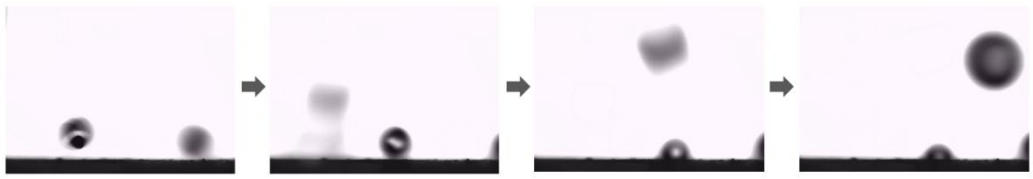

Figure 2.15 Optical images demonstrated that the falling droplet was divided into smaller droplets on our superhydrophobic surface and these small droplets bounced off from the surface.

Radius of drop ~1mm

Weight percentage (%)	Surface tension (mN m^{-1})	Impact velocity (m/s)				
		0.3	0.7	1.0	1.4	1.7
0	70.0	Rebound	Rebound	Rebound	Rebound	Fragmentation
5	64.0	Rebound	Rebound	Rebound	Fragmentation	Fragmentation
10	57.3	Rebound	Rebound	Rebound	Fragmentation	Fragmentation
15	51.5	Rebound	Rebound	Fragmentation	Fragmentation	Fragmentation
20	46.6	Rebound	Rebound	Fragmentation	Fragmentation	Fragmentation
25	44.1	Rebound	Rebound	Fragmentation	Fragmentation	Fragmentation
30	42.5	Pinning	Pinning	Pinning	Pinning	Pinning
40	38.3	Pinning	Pinning	Pinning	Pinning	Pinning
50	34.5	Pinning	Pinning	Pinning	Pinning	Pinning

Table 2.1 Summary of bouncing characteristics of the water-based solution with different methanol weight percentage.

In addition, an extremely small roll-off angle (< 1°) was observed for the deposited PFOTES-coated TiO_2 nanoparticle layers whereas relatively large roll-off angle of 34° was observed for the bare pentacene. The roll-off angle is the angle of inclination of a surface where a water-droplet rolls-off it (Figure 2.16). If a water-droplet is dropped onto a superhydrophobic surface, it will roll down the surface at a relatively small tiling angle. The superhydrophobic protection layer allowed rolling-off of a water droplet even if the substrate was tilted with an angle < 1°.

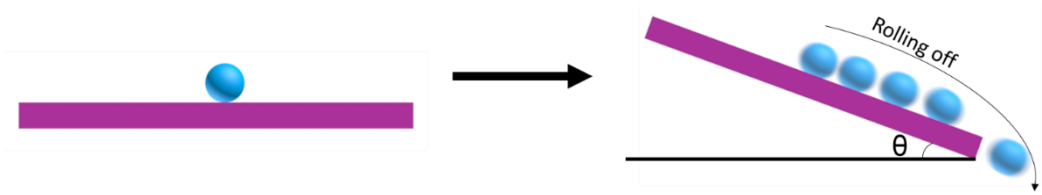

Figure 2.16 Schematic images of water-droplet rolling off on a surface.

The small roll-off angle of the PFOTES-coated TiO_2 nanoparticle layers allows the self-cleaning ability upon exposure to water-based solvents. The pentacene layer protected by the PFOTES-coated TiO_2 nanoparticle layers could successfully sweep heavy soils by dropping water droplets since the sliding water droplets take the soils away from the surface and absorb them into themselves (Figure 2.17). Therefore, all soils in the path of the sliding water-droplet were removed away from the protected surfaces, which is known as the self-cleaning effect.[21,22]

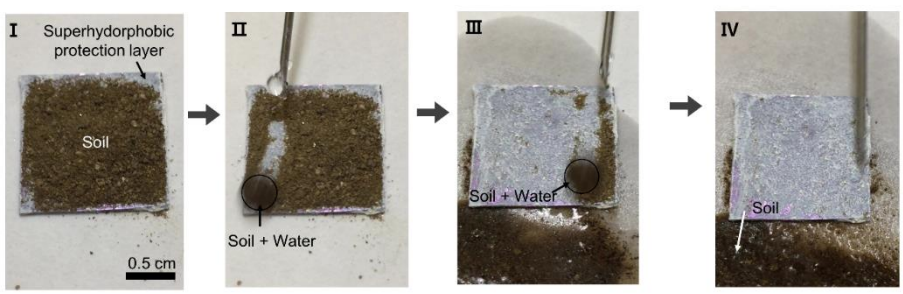

Figure 2.17 Optical images demonstrating the self-cleaning properties of the pentacene protected with the PFOTES-coated TiO_2 nanoparticle layers.

2.3.3. Chemical composition and organo-compatibilities of PFOTES-coated TiO_2 nanoparticle layers

I use X-ray photoelectron spectroscopy (XPS) to analyze the TiO_2 nanoparticle films with and without the PFOTES layer. The XPS spectrum showed intense photoelectron signals on the surface at binding energies of 457 eV and 463 eV which were related to the Ti $2p_{1/2}$ and $2p_{3/2}$ levels of the titanium atoms, respectively.[21,32] I observed that the F 1s peak was at the binding energy of 687 eV on the PFOTES-coated TiO_2 nanoparticle film. (Figure 2.18) And, to investigate the chemical composition of TiO_2 nanoparticles without the PFOTES coating layer, I mixed 8 g of TiO_2 nanoparticles into 29.8 ml of HFE-7500. Then, the TiO_2 nanoparticle layers were formed on a SiO_2 (270 nm thick)/heavily *p*-doped Si substrate using a dipping process. Figure 2.19 shows X-ray photoelectron spectroscopy (XPS) spectra. For the TiO_2 nanoparticles without the PFOTES coating layer, intense photoelectron signals on the surface showed peaks at binding energies of 460 eV and 465 eV, which are related to the Ti $2p_{1/2}$ and Ti $2p_{3/2}$ levels,[21,32] respectively, while no clear peak for fluorine was observed near 687 eV (Figure 2.19).[21] Because no clear peak related to the F 1s orbital was observed in the TiO_2 nanoparticle film without PFOTES, the fluorine contained in HFE-7500 did not remain on the surface of the TiO_2 nanoparticles after the drying process.

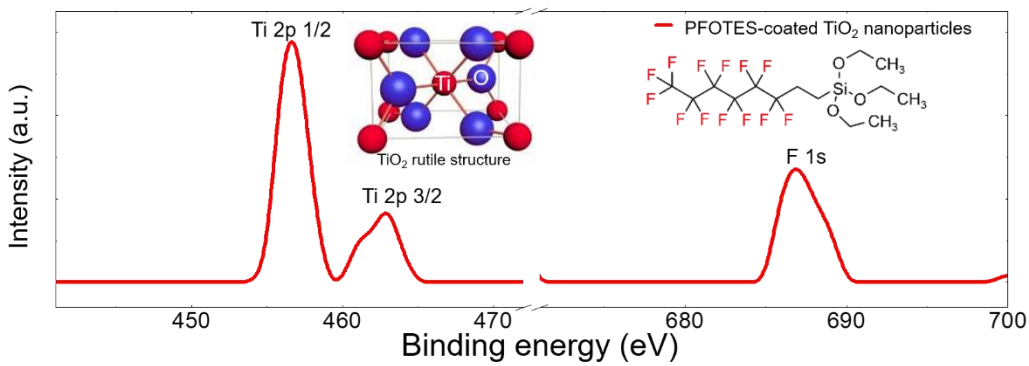

Figure 2.18 XPS spectrum of PFOTES-coated TiO_2 nanoparticle layers. The inset image shows the rutile phase of TiO_2 and the molecular structure of PFOTES with the fluorine atoms highlighted in red.

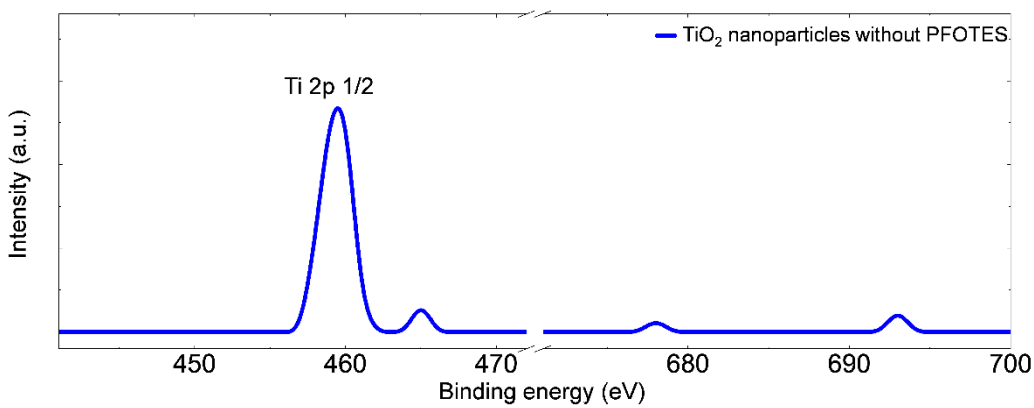

Figure 2.19 XPS spectrum of the TiO_2 nanoparticle layers without the PFOTES coating.

To confirm that the methods and materials used in this work are organo-compatible, cross-sectional images of the organic semiconducting layers with and without the PFOTES-coated TiO_2 nanoparticle layers were obtained. Scanning electron microscopy (SEM) images revealed that the PFOTES-coated TiO_2 nanoparticle layers were well deposited on the pentacene semiconducting layer, and they did not produce any physical damages to the

pentacene layer (Figure 2.20a,b). Moreover, the cross-sectional transmission electron microscope (TEM) and energy-dispersive X-ray spectroscopy (EDS) results also indicated that no undesirable penetration was observed after the superhydrophobic protection layer deposition because the titanium and oxygen elements were evidently detected only in the upper PFOTES-coated TiO_2 nanoparticle layers but were undetected in the underlying pentacene layer (Figure 2.20c).

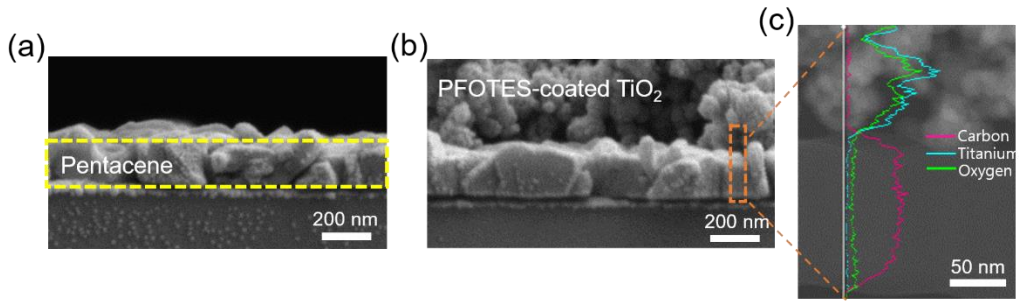

Figure 2.20 (a,b) SEM images of the pentacene layers (a) without and (b) with the PFOTES-coated TiO_2 nanoparticle layers. (c) TEM image and EDS data of the PFOTES-coated TiO_2 nanoparticle layers on a pentacene layer.

Also, the cross-sectional transmission electron microscope (TEM) images of the solution-processed TIPS-pentacene and P3HT layers protected by the PFOTES-coated TiO_2 nanoparticle layers indicated that the suggested materials and processes in this work did not produce any physical damages to the organic semiconducting layer. Moreover, energy-dispersive X-ray spectroscopy (EDS) profiles supported no undesirable penetration was observed after the superhydrophobic protection layer deposition because the titanium and oxygen elements were evidently detected only in the upper PFOTES-coated TiO_2 nanoparticle layers but were undetected in the underlying TIPS-pentacene and P3HT layers (Figure 2.21).

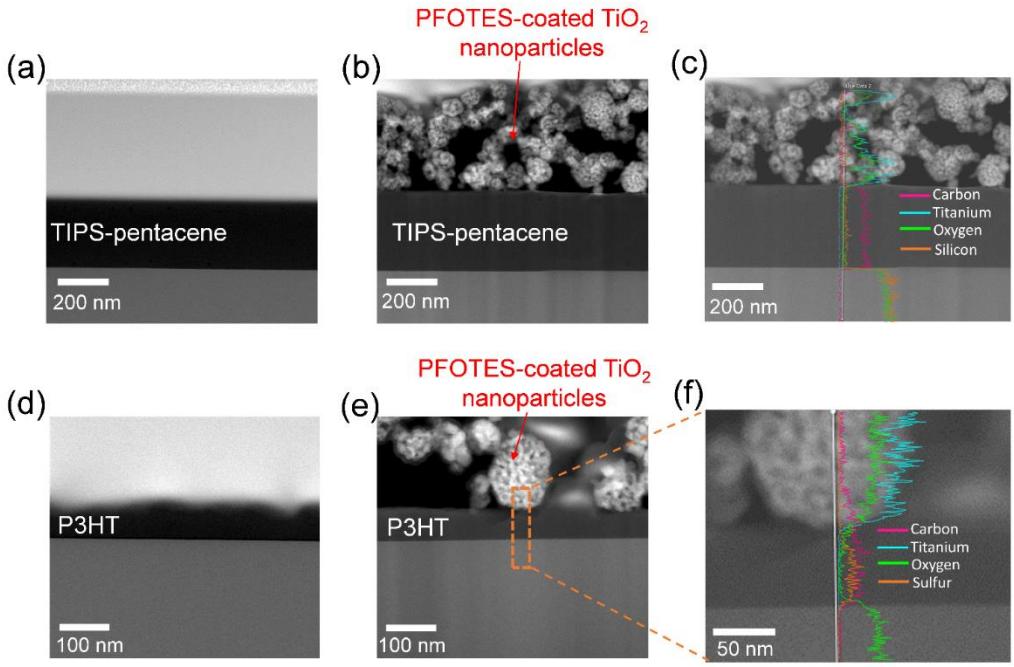

Figure 2.21 (a) TEM image of a bare TIPS-pentacene layer. (b) TEM image of a bare TIPS-pentacene layer with the PFOTES-coated TiO_2 nanoparticle layers. (c) EDS profiles of the PFOTES-coated TiO_2 nanoparticle layers on the TIPS-pentacene layer. (d) TEM image of a bare P3HT layer. (e) TEM image of a bare P3HT layer with the PFOTES-coated TiO_2 nanoparticle layers. (f) EDS profiles of the PFOTES-coated TiO_2

To investigate compatibilities of PFOTES-coated TiO_2 nanoparticle layers for a n-type semiconductor, {[N, N′-bis (2-octyldodecyl)-1, 4, 5, 8-naphthalenedicarboximide-2, 6-diyl]-alt-5, 5′-(2, 2′-bithiophene)} P(NDI2OD-T2) was used to be dissolved in anhydrous chlorobenzene (10 mg ml^{-1}). After filtered using a 0.2 mm polytetrafluoroethylene syringe filter in a N_2 glove box, the prepared solution was spin-coated onto a heavily p-doped Si substrate with SiO_2 (270 nm thick) at 2000 rpm. Then, the P(NDI2OD-T2) layers were annealed at 110 °C for 30 min. The completely dried semiconducting layers were dipped into PFOTES-coated TiO_2 nanoparticle solution, and the PFOTES-coated TiO_2 nanoparticle layers were deposited onto the n-type semiconductor.

From the TEM images shown in Figure 2.22a,b, I could not find any significant damages on the P(NDI2OD-T2) layers after depositing PFOTES-coated TiO_2 nanoparticle layers. Moreover, EDS profiles also supported that undesirable penetration by the TiO_2 nanoparticles was not observed (Figure 2.22c). In addition, it was confirmed that the PFOTES-coated TiO_2 nanoparticle layers were uniformly deposited onto P(NDI2OD-T2) layers (Figure 2.22d) exhibiting high water contact angles (Figure 2.22e). From these results, my superhydrophobic protection layer could be also applied to n-type organic semiconductors.

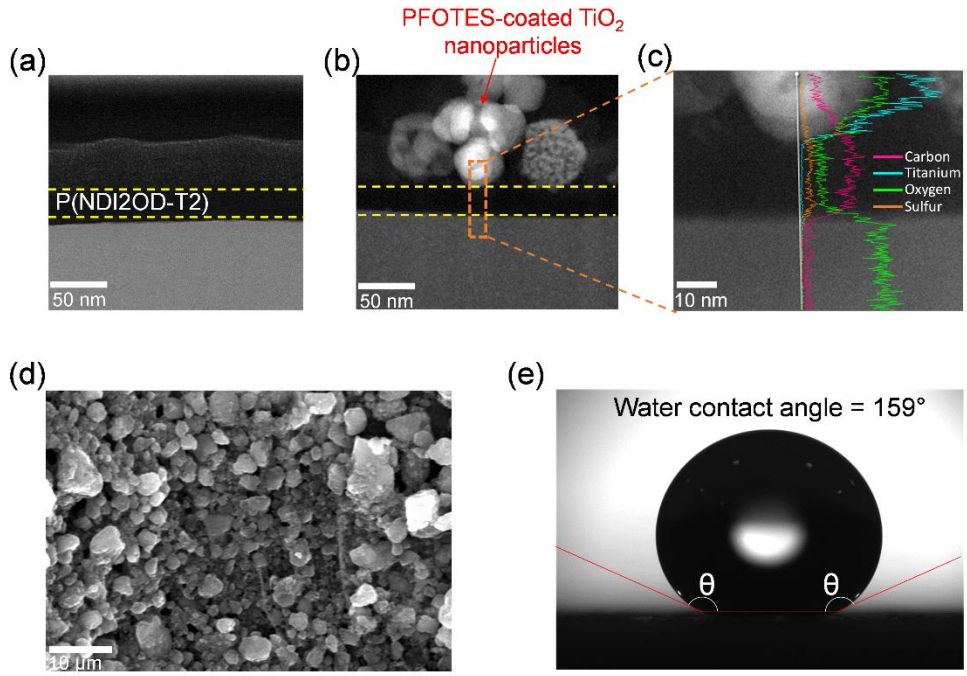

Figure 2.22 (a) TEM image of a bare P(NDI2OD-T2) layer (the top layer is carbon coating). (b) TEM image of a bare P(NDI2OD-T2) layer with the PFOTES-coated TiO_2 nanoparticle layers. (c) EDS profiles of the PFOTES-coated TiO_2 nanoparticle layers on the P(NDI2OD-T2) layer. (d) SEM images of the surface of PFOTES-coated TiO_2 nanoparticle layers on a P(NDI2OD-T2) layer. (e) Optical image of the water contact angle on the protected P(NDI2OD-T2) layer with the PFOTES-coated TiO_2 nanoparticle layers.

2.3.3 Durability of organo-compatible superhydrophobic protection layer

To use organic devices in practical applications, an excellent tolerance to realistic circumstances is necessary to achieve reliable operation maintaining their electrical characteristics when exposed to, for example, water, acid rain (pH < 5.6),[33] various beverages (pH 3.0-6.5),[34] and cleaning soaps (pH 9.0-12.0)[35,36] that can be met in daily life. Therefore, an effective protection layer should have a good robustness against liquid-based substances with a wide range of pH values to prevent operation failure. To confirm the robustness of the protection film, contact angles were measured after exposure to various corrosive liquids, such as hydrochloric acid (HCl, pH 1.0), sodium hydroxide (NaOH, pH 13.0), acetic acid (CH_3COOH, pH 2.7), ammonium hydroxide (NH_3OH, pH 11.7), and deionized (DI) water for 10 s. Even though the prepared protection film was exposed to strong acid and alkaline solvents, its superhydrophobicity was well-maintained exhibiting a contact angle of over 150° (Figure 2.23a). Although superhydrophobicity of the PFOTES-coated TiO_2 nanoparticle layers slightly degraded showing a contact angle of ~130° due to increased surface energy after exposure to air for one year, the PFOTES-coated TiO_2 nanoparticle layers still exhibited sufficient hydrophobicity to prevent water-based threats, which indicates good durability in ambient (Figure 2.23b).

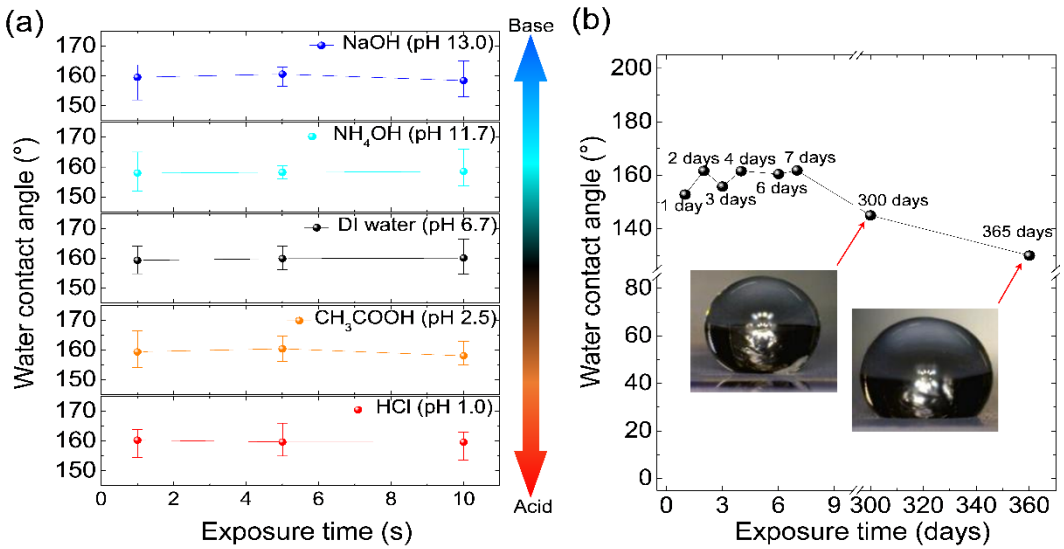

Figure 2.23 (a) Water contact angles of the superhydrophobic layer after exposure to HCl (pH 1.0), CH_3COOH (pH 2.5), DI water (pH 6.7), NH_4OH (pH 11.7), and NaOH (pH 13.0) droplets for 1, 5, and 10 s. (b) Water contact angles of the PFOTES-coated TiO_2 nanoparticle layers after exposure to air for 1 year.

To investigate the mechanical stability under lateral pressure, a commercially available rubber roller was used to apply shear pressure by friction between the roller and the prepared PFOTES-coated TiO_2 nanoparticle layers. While superhydrophobicity with a high water contact angle of > 150° was well-maintained during the 50-rollings with shear pressure of 1 kPa and a speed of 1 cm s^{-1}, a rolling with shearing force of 25 kPa resulted in a delamination of the prepared TiO_2 nanoparticle layers, so the superhydrophobicity was lost after 20-rollings with a reduction of the TiO_2 nanoparticle layer-thickness simultaneously (Figure 2.24a,b). As shown in Figure 2.24c, extremely rough surface was observed on the superhydrophobic PFOTES-coated TiO_2 nanoparticle layer before applying shearing force. However, the PFOTES-coated TiO_2 nanoparticle layers lost its superhydrophobicity partly as the surface was flatten during the rolling cycles (Figure 2.24d,e). In other words, shearing force makes a flatten surface, resulting in a water contact

angle < 90°. It should be noted that because the applied lateral pressure in my experiments is much larger than daily-life conditions, for example, wind pressure (<< 1 kPa) of which speed is distributed between 1 to 13 m s^{-1}, the mechanical stability of the PFOTES-coated TiO_2 nanoparticle layers is enough to be employed in the open air.[37-39] Moreover, during the rolling cycles, the PFOTES-coated TiO_2 nanoparticle layers was peeled-off due to friction force with the roller, which is also a critical reason to collapse the rough structure. Under vertical pressure from 10 N cm^{-2} to 50 N cm^{-2} (limitation of my facility), the PFOTES-coated TiO_2 nanoparticle layers well-maintained its superhydrophobicity, exhibiting an average water contact angle over 150° for up to 1000 s, because the surface roughness of the TiO_2 nanoparticle layers was still well-preserved without structure-collapsing, as shown in Figure 2.25.

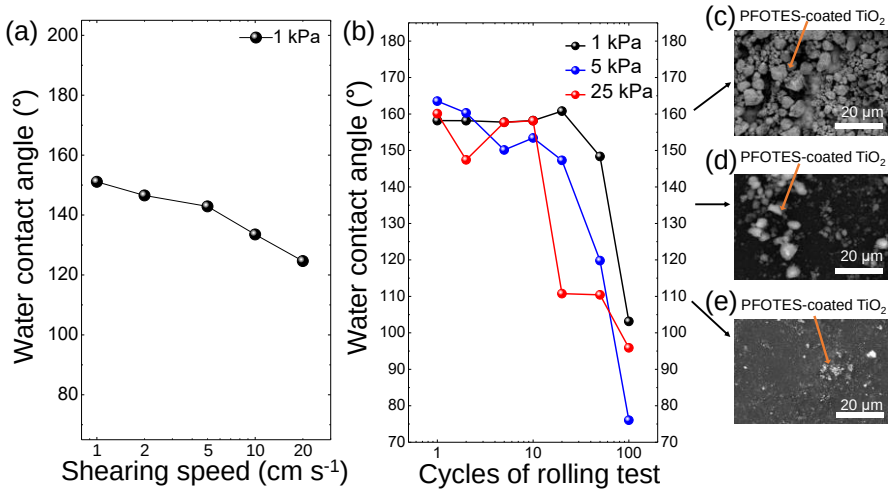

Figure 2.24 (a) Water contact angles of the PFOTES-coated TiO_2 nanoparticle layer after 20-times rolling with lateral pressure of 1 kPa depending on shearing speed. (b) Water contact angles of the layers after each rolling cycles with applying different lateral pressure 1, 5 and 25 kPa with shearing speed of 1 cm s^{-1}. (c-e) SEM images of (c) the layers before the rolling cycles, (d) the layers which lost its roughness partially showing a water contact angle ~135° after the rolling cycles, and (e) the layers which lost superhydrophobicity completely after the rolling over 100-cycles.

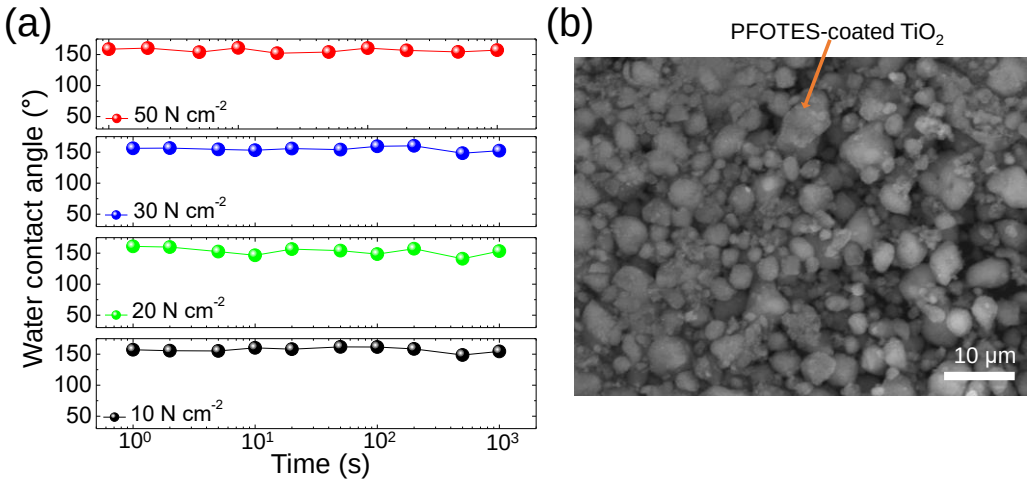

Figure 2.25 (a) Water contact angles of the superhydrophobic layer under vertical pressures for 1000 s. (b) SEM images of the PFOTES-coated TiO_2 nanoparticle layers after pressed at 50 N cm^{-2} for 1000 s.

I studied superhydrophobicity of the PFOTES-coated TiO_2 nanoparticle layers by measuring water contact angles on the surface under tensile stain (Figure 2.26). High water contact angles of the PFOTES-coated TiO_2 nanoparticle layers on polyethylene terephthalate (PET) substrates were well maintained at the bent condition under bending radius of 3 mm, 5 mm, and 10 mm (Figure 2.27a). Furthermore, high water contact angles were also maintained after 10,000 bending cycles (Figure 2.27b). In addition, when I applied the PFOTES-coated TiO_2 nanoparticle layers on a rubber based stretchable platform, the high water contact angles were observed even under 100 % stretched condition (Figure 2.27c).

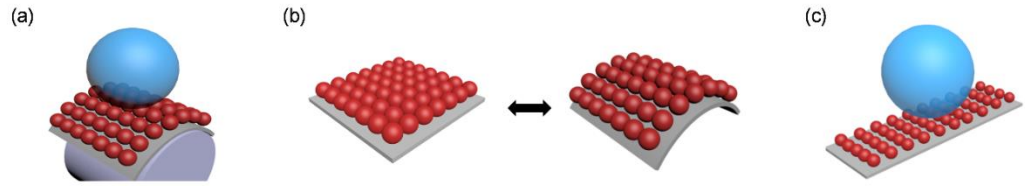

Figure 2.26 Contact angle measurements of PFOTES-coated TiO_2 nanoparticle layers under tensile strain: (a) under bent condition, (b) after bending cycles, and (c) at stretched conditions.

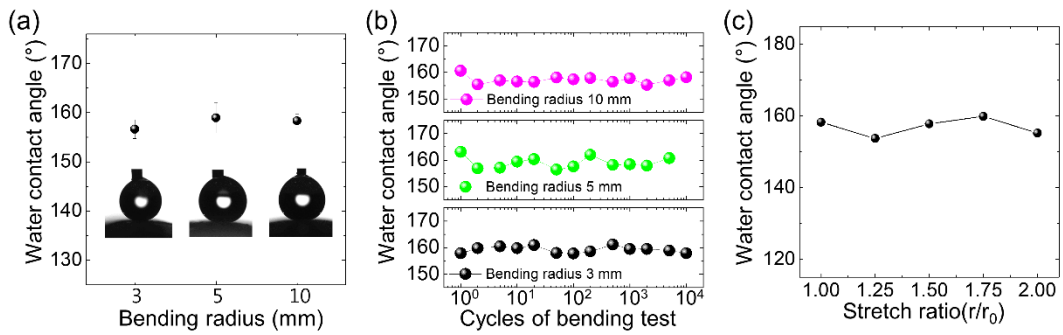

Figure 2.27 Water contact angles of PFOTES-coated TiO_2 nanoparticle layers (a) after each bending cycle, and while (b) bending and (c) stretching.

Even after exposure to tap water with pressure ~ 100 kPa for 100 s, the PFOTES-coated TiO_2 nanoparticle layers exhibited a stable superhydrophobicity (Figure 2.28). The dynamic pressure in this experiment was comparable to the dynamic pressure of rain droplets since the average speed of raindrops is between 0 and 14 m s^{-1}, corresponding to dynamic pressure up to 1 bar (= 100 kPa).[40,41]

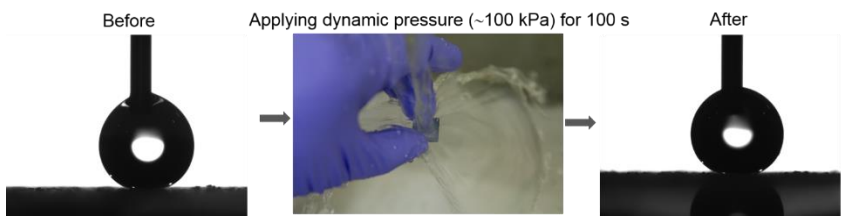

Figure 2.28 Before and after applying water-pressure, the superhydrophobic protection layer preserved its high water contact angle.

I performed an adhesion test with a piece of commercial Scotch tape over 15 times for the superhydrophobic protection layer on different organic semiconductors. The results showed that the PFOTES-coated TiO_2 nanoparticle layers exhibited good adhesion properties without delamination issues on various organic semiconductors, maintaining their superhydrophobicity with a contact angle over 150° in these durability tests (Figure 2.29).

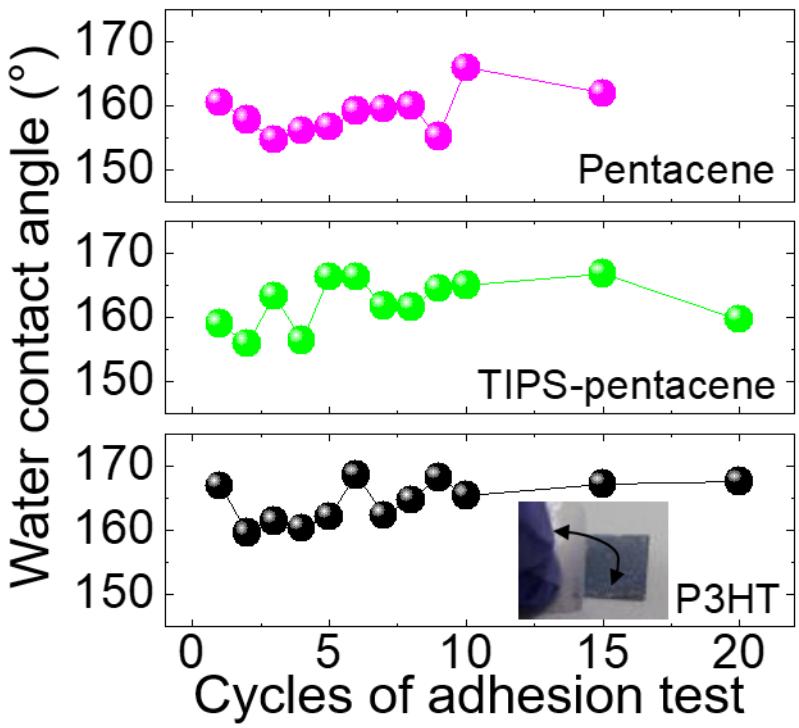

Figure 2.29 Water contact angles of the superhydrophobic layer on three organic semiconductors in the adhesion test using a commercial scotch tape.

I evaluated the thermal resistance on a 80 °C hot-plate for a day (Figure 2.30a). Furthermore, it was placed on a hot-plate up to 3 h. Regardless of underlying organic semiconductors (pentacene, TIPS-pentacene, and P3HT), its superhydrophobicity was maintained up to 200 °C (Figure 2.30b-e). The water contact angle on the PFOTES-coated TiO_2 nanoparticle layer on SiO_2 was drastically reduced after annealing over 200 °C for 3 h or 250 °C for 10 min which is closed to the reported temperature of PFOTES desorption.[42]

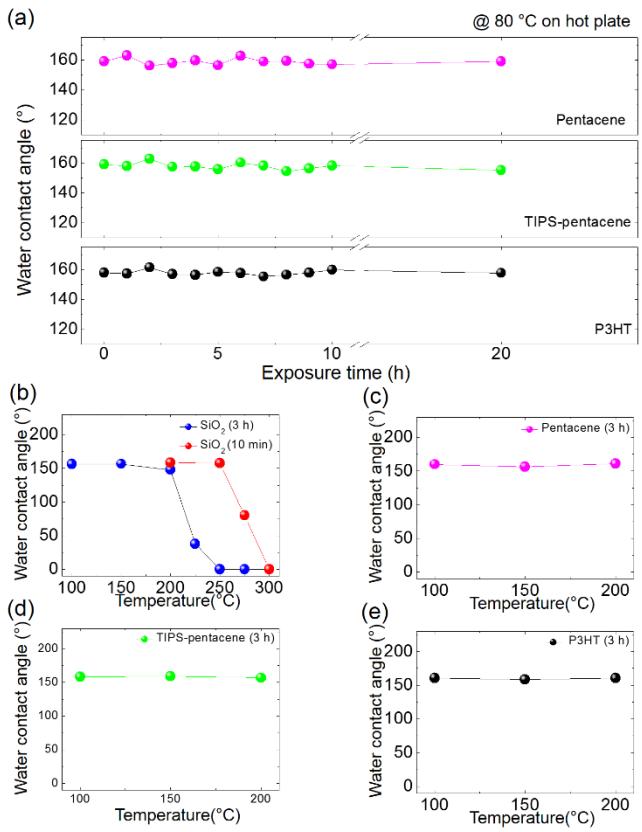

Figure 2.30 (a) Water contact angles of the superhydrophobic layer on three organic semiconductors (pentacene, TIPS-pentacene, P3HT) in thermal durability test at 80 °C on a hot-plate for 20 h. (b-e) Thermal durability test on a hot-plate in air for PFOTES-coated TiO_2 nanoparticle layer on (b) SiO_2, (c) pentacene, (d) TIPS-pentacene, and (e) P3HT.

Two ultraviolet (UV) lamps with a peak wavelength of 300 nm and 360 nm were used to investigate the changes of superhydrophobicity after exposure to UV light. The following results in Figure 2.31a and b indicated that the contact angle decreased after exposure to UV light with power of 3500 erg s^{-1} cm^{-2} corresponding to 0.35 mW cm^{-2} for 10^3 s. The degradation of the contact angle was delayed up to 10^5 s as UV lamp power was reduced (~100 erg s^{-1} cm^{-2} corresponding to 0.01 mW cm^{-2}). To investigate the stability of the PFOTES-coated TiO_2 nanoparticle layers under light-stress, they were exposed to visible light laser with 4×10^5 erg cm^{-2} s^{-1} with a spot size of 2 cm^2. As shown in Figure 2.32a and b, while they lost superhydrophobicity within 10^4 s (~3 h) and 2×10^5 s (~3 days) after intensively exposed to laser with a short-wavelength of 405 and 520 nm, respectively, superhydrophobicity was still well-maintained under light-stress with a long wavelength (658 nm and 780 nm in this study) for ~3 days, exhibiting a contact angle over 150°. In addition, the PFOTES-coated TiO_2 nanoparticle layer which lost superhydrophobicity after exposed to UV or visible light could have superhydrophobicity again by re-adhering PFOTES onto the surface of TiO_2 through a simple drop-casting of HFE-7500 containing PFOTES. This recovery-ability could be shown repeatedly (Figure 2.32c).

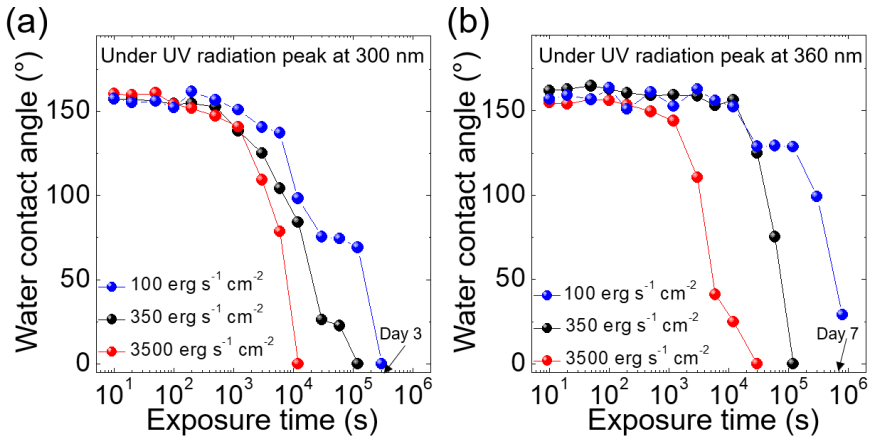

Figure 2.31 (a, b) Degradation of water contact angles under UV light exposure with a peak-wavelength of (a) 300 and (b) 360 nm for different light-power.

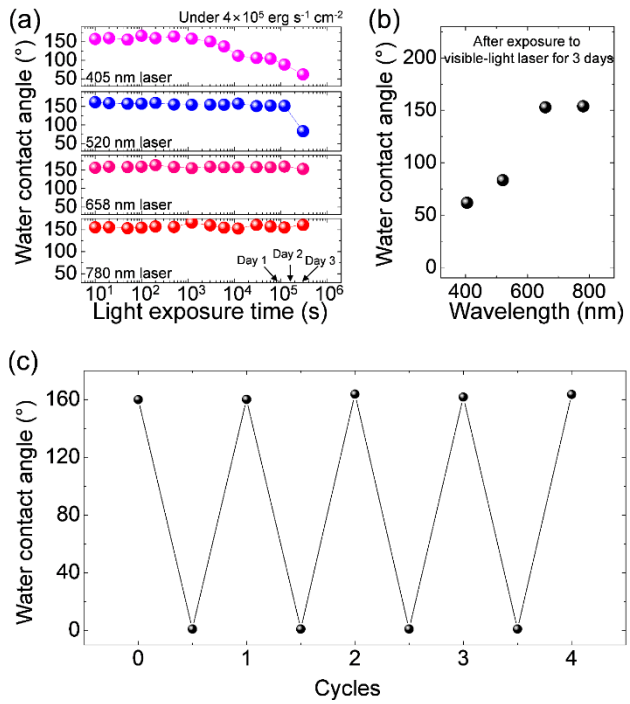

Figure 2.32 (a, b) Water contact angles of the superhydrophobic layer under light-stress using visible light laser with 405, 520, 658 and 720 nm-wavelength (a) for 3 days and (b) after 3 days. (c) Cycles of water contact angles of the PFOTES-coated TiO_2 nanoparticle layers after exposure to UV light (~0º) and re-adhering PFOTES (~160º).

2.3.4 Electrical characteristics of organic thin film transistors with and without superhydrophobic protection layers

I systematically performed to figure out that my superhydrophobic protection layers produced by the facile, organo-compatible and universal process could be a good alternative strategy to improve electrical reliability of OTFTs for water-based threats. I characterized the electrical characteristics of various OTFTs without and with PFOTES-coated TiO_2 nanoparticle protection layers before and after exposure to DI water (pH 6.7), HCl (pH 1.0), and NaOH (pH 13.0). Aforementioned, three representative organic semiconductors (evaporated pentacene, solution processed TIPS-pentacene, and P3HT) were chosen to demonstrate that the suggested superhydrophobic protection layer can be applied to a wide range of organic semiconductors, maintaining their electrical characteristics. The transfer (drain-source current *versus* gate voltage, I_{DS}–V_{GS}) characteristics were measured by sweeping V_{GS} from 40 to -60 V at a fixed drain-source voltage (V_{DS}) of -60 V (Figure 2.33a for pentacene OTFTs and Figure 2.34a,b for TIPS-pentacene and P3HT OTFTs), and the output (drain-source current *versus* drain-source voltage, I_{DS}–V_{DS}) was measured by sweeping V_{DS} from 0 to -60 V at different V_{GS} from 0 to -60 V with an increment of -10 V (Figure 2.32b-d for pentacene OTFTs, Figure 2.35 for TIPS-pentacene OTFTs and Figure 2.36 for P3HT OTFTs).

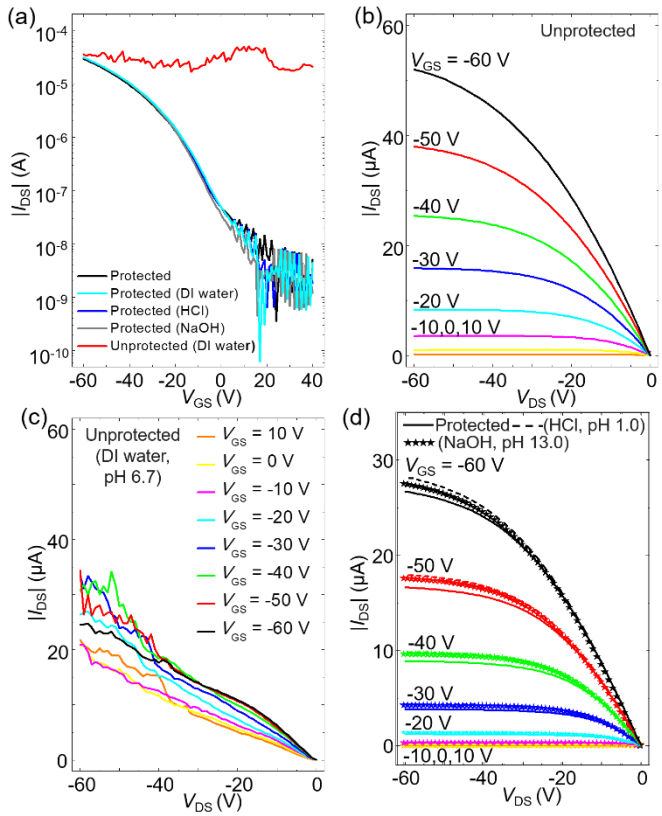

Figure 2.33 (a) Transfer curves on the semilogarithmic scale for an unprotected pentacene OTFT (i.e., without PFOTES-coated TiO_2 nanoparticle layers) after exposure to DI water and for a protected pentacene OTFT (i.e., coated with PFOTES-coated TiO_2 nanoparticle layers) before and after exposure to aqueous solutions of different pH ranging from 1 to 13. (b) Output curves for unprotected pentacene OTFTs before exposure to DI water. (c) Output curves for unprotected pentacene OTFTs after exposure to DI water. (d) Output curves of the protected pentacene OTFT with the PFOTES-coated TiO_2 nanoparticle layers before and after exposure to strong acid (HCl) and base (NaOH).

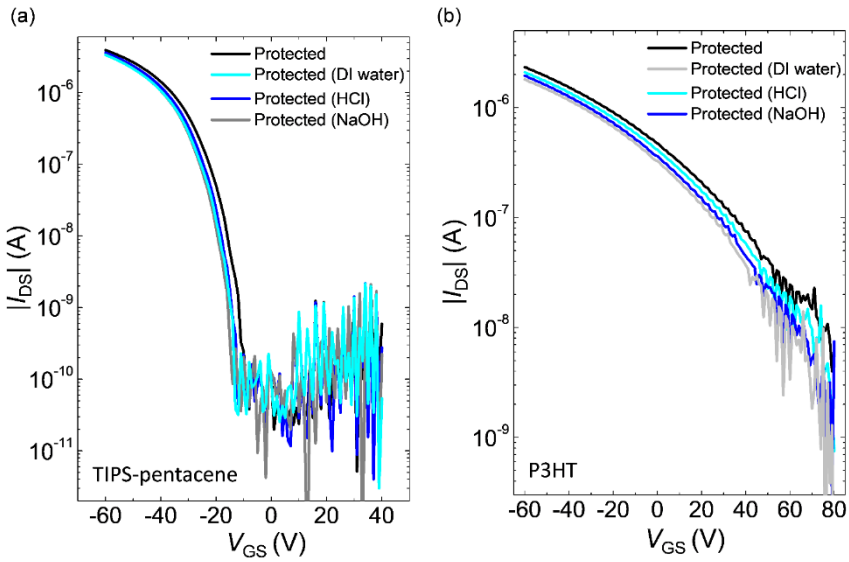

Figure 2.34 (a, b) Transfer curves on semilogarithmic scale for protected (a) TIPS-pentacene and (b) P3HT OTFTs (i.e., coated with the PFOTES-coated TiO_2 nanoparticle layers) before and after exposure to aqueous solutions of different pH for 10 s.

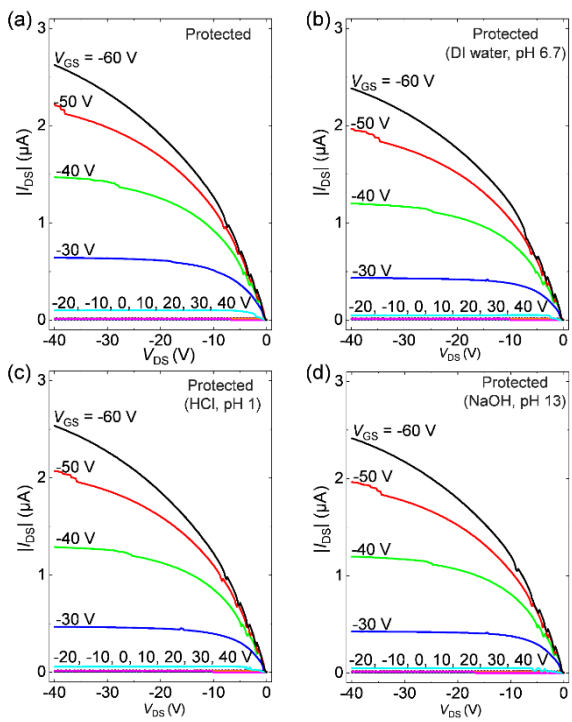

Figure 2.35 Output curves for TIPS-pentacene OTFTs protected by the PFOTES-coated TiO_2 nanoparticle layers before and after exposure to aqueous solutions of different pH for 10 s.

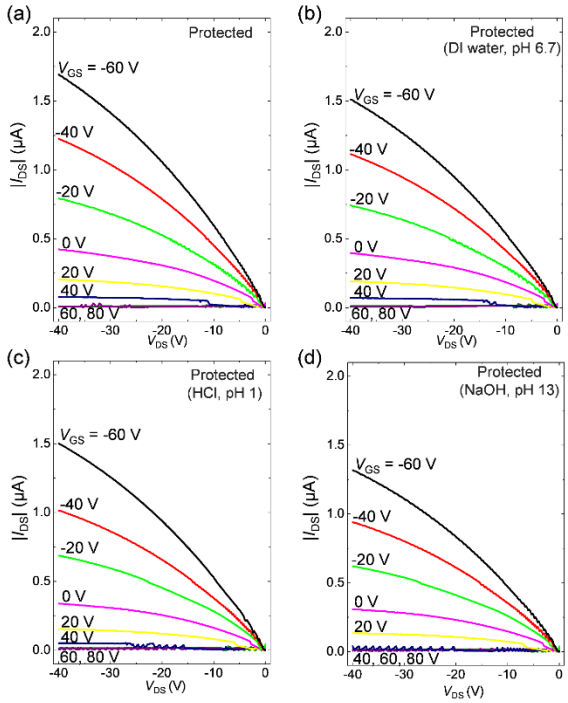

Figure 2.36. Output curves for the P3HT OTFTs protected by the PFOTES-coated TiO_2 nanoparticle layers before and after exposure to aqueous solutions of different pH for 10 s.

To induce ordered crystals of organic semiconductors, surface treatment using a fluorinated solution was conducted on the SiO_2 dielectric layer, which provides a sufficient hydrophobic surface with a water contact angle of 108° and thus the improved electrical performances were achieved (see Figure 2.37).[20] For more detailed process, the water contact angle of thermally grown 270 nm-thick SiO_2 was measured and found to be 78°, which indicates the hydrophilicity of the bare SiO_2 surface (Figure 2.37a).[43] A surface treatment using a fluorinated solution of PFOTES was conducted on the SiO_2 layer to provide a hydrophobic surface.[20] After UV-ozone treatment for 10 s to achieve better wetting properties for PFOTES on the SiO_2 layer, a PFOTES (0.5 g) solution in HFE-7200 (7 ml) was spin-coated with a spin speed of 500 rpm for 30 s. Then, it was annealed on a hot plate at 100 °C for 10 min. The PFOTES layer on SiO_2 produced a higher water contact

angle of 108° (Figure 2.37b), which helped to induce well-ordered pentacene crystals and thus improved the electrical performance of the pentacene OTFTs. The pentacene OTFTs without this surface treatment showed a mobility of ~0.1 $cm^2 V^{-1} s^{-1}$, which is comparable to the electrical characteristics in previously reported results.[44] However, the surface engineered pentacene OTFTs with the PFOTES exhibited a higher mobility of ~0.4 $cm^2 V^{-1} s^{-1}$.For the OTFTs without the superhydrophobic protection layer, the unprotected devices exhibited a high I_{DS} over 10^{-5} A over the entire range of gate biases when exposed to water (Figure 2.33a,c and Figure 2.38). Before exposure to water droplets, the unprotected pentacene OTFTs exhibited distinguished current levels depending on the gate bias of 10 V and -30 V. However, the current levels of the unprotected devices in the ON-state increased ten-fold regardless of the gate bias immediately after water droplets were dropped on the pentacene channel area because of ionic conduction through water (see Figure 2.38a). The protected pentacene OTFTs with the superhydrophobic layer maintained the ON- and OFF-current levels even when water droplets were dropped on the pentacene channel area because they rolled off the device due to the superhydrophobic protection layer (see Figure 2.38b). However, all of the protected OTFTs showed no significant degradation of the electrical characteristics including a good current ratio (I_{on}/I_{off}) and field effect mobility (μ_{FET}) even when they were exposed to various corrosive solutions (Figure 2.33a,d, Figure 2.38 and Table 2.2). Furthermore, additional experiment was performed to prove that the device stability after exposure to water in much more harsh conditions (tap water with dynamic pressure of 50 kPa for 1000 s). Even after long-term water exposure, the transfer curves were not significantly shifted or degraded, with maintaining the mobility and ON/OFF ratio, as shown in Figure 2.39 and Table 2.3. Therefore, the PFOTES-coated TiO_2

nanoparticle layers can be a good protection layer against water-based threats, even with dynamic pressure.

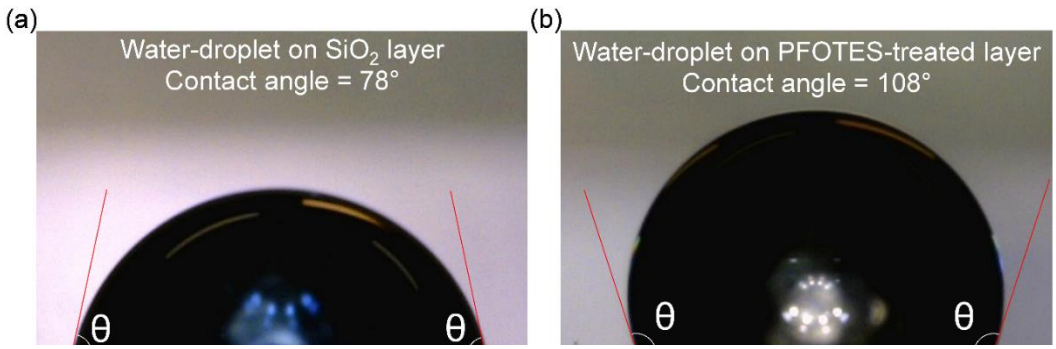

Figure 2.37 (a, b) Water contact angle of (a) SiO_2 surface and (b) PFOTES-treated SiO_2 layer.

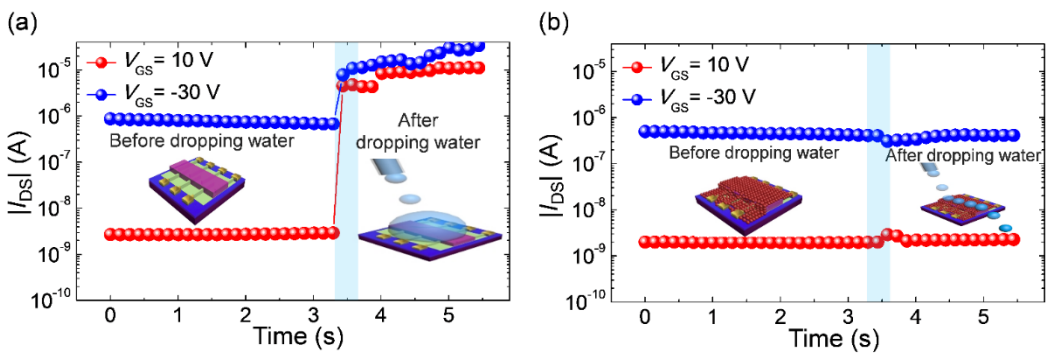

Figure 2.38 (a, b) Current–time graph for an (a) unprotected and (b) protected pentacene OTFT before and after exposure to water droplets.

Organic semiconductor	Condition	Field effect mobility ($cm^2 V^{-1} s^{-1}$)	|ΔThreshold voltage (V)|†	ON/OFF ratio
Pentacene	As deposited*	0.41 ± 0.07	0.0 ± 1.4	~10^4
	After exposure to DI water (pH 6.7)	0.41 ± 0.08	1.8 ± 1.2	~10^4
	After exposure to HCl (pH 1.0)	0.41 ± 0.07	2.1 ± 1.6	~10^4
	After exposure to NaOH (pH 13.0)	0.40 ± 0.07	2.9 ± 3.6	~10^4
TIPS-pentacene	As deposited*	0.23 ± 0.03	0.0 ± 1.3	~10^4
	After exposure to DI water (pH 6.7)	0.21 ± 0.03	2.7 ± 1.0	~10^4
	After exposure to HCl (pH 1.0)	0.22 ± 0.03	2.3 ± 1.6	~10^4
	After exposure to NaOH (pH 13.0)	0.20 ± 0.04	3.4 ± 0.8	~10^4
P3HT	As deposited*	0.016 ± 0.004	0.0 ± 1.5	~10^3
	After exposure to DI water (pH 6.7)	0.017 ± 0.002	0.6 ± 1.9	~10^3
	After exposure to HCl (pH 1.0)	0.015 ± 0.003	2.6 ± 2.3	~10^3
	After exposure to NaOH (pH 13.0)	0.014 ± 0.003	0.6 ± 2.6	~10^3

Table 2.2. Summary of the electrical parameters of protected OTFTs before and after exposure to various liquids of different pH.

*'As deposited' condition means that the electrical parameters were characterized as soon as the superhydrophobic protection layers were deposited on OTFTs.

†'ΔThreshold voltage' means that the threshold voltage difference after exposure to liquid-based substances compared to that measured at the 'As deposited' condition.

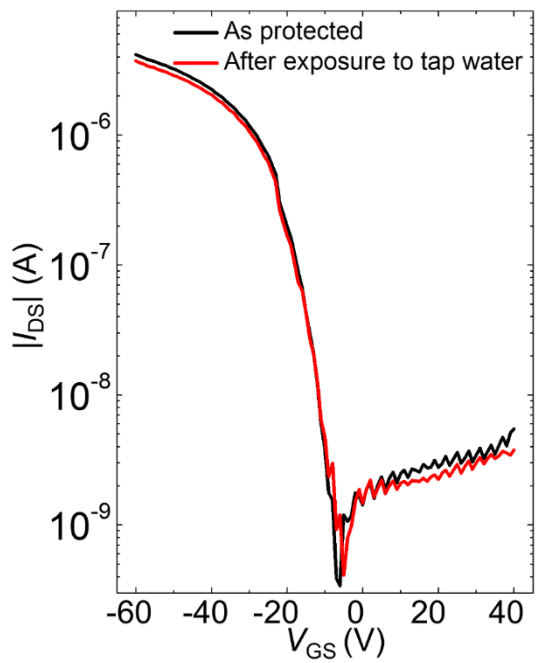

Figure 2.39. Transfer curves in the semilogarithmic scale for a protected TIPS-pentacene OTFT. The data curve in black and red were measured for the protected OTFT before and after exposure to tap water for 1000 s, respectively.

Exposure to tap water	Mobility ($cm^2 V^{-1} s^{-1}$)	Threshold voltage (V)
Before	0.24	-7.8
After	0.23	-8.3

Table 2.2. Electrical parameters of the protected OTFTs before and after exposure to tap water.

Also, I examined the contact properties between the source-drain electrodes and the pentacene semiconductor in a pentacene OTFT protected with a superhydrophobic protection layer. Figure 2.40 shows the I_{DS}–V_{DS} relationship on the log-log scale. Assuming $I_{DS} \propto V_{DS}^{\gamma}$, the determined γ values close to 1 indicate that the output characteristics of the protected pentacene OTFT showed good linearity in the low V_{DS} regime (i.e., good electrical contact to pentacene) after exposure to liquid-based hindrances.

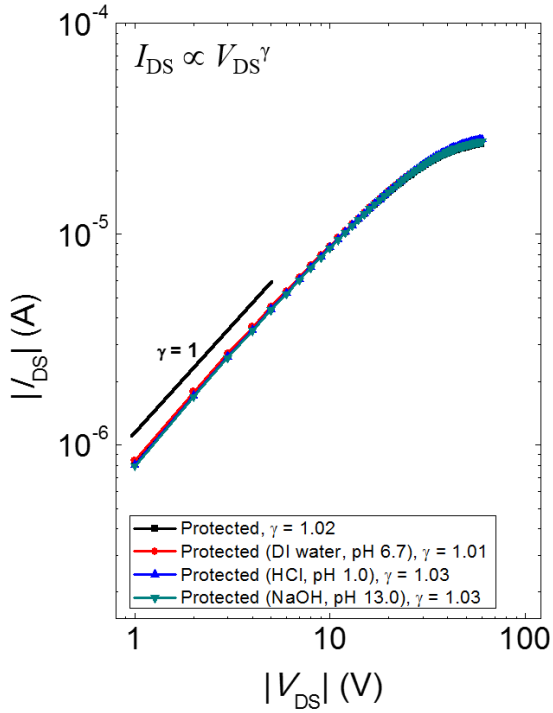

Figure 2.40 Log-log plot of I_{DS}–V_{DS} characteristics with V_{DS} ranging from 1 to 60 V.

Furthermore, I performed the stability test measuring the electrical characteristics of the protected OTFTs after storing them in a chamber with high humidity (@ 75% relative humidity (RH), 20 °C). The threshold voltages (V_{TH}) of the unprotected OTFTs evidently shifted over 5 V on average toward the positive gate voltage direction as soon as they were exposed to high humidity, unlike the behavior of the protected ones showing no notable degradations. The reason for the V_{TH} shift was known for the water adsorption on organic semiconductors (Figure 2.41, 2.42 and Table 2.4).[45-47] For example, the transfer characteristics of the pentacene OTFTs shifted drastically to the positive gate voltage direction while maintaining the field-effect mobility as exposed to ambient, which is consistent with my results.[48] The V_{TH} of the unprotected OTFTs significantly shifted to the positive gate voltage direction for a day unlike the V_{TH} of the protected OTFTs. During

long period (1 day to 20 days), there was also the noticeable V_{TH} change of the protected devices, but it was much smaller (by ~50%) than that of unprotected ones (Figure 2.42 and Table 2.4). Note that if the OTFTs were exposed to high-humid air (@ 75% relative humidity (RH), 20 °C) over three weeks, both of the OTFTs exhibited the noticeable V_{TH} shift. Because of the water-molecules adsorption into the organic semiconductors, the representative extracted V_{TH} of the unprotected TIPS-pentacene OTFT shifted to the positive gate voltage direction after storing them under the prepared high humidity conditions. While V_{TH} of the unprotected OTFT greatly shifted over 10 V for 1 day, those of the protected ones shifted only less than 4 V (Figure 2.42 and Table 2.4).

To investigate the reversibility of water molecules adsorption on organic semiconductors, TIPS-pentacene OTFTs were exposed to humid condition (@ ~ 75% RH, 20 °C) for 2 days, then their transfer curves were observed to be largely shifted to positive gate voltage direction as shown in Figure 2.43 (gray to black curves). Then, the degraded devices were stored in a dry environment under vacuum at ~1 torr for two days. The transfer curves after being stored in vacuum were gradually recovered in the negative gate voltage direction as shown in Figure 2.43 (green to red curves), which indicates that the shifted threshold voltages due to the water molecules adsorption on organic semiconductors could be somewhat recovered through a dry condition under vacuum.

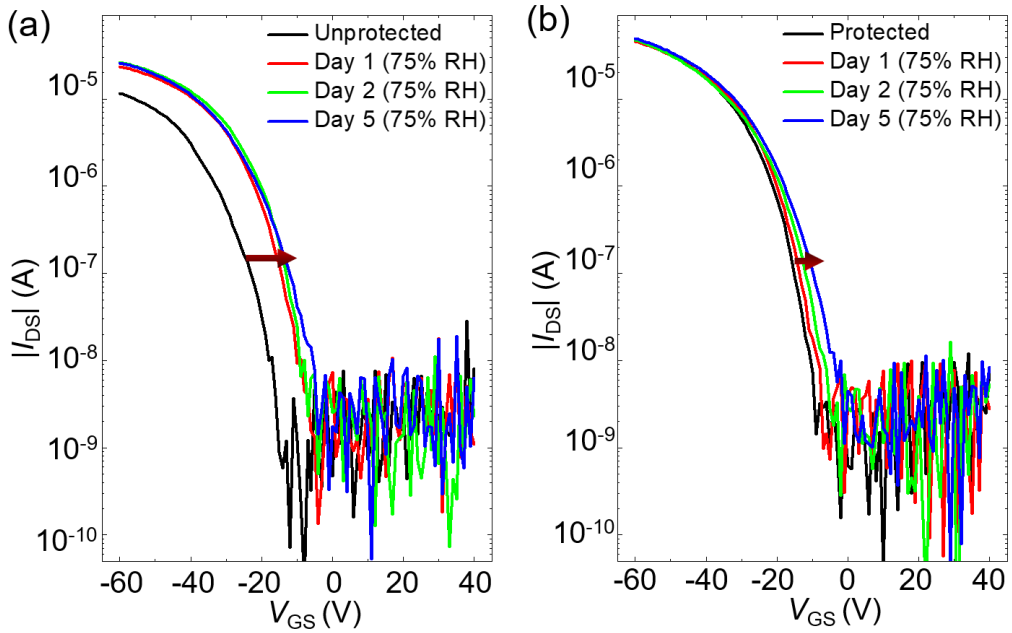

Figure 2.41 (a, b) Transfer curves on the semilogarithmic scale for the (a) unprotected and (b) protected TIPS-pentacene OTFTs after exposure to water vapor (75% relative humidity, 20 °C).

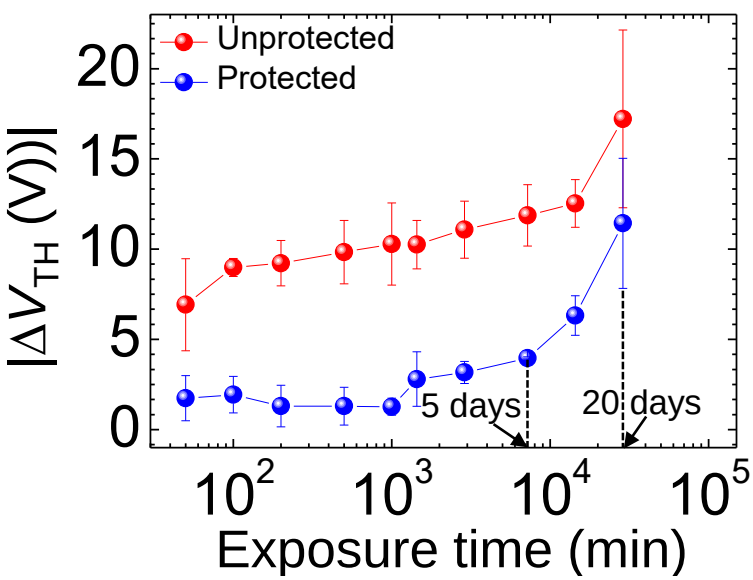

Figure 2.42 Threshold voltage (V_{TH}) shift of protected and unprotected OTFTs in the semilogarithmic scale for 20 days. Error bars were obtained from measurements of several devices.

Time	|ΔField effect mobility ($cm^2 V^{-1} s^{-1}$) |*		|ΔThreshold voltage (V)|†		ON/OFF ratio	
	Unprotected	protected	Unprotected	protected	Unprotected	protected
0 min	0	0	0	0	~10^4	~10^4
20 min	0.01	0.01	5.40	1.23	~10^4	~10^4
50 min	0.01	0.02	6.92	1.73	~10^4	~10^4
100 min	0.02	0.01	8.99	1.93	~10^4	~10^4
200 min	0.02	0.03	9.22	1.30	~10^4	~10^4
500 min	0.02	0.03	9.83	1.30	~10^4	~10^4
1000 min	0.03	0.04	10.3	1.27	~10^4	~10^4
1 day	0.02	0.02	10.3	2.80	~10^4	~10^4
2 day	0.05	0.04	11.1	3.12	~10^4	~10^4
5 day	0.06	0.03	11.9	3.97	~10^4	~10^4
10 day	0.07	0.02	12.5	6.32	~10^4	~10^4
20 day	0.07	0.02	17.2	11.4	~10^4	~10^4

Table 2.4. Extracted electrical parameters in average values of the protected and unprotected OTFTs before and after exposure to humid air (75% RH). *'Δ Field effect mobility ($cm^2 V^{-1} s^{-1}$)' indicates that the mobility difference after exposure to humid air (75% RH). The average initial mobility of unprotected and protected OTFTs were 0.13 $cm^2 V^{-1} s^{-1}$ and 0.29 $cm^2 V^{-1} s^{-1}$, respectively.

†'Δ Threshold voltage' indicates that the threshold voltage difference after exposure to humid air (75% RH), The average initial threshold voltage of unprotected and protected OTFTs were -18.4 V and -15.8 V, respectively.

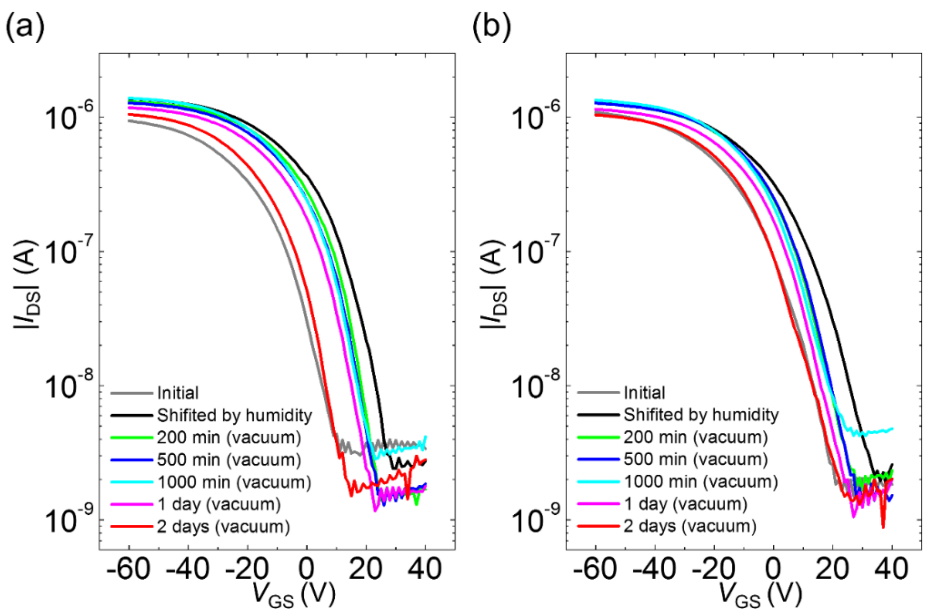

Figure 2.43. Transfer curves on the semilogarithmic scale for two TIPS-pentacene OTFTs before and after exposed to water vapor for two days in 75% RH and transfer curves of the exposed OTFTs storing in vacuum conditions (~1 torr) during two days.

To analyze the protection-ability of the PFOTES-coated TiO_2 nanoparticle layers against water-molecules quantitatively, WVTR of the PFOTES-coated TiO_2 nanoparticle layers was also characterized. Because the PFOTES-coated TiO_2 nanoparticle layers could not be suspended itself, they were deposited between two PET films which were employed as a supporting substrate in a sandwich structure. The test was performed under ASTM-F-1249 condition (RH 90%, temperature 37.8 ˚C). While the reference film, *i.e.*, the stacked PET films without the PFOTES-coated TiO_2 nanoparticle layers, had a WVTR value of 0.391 g m^{-2} day^{-1}, the prepared PET films with the PFOTES-coated TiO_2 nanoparticle layers exhibited a 20% lower WVTR value of 0.316 g m^{-2} day^{-1}. Note that the WVTR value of PFOTES-coated TiO_2 nanoparticle layers was calculated by laminate theory[49,50]

$$\frac{1}{W_{Total}} = \frac{1}{W_{PET}} + \frac{1}{W_{TiO_2}}$$

where $W_{Total,}$ W_{PET}, and W_{TiO2}, denote that the WVTR value of PET/PFOTES-coated TiO_2 nanoparticle layers/PET, the WVTR value of two PET films stacked without the PFOTES-coated TiO_2 nanoparticle layers, and the WVTR value of the PFOTES-coated TiO_2 nanoparticle layers itself, respectively. From the calculation, the estimated WVTR value of the PFOTES-coated TiO_2 nanoparticles layers was found as ~1.61 g m^{-2} day^{-1}. The extracted value was comparable to that of μm-thick plastic films having a WVTR value of ~1 g m^{-2} day^{-1} which can be used for an antimicrobial plastic-packaging or parenteral-solutions encapsulation[51-54] Although the proposed PFOTES-coated TiO_2 nanoparticle layers shows insufficient performance to encapsulate organic devices perfectly, the tightly packed nanoparticle film can impede the degradation of organic semiconductors caused by water-molecules adsorption.

2.4. Conclusion

In this study, the functionalized TiO_2 nanoparticle-based superhydrophobic protection layer was utilized to realize reliable OTFTs. Because of the roughened surface and low surface energy of the protection layer, excellent water repellency and self-cleaning abilities were achieved, which could preserve the electrical characteristics of enviromentally sensitive organic semiconducotrs. The suggested superhydrophobic protection layers were applied onto various organic semiconductors directly by a facile dipping process, exhibiting good resistances against mechanical-, thermal-, and light-stress and chemical-threats. In addition, they allowed more reliable electrical characteristics of OTFTs in ambient, even exposed to strong solvents due to its superhydrophobicity. This approach can be a good alternative solution to protect low-cost and flexible organic electronics working in the opened air.

References

[1] Forrest, S. R. *Nature* **2004**, *428***,** 911-918.

[2] Sekitani, T.; Yokota, T.; Zschieschang, U.; Klauk, H.; Bauer, S.; Takeuchi, K.; Takamiya, M.; Sakurai, T.; Someya, T *Science* **2009,** *326*, 1516-1519.

[3] Song, Y.; Jeong, H.; Jang, J.; Kim, T.-Y; Yoo, D.; Kim, Y.; Jeong, H.; Lee, T. *ACS Nano*, **2015**, *9*, 7697–7703.

[4] Zhou, Y.; Fuentes-Hernandez, C.; Shim, J.; Meyer, J.; Giordano, A. J.; Li, H.; Winget, P.; Papadopoulos, T.; Cheun, H.; Kim, J.; Fenoll, M.; Dindar, A.; Haske, W.; Najafabadi, E.; Khan, T. M.; Sojoudi, H.; Barlow, S.; Graham, S.; Brédas, J. -L ; Marder, S. R. *et al. Science* **2012**, *336*, 327–332.

[5] Sirringhaus, H. *Adv. Mater.* **2014**, *26*, 1319-1335.

[6] Klauk, H.; Zschieschang, U.; Pflaum, J.; Halik, M. *Nature* **2007**, *445*, 745-748.

[7] Diao, Y.; Tee, B. C-K.; Giri, G.; Xu, J.; Kim, D. H.; Becerril, H. A.; Stoltenberg, R. M.; Lee, T. H.; Xue, G.; Mannsfeld, S. C. B.; Bao, Z. *Nat. Mater.* **2013**, *12*, 665-671.

[8] Baeg, K. J.; Caironi, M.; Noh, Y. Y. *Adv. Mater.* **2013**, *25*, 4210-4244.

[9] Kang, H.; Kitsomboonloha, R.; Jang, J.; Subramanian, V. *Adv. Mater.* **2012,** *24*, 3065-3069.

[10] Chung, S.; Jang, M.; Ji, S. B.; Im, H.; Seong, N.; Ha, J.; Kwon, S.-K.; Kim, Y.-H.; Yang, H.; Hong, Y. *Adv. Mater.* **2013**, *25*, 4773-4777.

[11] Sonar, P.; Singh, S. P.; Li, Y.; Soh, M. S.; Dodabalapur, A. *Adv. Mater.* **2010**, *22*, 5409-5413.

[12] Sirringhaus, H. *Adv. Mater*. **2009**, *21*, 3859-3873.

[13] Kaltenbrunner, M.; Sekitani, T.; Reeder, J.; Yokota, T.; Kuribara, K.; Tokuhara, T.; Drack, M.; Schwödiauer, R.; Graz, I.; Baier-Gogonea, S.; Bauer, S.; Someya, T. *Nature* **2013**, *499***,** 458-463.

[14] McCulloch, I.; Heeney, M.; Bailey, C.; Genevicius, K.; MacDonald, I.; Shkunov, M.; Sparrowe, D.; Tierney, S.; Wagner, R.; Zhang, W.; Chabinyc, M. L.; Kline, R. J.; McGehee, M. D.; Toney M. F. *Nat. Mater*. **2006**, *5*, 328-333.

[15] Knopfmacher, O.; Hammock, M. L.; Appleton, A. L.; Schwartz, G.; Mei, J.; Lei, T.; Pei, J.; Bao, Z. *Nat. Commun.* **2014**, *5*, 2954.

[16] Jinno, H.; Fukuda, K.; Xu, X.; Park, S.; Suzuki, Y.; Koizumi, M.; Yokota, T.; Osaka, I.; Takimiya, K.; Someya, T. *Nat. Energy* **2017**, *2*, 780-785.

[17] Simon, D. T.; Kurup, S.; Larsson, K. C.; Hori, R.; Tybrandt, K.; Goiny, M.; Jager, E. W. H.; Berggren, M.; Canlon, B.; Richter-Dahlfors, A. *Nat. Mater.* **2009**, *8*, 742–746.

[18] Sandström, A.; Dam, H.; Krebs, F.; Edman, L. *Nat. Commun.* **2012**, *3*, 1002.

[19] Deng, X.; Mammen, L.; Zhao, Y.; Lellig, P.; Müllen, K.; Li, C.; Butt, H. -J.; Vollmer, D. *Adv. Mater.* **2011**, *23*, 2962-2965.

[20] Kim, S. H.; Jang, M.; Yang, H.; Anthony, J. E.; Park, C. E. *Adv. Funct. Mater.* **2011**, *21*, 2198-2207.

[21] Lu, Y.; Sathasivam, S.; Song, J.; Crick, C. R.; Carmalt, C. J.; Parkin I. P. *Science* **2015**, *347*, 1132-1135.

[22] Lai, Y.; Tang, Y.; Gong, J.; Gong, D.; Chi, L.; Linc, C.; Chen, Z. *J. Mater.Chem.* **2012**, *22*, 7420-7426.

[23] A. A. Zakhidov, J.-K. Lee, H. H. Fong, J. A. DeFranco, M. Chatzichristidi, P.G. Taylor, C. K. Ober, G. G. Malliaras, *Adv. Mater.* **2008**, *20*, 3481.

[24] Wang, C.-Y.; Groenzin, H.; Shultz, M. J. *Langmuir* **2003**, *19*, 7330-7334.

[25] Nishino, T.; Meguro, M.; Nakamae, K.; Matsushita, M.; Ueda, Y. *Langmuir* **1999**, *15*, 4321-4323.

[26] Phenrat, T.; Saleh, N.; Sirk, K.; Tilton, R. D.; Lowry, G. V. *Environ. Sci. Technol.* **2007**, *41*, 284-290.

[27] Feng, L.; Li, S.; Li, Y.; Li, H.; Zhang, L.; Zhai, J.; Song, Y.; Liu, B.; Jiang, L.;
Zhu, D. Adv. Mater. 2002, 14, 1857-1860.

[28] Bonn, D.; Eggers, J.; Indekeu, J.; Meunier, J.; Rolley, E. *Rev. Mod. Phys.* **2009**, *81*, 739.

[27] Vazquez, G.; Alvarez, E.; Navaza, J. M. *J. Chem. Eng. Data* **1995**, *40*, 611-614.

[28] Lafuma, A.; Quéré, D. *Nat. Mater.* **2003**, *2*, 457-460.

[29] Wang, S.; Jiang, L *Adv. Mater.* **2007**, *19*, 3423–3424.

[30] Rioboo, R.; Voué, M.; Vaillant, A.; De Coninck, J. *Langmuir* **2008**, *24*, 14074-14077.

[31] Liu, Y.; Moevius, L.; Xu, X.; Qian, T.; Yeomans, J. M.; Wang, Z. Pancake bouncing on superhydrophobic surfaces. *Nat. phys.* **2014**, *10*, 515-519.

[32] Song, Z.; Hrbek, J.; Osgood, R. *Nano. Lett.* **2005**, *5*, 1327-1332.

[33] Zhang, X.; Jiang, H.; Jin, J.; Xu, X.; Zhang, Q. *Atmos. Environ.* **2012**, *46*, 590-596.

[34] Shoenut, J. P.; Duerksen, D.; Yaffe, C. S. *Dig. Dis. Sci.* **1998**, *43*, 834-839.

[35] Moreira, K. A.; Albuquerque, B. F.; Teixeira, M. F. S.; Porto, A. L. F.; Lima Filho, J. L. *World J. Microbiol. Biotechnol*. **2002**, *18*, 309-315.

[36] Ananthapadmanabhan, K. P.; Moore, D. J.; Subramanyan, K.; Misra, M.; Meyer, F. *Dermatol. Ther*. **2004**, *17*, 16-25.

[37] Tar, K. *Renew and Sustain Energy Rev.* **2008***, 12*, 1712-1724.

[38] Safari, B.; Gasore, J. A. *Renew Energy* **2010**, *35*, 2874-2880.

[39] Kramer, C.; Gerhardt, H. J.; Scherer, S. *Journal of Wind Engineering and Industrial Aerodynamics* **1979**, *4*, 229-242.

[40] Hauser, D.; Amayenc, P.; Nutten, B.; Waldteufel, P. *J. Atmos. Oceanic Technol.* **1984**, *1*, 256-269.

[41] van Boxel, J. H. *I.C.E. Special Report* **1998**, *1*, 77-85.

[42] Nørgaard, A. W.; Jensen, K. A.; Janfelt, C.; Lauritsen, F. R.; Clausen, P. A.; Wolkoff, P. *Environ. Sci. Technol.* **2009**, *43*, 7824-7830.

[43] Ganesh, V. A.; Raut, H. K.; Nair, A. S.; Ramakrishna, S. *J. Mater. Chem.* **2011**, *21*, 16304–16322.

[44] Jang, J.; Song, Y.; Oh, H.; Yoo, D.; Kim, D.; Lee, H.; Hong, S.; Lee, J.-K.; Lee, T. *Appl. Phys. Lett.* **2014**, *104*, 053301.

[45] Park, S. K.; Mourey, D. A.; Han, J.-I.; Anthony, J. E.; Jackson, T. N. *Org. Electron.* **2009**, *10*, 486-490.

[46] Li, D.; Borkent, E. J.; Nortrup, R.; Moon, H.; Katz, H.; Bao, Z. *Appl. Phys. Lett.* **2005**, *86*, 042105.

[47] Bobbert, P. A.; Sharma, A.; Mathijssen, S. G.; Kemerink, M.; de Leeuw, D. M. *Adv. Mater*. **2012**, *24*, 1146-1158.

[48] Kumaki, D.; Umeda, T.; Tokito, S. *Appl. Phys. Lett*. **2008**, *92*, 093309.

[49] Henry, B. M.; Erlat, A. G.; McGuigan, A.; Grovenor, C. R. M.; Briggs, G. A. D.; Tsukahara, Y.; Miyamoto, T.; Noguchi, N.; Niijima, T. *Thin Solid Films* **2001**, *382***,** 194-201.

[50] Graff, G. L.; Williford, R. E.; Burrows, P. E. *J. Appl. Phys.* **2004**, 96, 1840-1849. Sung, S. Y.;

[51] Sin, L. T.; Tee, T. T.; Bee, S. T.; Rahmat, A. R.; Rahman, W. A. *Food Control* **2014**, *39*, 214-221.

[52] Nakatsuka, S.; Andrady, A. *J. Environ. Polym. Degrad.* **1994**, *2*, 161-167.

[53] Wood, R. W.; Mulski, M. J *Inter. J. Pharm.* **1989**, *50*, 61-66.

[54] Hirvikorpi, T.; Laine, R.; Vähä-Nissi, M.; Kilpi, V.; Salo, E.; Li, W. M.; Lindfors, S.; Vartianen, J.; Kenttä, E.; Nikkola, J.; Harlin, A.; Kostamo J. *Thin Solid Films* **2014**, *550*, 164-169.

Chapter 3. Transparent superhydrophobic layer for organic phototransistors

In this chapter, I discussed improving the reliability of organic phototransistors against water by providing extreme water repellency through transparent superhydrophobic nanoparticle layers. A transparency and water contact angles of the transparent nanoparticle layers were analyzed, and how the surface morphologies influenced these characteristics were discussed. I also verified how my superhydrophobic layer could maintain high water contact angles against physical stresses like light, thermal and mechanical stresses. Finally, it was shown that the transparent superhydrophobic layer provided self-cleaning abilities without degrading the optoelectronic properties of the organic phototransistor. Thus, the study investigated that the nanoparticle layer has water repellency and transparency when it has a certain surface morphology, while further improving the reliability of the organic optoelectronic devices.

3.1. Introduction

For the last decades, organic electronic materials have paved a promising route for realizing large-area flexible applications using low-cost solution processing.[1-6] Specifically, their improved environmental-stability have shown possibilities that organic electronics can be utilized in practical applications in the open air beyond controlled laboratory conditions.[7-10] To achieve better reliability in a perspective of devices, one of the key challenges is to integrate effective protection layers against external threats in daily conditions. In this thread, introducing superhydrophobic layers having a water contact angle over 150 ° onto organic electronics have regarded as an attractive solution because excellent water-repellency can remove harmful dusts or water-based treats efficiently from the self-cleaning ability.[7,11-14] Recently, organo-compatible superhydrophobic

protection layers have been reported that can improve the environmental stability of organic thin film transistors (OTFTs).[7] However, the previously reported opaque layers having a thickness over 10 μm can be a critical hurdle to be utilized in thin film optoelectronic applications. As a solution to provide transparency to the protection layers, the optimization of their thickness and surface roughness is a most facile methodology that allow the enhanced transmittance via reduced light scattering.[13,15] Specifically, because the high surface roughness is a key parameter for maintaining the superhydrophobicity, the investigation on the optimized conditions for realizing transparent superhydrophobic layers is highly desirable as well as preserving organo-compatibility. In addition, environmental stabilities of superhydrophobic layers under mechanical deformation, thermal stress, and light-exposure are necessary to be integrated onto practical applications.

Here, I report transparent superhydrophobic layers for organic optoelectronic devices by employing organo-compatible solution processing. Functionalized titanium dioxide (TiO2) nanoparticles with fluorinated silane dispersed in a highly fluorinated solvent were directly spin-coated onto organic phototransistors without any additional pre-treatments. Their surface roughness was modulated to suppress Rayleigh and Mie scattering by the organo-compatible rinsing process.[13,15] By reducing the nanoparticle size and surface roughness below 100 nm, the prepared TiO_2 nanoparticle layers exhibited high transmittance over 75 % in visible wavelength range (> 400 nm) preserving the superhydrophobicity that provide the excellent self-cleaning ability.[13,15] In addition, my rough nanoparticle surfaces could repel various liquid with a lower surface tension than water and a water droplet having a volume less than 1 μL, demonstrating excellent liquid-repellency by facile and organo-compatible process. Furthermore, the much thinner superhydrophobic layers promises outstanding mechanical flexibility, even reliable

behaviors under stretched conditions. Their superhydrophobicity was well maintained not only under temperature-acceleration tests until the decomposition temperature of the attached fluorinated alkyl silane molecules, but under exposure to high intensity laser for 3 days. Finally, I fabricated 6,13-Bis(triisopropylsilylethynyl) pentacene (TIPS-pentacene) based organic phototransistors with the transparent superhydrophobic layers. Both TIPS-pentacene phototransistor with and without the transparent self-cleaning layers exhibited similar optoelectronic properties while transparent superhydrophobic protective layers could provide enhanced environmental reliabilities to the underlying phototransistor against water droplets and dusts in daily conditions. This work can provide a key pathway to implement a transparent superhydrophobic layers for further reliable organic optoelectronic devices.

3.2. Experiments

3.2.1. Device fabrication process

For preparing TIPS-pentacene phototransistors, Indium tin oxide (ITO)-coated PET (Sigma Aldrich) was sequentially cleaned with acetone, isopropanol and deionized water for 10 min, respectively. Next, the cleaned ITO-coated PET substrates were exposed to ultraviolet ozone cleaner for 5 min, which enhanced film uniformity. A solution containing 20 wt % poly(4-vinylphenol) (PVP, Mw = 25 000 g mol^{-1}, Sigma Aldrich) and 5 wt % (PMF, number-average molecular weight (Mn) ~ 432 g mol^{-1}, Sigma-Aldrich) dissolved in propylene glycol methyl ether acetate (PGMEA) was spin-coated onto the cleaned ITO for the formation of gate dielectric with 500 rpm rate for 5 s and 2000 rpm for 40 s. Then, it was annealed at 100 °C for 10 min and at 210 °C for 10 min, sequentially. Ti (5 nm)/Au (60 nm) source/drain (S/D) electrodes with a channel width and length of 300

μm and 50 μm, respectively is deposited onto the PVP gate dielectric layers using electron-beam evaporator at a rate of 0.5 Å/s. Then, 0.5 wt% TIPS-pentacene dissolved in toluene was drop-casted on the patterned Ti/Au S/D electrodes and then dried in air for 1 h. To prepare the transparent superhydrophobic protection layer, I purchased 3-ethoxy-1,1,1,2,3,4,4,5,5,6,6,6-dodecafluoro-2-trifluoromethylhexane (HFE-7500) from 3M^{TM}, and titanium (IV) oxide in having 21 nm as primary particle size (TiO_2 nanoparticles) and 1*H*,1*H*,2*H*,2*H*-perfluorooctyltriethoxysilane (PFOTES) from Sigma Aldrich. First, 1 g of PFOTES was placed into 15.0 ml of HFE-7500, and then it was mixed with 1.0 g of TiO_2 nanoparticles. After exposing the solution to ultraviolet lamp for 1 h for better dispersion, I spin-coated the solution onto organic optoelectronics with a spin speed of 500 rpm for 35 s (Figure 3.1). Finally, I dipped the devices into the rinsing solution which is composed of HFE-7200 (100 ml) and acetone (10 ml) for 5 s (Figure 3.1).

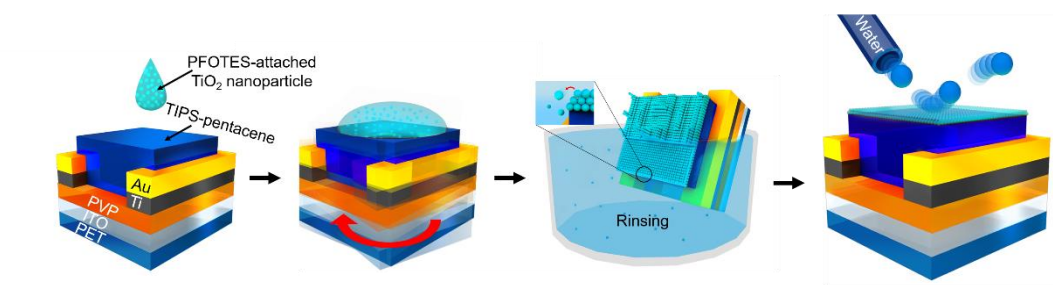

Figure 3.1 Schematic images for fabricating the transparent superhydrophobic layers onto an organic phototransistor.

3.2.2. Environmental reliability tests

To investigate the stability of my transparent superhydrophobic layers under light-stress, they were exposed to visible light laser with the power of 40 mW cm-2 in a spot size of 0.2 cm2. (Wavelength of 405 nm, 520 nm, 658 nm and 780 nm). The thermal reliability was examined by measuring water contact angles on the transparent superhydrophobic layers after annealing on a hot-plate with increasing temperature from 80 °C to 300 °C for 1 h. A mechanical stability test over 10 k repetitive bending-relaxation cycles at a bending radius of 3 nm, 5 nm, and 10 nm was also conducted to investigate the mechanical reliability using home-made equipment.

3.3. Results & Discussions

3.3.1. Surface characteristics of transparent superhydrophobic layers on various surfaces

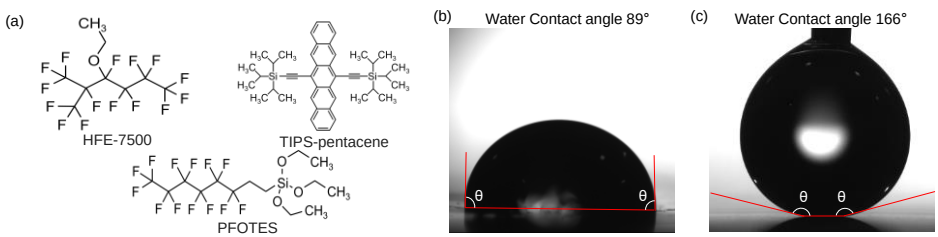

Figure 3.2 (a) Molecular structures of HFE-7500, TIPS-pentacene and PFOTES. (b) Optical image of a water contact angle on a TIPS-pentacene layer. (c) Optical image of a water contact angle on a transparent superhydrophobic layers on the TIPS-pentacene layer.

The attached PFOTES having the trifluoromethyl (-CF_3) group with extremely low surface tension of 6.7 mJ m^{-2} and surface roughness by the TiO_2 nanoparticles (~ 30 nm as a root-mean-square (RMS) height in 1 μm^2) offered the superhydrophobic

properties.[7,13,15,18,19] Because the spin-coated TiO_2 nanoparticle layers were still opaque, a rinsing process was conducted with highly fluorinated solvent based on HFE-7200 (mixture of the isomers 1-ethoxy-1,1,2,2,3,3,4,4,4-nonafluorobutane and 1-ethoxy-1,1,2,3,3,3-hexafluoro-2-(trifluoromethyl)propane) and acetone in a volume ratio of 10:1 to remove excessive TiO_2 nanoparticles resulting in transparent superhydrophobic layers (Figure 3.1a). Typically, because the fluorinated solvent would not give physical or chemical damages to organic materials, a superhydrophobic layers could be deposited onto TIPS-pentacene organic phototransistors while not interfering with underlying organic layers (Figure 3.1a and 3.2a).[7,20] Also, acetone could be mixed into the rinsing solution since it is known that fluorine and fluorinated solution slowed down chemical reactions such as polymerization so that acetone in fluorinated solvent would not dissolve or damage underlying organic materials.[21,22] The TIPS-pentacene semiconducting layer with the PFOTES attached TiO_2 nanoparticle layers showed a high water contact angle up to 168° without the degradation of transmittance, while a water contact angle of 89° was shown on the pristine TIPS-pentacene semiconductor layer (Figure 3.2b-c). To utilize my method for universal flexible organic optoelectronic devices, it is important to prove that PFOTES-attached nanoparticle layers were well deposited onto cheap and flexible substrates. So, foldable commercially available white paper, bendable PET with thickness 188 μm from Buysemimall company and stretchable polydimethylsiloxane (PDMS, Sylgard 184) from Dow Corning, all of which were previously used as flexible substrates for organic phototransistors were selected to be deposited with my transparent superhydrophobic layers.[1,23-25] Without any specific pre-treatment, the transparent superhydrophobic layers fabricated onto the flexible substrates by the solution process exhibited its underlying patterns while showing high contact angles of water droplets as shown in Figure 3.3. For

the better proof that my method was universally applied to various platforms, my transparent superhydrophobic layers were deposited onto hydrophobic and hydrophilic surfaces by the solution process. To prepare a hydrophobic surface, a glass substrate from Sigma Aldrich was spin coated by the solution with 0.5g of PFOTES in 7 mL of HFE-7200 with a spin speed of 500 rpm for 30s and a water contact angle of the PFOTES-coated surface was 102°, which indicated hydrophobicity (Figure 3.4a).[26] In addition, PDMS, PET and glass showed different contact angles were 81°, 79° and 40°, respectively (Figure 3.4b-d), which indicated hydrophilic surfaces.[26] Regardless of their water contact angles, all of them could be coated by transparent superhydrophobic surfaces as shown in Figure 3.4. Also, transparent superhydrophobic layer on a white paper showed a superhydrophobicity with a contact angle of 159° (Figure 3.5). These high water contact angles indicated that my surface morphologies had small area fractions of liquid and solid contact while having similar root mean square (RMS) height as ~30 nm for 1 by 1 μm2 by atomic force microscope (AFM) images (Figure S3.6), and this RMS height value lead to transparency by reducing light scattering.[11,15,18, 27-31]

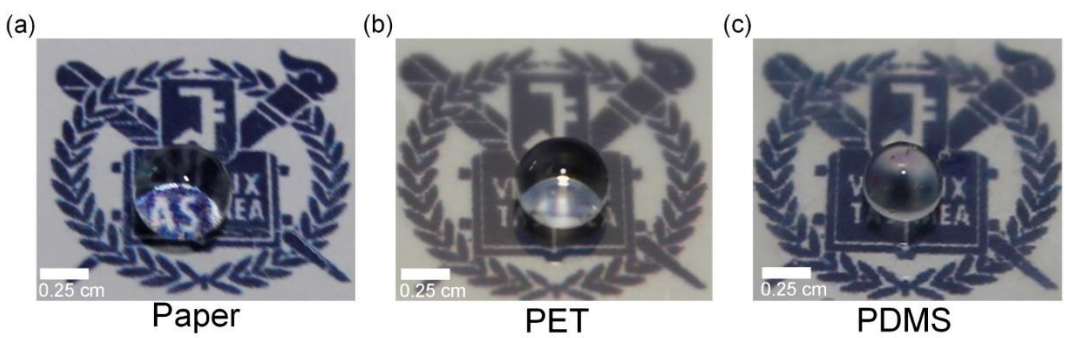

Figure 3.3 Optical images demonstrated that water droplets on the transparent superhydrophobic layers formed onto a) paper, b) PET and c) PDMS.

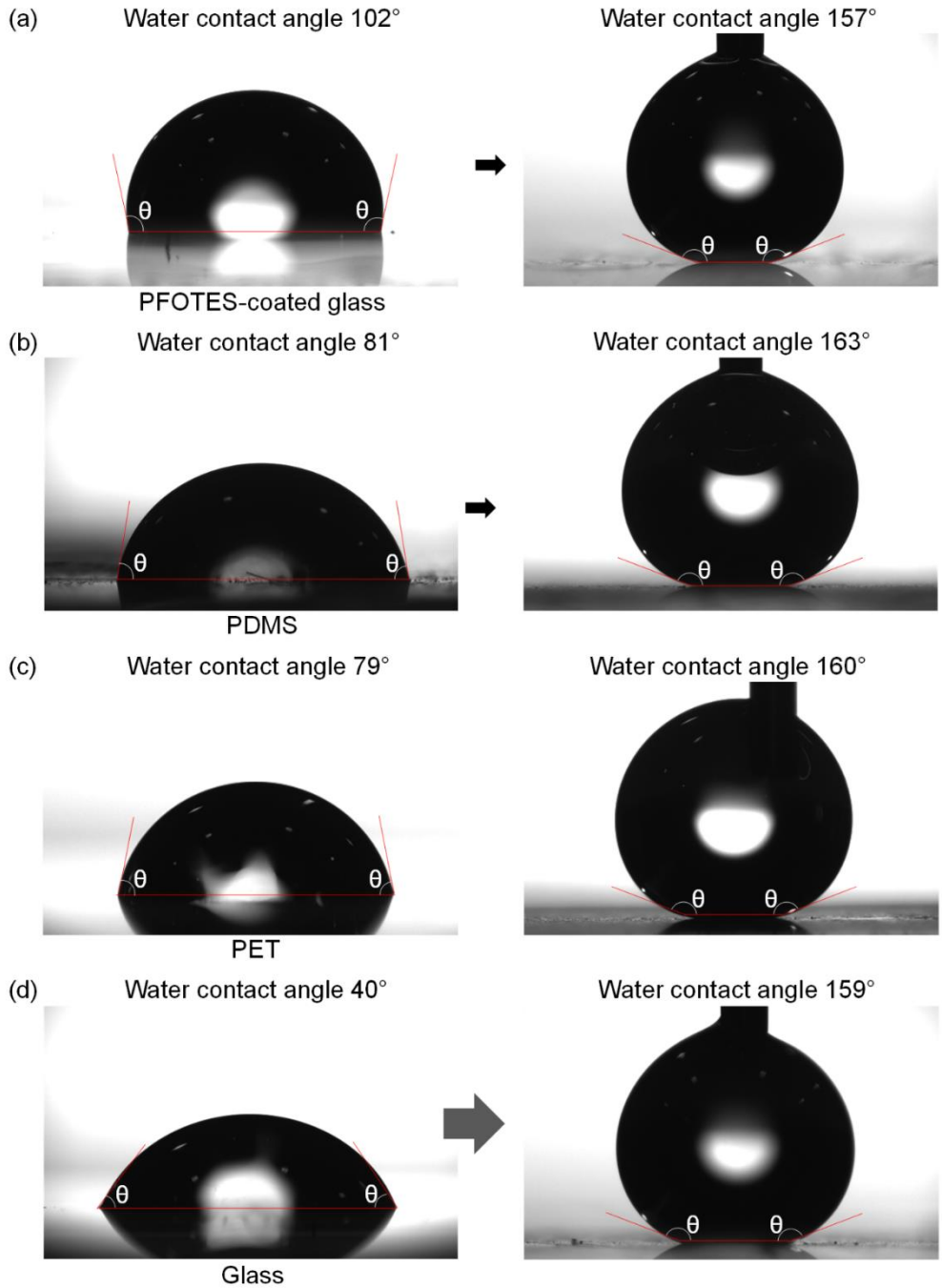

Figure 3.4 Optical images of water droplets on a) PFOTES-coated glass, b) PDMS, c) PET and d) Glass before and after depositing transparent superhydrophobic layers.

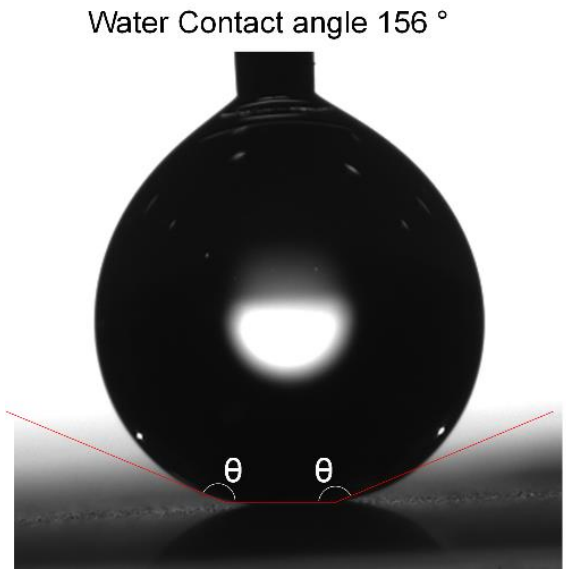

Figure 3.5 Optical image of a water droplet on the transparent superhydrophobic layers deposited onto the white paper.

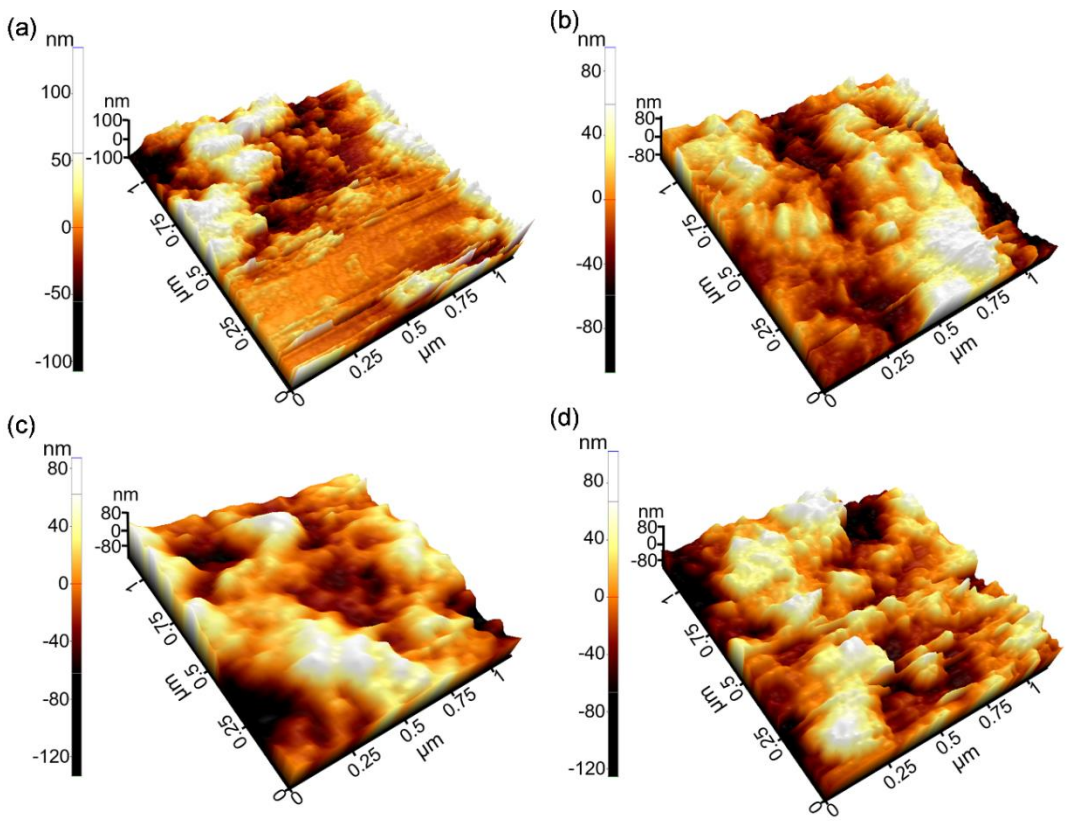

Figure 3.6 AFM images of the transparent superhydrophobic layers on a) PFOTES-coated glass, b) PDMS, c) PET and d) Glass by 1 by 1 μm^2.

3.3.2. Transmittance of transparent superhydrophobic layers before and after rinsing

From the transmitted electron microscope images as shown in Figure 3.7a and b, there were no physical or chemical damages in TIPS-pentacene layer after integrating transparent superhydrophobic layers due to organo-compatible processing. The PFOTES-attached TiO_2 nanoparticle layers showed much higher transparency with the transmittance over 84 % in the wavelength ranging from 450 nm (blue) to 635 nm (red) after rinsing in contrast with unrinsed counterpart as shown in Figure 3.7c, which was comparable to other transparent superhydrophobic layers.[13-15,17,32,33] As inset figures in Figure 3.7c indicated, most of light with wavelength of 520 nm (green) from a laser could not pass through the opaque layer due to light scattering in contrast with the transparent layers, which was also observed for light with wavelengths of 635 nm (red) and 450 nm (blue) (Figure 3.8).

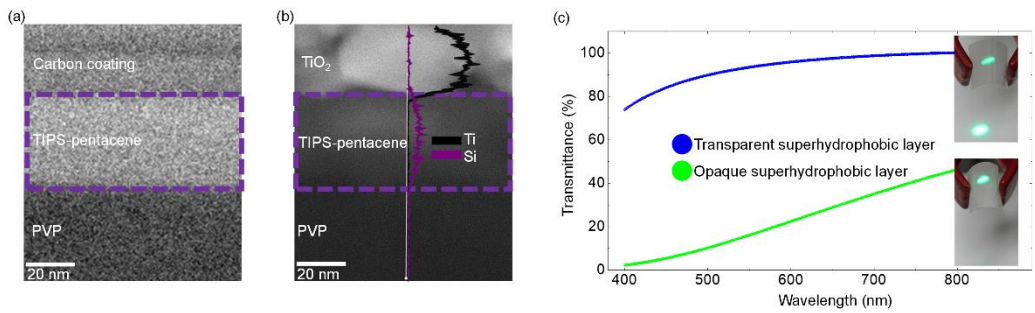

Figure 3.7 Transmittance and surface profile of the organo-compatible superhydrophobic transparent layers. (a,b) TEM images of TIPS-pentacene layers (a) without and (b) with PFOTES-attached nanoparticle layers. (c) Transmittance data in visible light range for transparent and opaque layers and inset images were optical images about green light transmittance for each layers.

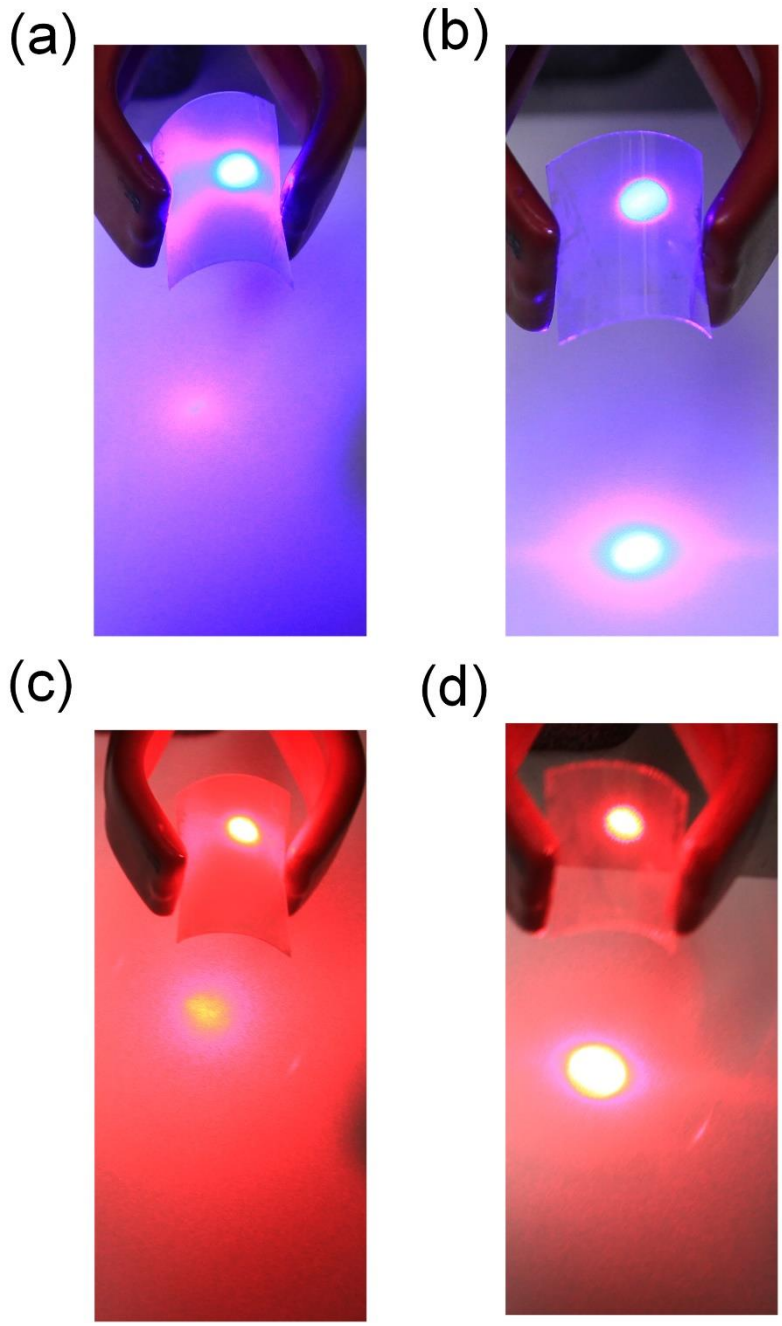

Figure 3.8 Optical images about light transmittance from blue laser (450 nm) and red laser (635 nm) for (a), (c) opaque and (b), (d) transparent superhydrophobic layers.

In addition, superhydrophobicity was also well maintained for the transparent layers even after rinsing out the unbound TiO_2 nanoparticles by clearly showing a spherical water droplet on the layers (Figure 3.9a). The surface of TiO_2 nanoparticle layers characterized by a 3D laser profiler obviously showed the difference of surface roughness and particle aggregations in a scan size of 1600 μm^2 for the opaque and transparent superhydrophobic layers (Figure 3.9b).

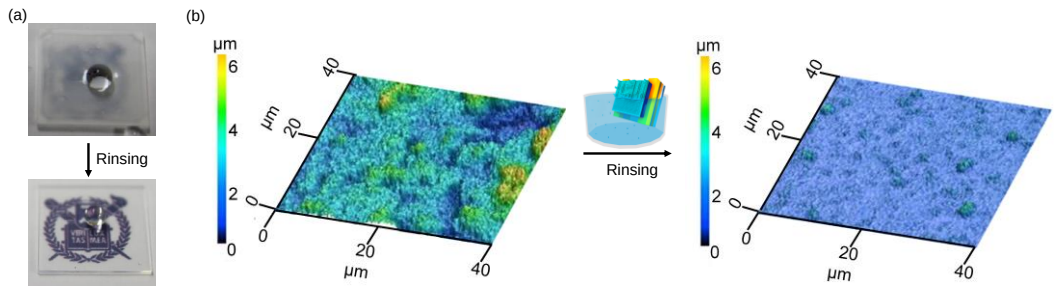

Figure 3.9 (a) Optical images of water droplets on a opaque superhydrophobic layer (Top) and the transparent superhydrophobic layer (Bottom). (b) 3D laser profiler images of the PFOTES-coated TiO_2 nanoparticle layers before (Left) and after (Right) rinsing.

Moreover, fully transparency was delivered in my transparent nanoparticle layers when wavelength of incident light was over 600 nm. These results could be explained by following equations because the surface roughness by a RMS height of the TiO_2 nanoparticle layers (~ 30 nm) was much smaller than wavelength of incident visible light from 400 nm to 800 nm.[34]

$$T_0 = 4n_a n_T/(n_a + n_T)^2 \quad (1)$$

$$\Delta T_S \cong -T_0[2\pi(n_a - n_T)\sigma/\lambda]^2 \quad (2)$$

$$\Delta T_L \cong T_0[2\pi(n_a - n_T)d/\lambda]^2, d = 2\sigma\sqrt{n_a/n_T} \quad (3)$$

where T_0, n_a, n_T, λ, σ, ΔT_S, and ΔT_L denote the transmittance of perfectly smooth surface of TiO_2 layers, refractive index of air, refractive index of TiO_2 nanoparticles, light wavelength, RMS height of the nanoparticles surface, the change of the transmittance due to scattering from the surface roughness and the change of transmittance due to change of reflectance from surface roughness, respectively.

These equations indicate that the decreased reflected light caused by surface roughness (3) may contribute more to the transmittance than the amount of transmittance lost due to light scattering by the surface roughness (2). If it is assumed that TiO_2 refractive index for visible light was distributed from 1.6 to 1.7 similar to other reported transparent TiO_2 nanotube arrays[35] and refractive index of air is 1, then each value of T_0, ΔT_S and ΔT_L could be approximately 0.93, -0.04 and 0.10 at 600 nm as light wavelength, which lead total light transmittance of the layer to almost 1, closed to my experimental transmittance value. However, absorbance of visible light even below the optical band gap of TiO_2 nanoparticles reduced light transmittance if wavelength of light was shorter than 600 nm (Figure 3.7c). By scanning electron microscope (SEM) images, it was clearly observed that aggregated unbound TiO_2 nanoparticle clusters before rinsing process were removed by the rinsing solution based on fluorinated solution, which was organo-compatible as reported (Figure 3.10).[7,20] In the case of thickness, it did not affect the contacting area between TiO_2 nanoparticles and air, therefore, thickness only hindered a transparency of the transparent superhydrophobic layers since TiO_2 could absorbed visible light in certain range.[35] To find out how rinsing process decreased thickness of the nanoparticle layers, AFM images was observed to show that a thickness of opaque superhydrophobic layers was reduced 4.27 μm and the one of the transparent superhydrophobic layers was reduced to 0.27 μm as shown in Figure 3.11. For more quantitively analysis for surface roughness

of opaque superhydrophobic layers, a RMS height which also determined transmittance was analyzed by AFM images as shown in Figure 3.12 like the transparent superhydrophobic layers as shown in Figure 3.6.[15,17,34] The transmittance of the opaque layers was low as shown in Figure 3.7 since RMS height of opaque layers was measured to be 121 nm, which could induced Mie scattering.[15]

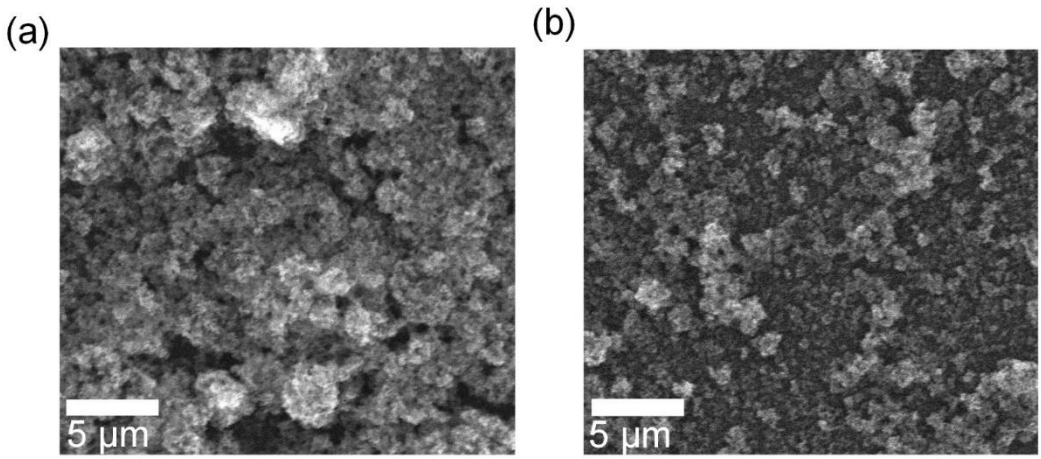

Figure 3.10 SEM images for the PFOTES-attached TiO_2 nanoparticles (a) before and (b) after rinsing process.

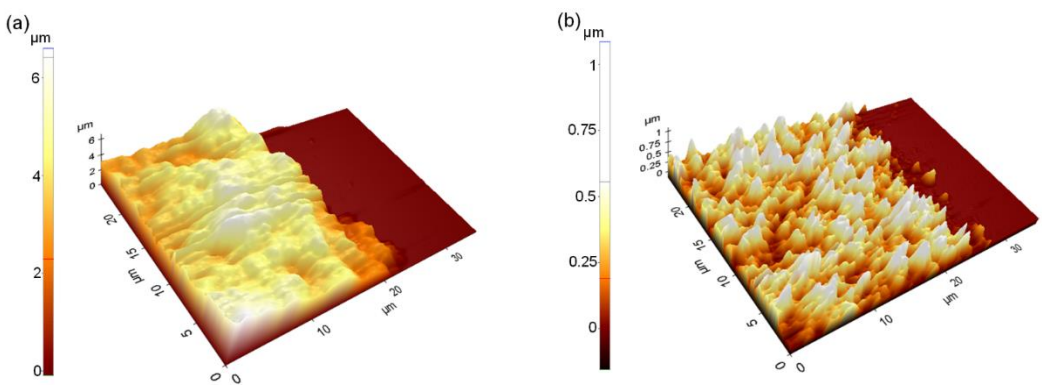

Figure 3.11 AFM images showed thickness of the PFOTES-attached TiO2 nanoparticles (a) after and (b) before rinsing process.

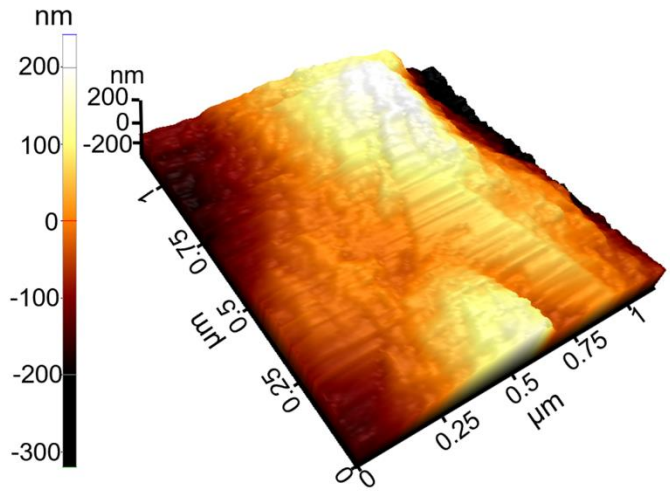

Figure 3.12 AFM images showed surface morphology of the PFOTES-attached TiO_2 nanoparticles before rinsing process by size 1 by 1 μm^2.

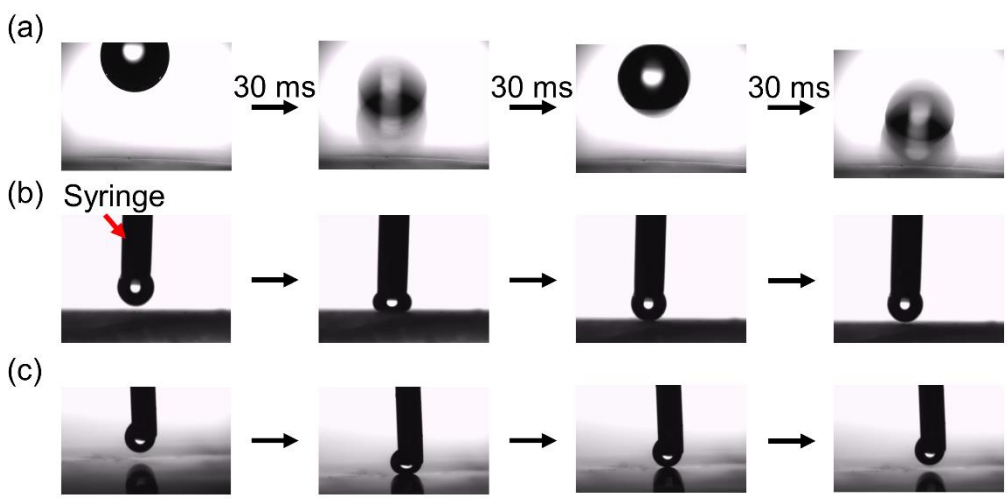

Figure 3.13 Water repellency and mechanical disabilities of our transparent superhydrophobic layers. a) Optical images of a bouncing water droplet on a superhydrophobic surface.

3.3.3. Liquid repellency of transmittance of transparent superhydrophobic layers

The controlled surface roughness enabled to show water-droplet bouncing and excellent water-repellency to even small water droplets (~ 1 μL) maintaining excellent transparency (Figure 3.13a and b). For extreme water repellency of the superhydrophobic surfaces, there are two important factors of surface morphologies. One is a total area ratio of a solid surface to contact with liquid or air under unit projected area, which was connected to water contact angles of the surface. In order to reduce the contact area ratio between solid surface and liquid, reported superhydrophobic layers generally had hierarchical structure with micro and nanoscale roughness.[37] In case of my transparent superhydrophobic layers, its line profile of AFM image showed that there are both nanoscale curvature within 1 μm scale and microscale curvature within 45 μm scale (Figure 3.14). The other factor for extreme water repellency is spacings between local maximums of superhydrophobic surfaces. Since small water droplets might be pinned onto even superhydrophobic surfaces if the spacings between local maximum peaks within area contacting with water droplets were larger than the critical values which were proportional to sizes of water droplets.[29-31] However, a surface became rougher if spacings between local maximum peaks of the surface became shorter and heights of local maximum peaks were higher, and increased surface roughness reduced transmittance by light scattering.[15] Therefore, to achieve both extreme water repellency and transparency, heights of local maximum peaks should be decreased to attain low RMS height to reduce light scattering due to surface roughness while spacings of local maximums should be small enough to repel small water droplets.[15,29-31] For my transparent superhydrophobic layers, its line profile of AFM image showed average heights of peak and valley of surface roughness

within length of 45 μm was ~ 0.1 μm and the spacings between the peaks of surface roughness was less than 5 μm, which satisfied the conditions described above.

Assuming the nanoparticle-based surface structure is pillar arrays, the critical curvature radius of water droplets not to be rolled off from the surface was about ~100 μm by following equation, which correspond to 4 x 10^{-4} μL [31]

$$1/R_{cr} = 4h_0/(w_0^4 + 4h_0^4)^{0.5} \quad (4)$$

($R_{cr,}$ w_0, and h_0 denotes the critical curvature radius of water droplet, the spacing between maximum peaks and height of peaks)

My superhydrophobic TiO_2 nanoparticle layers could repel water droplets having a volume less than ~1 μL due to the excellent structure properties even 50% stretched conditions as shown in Figure 3.13b and c.

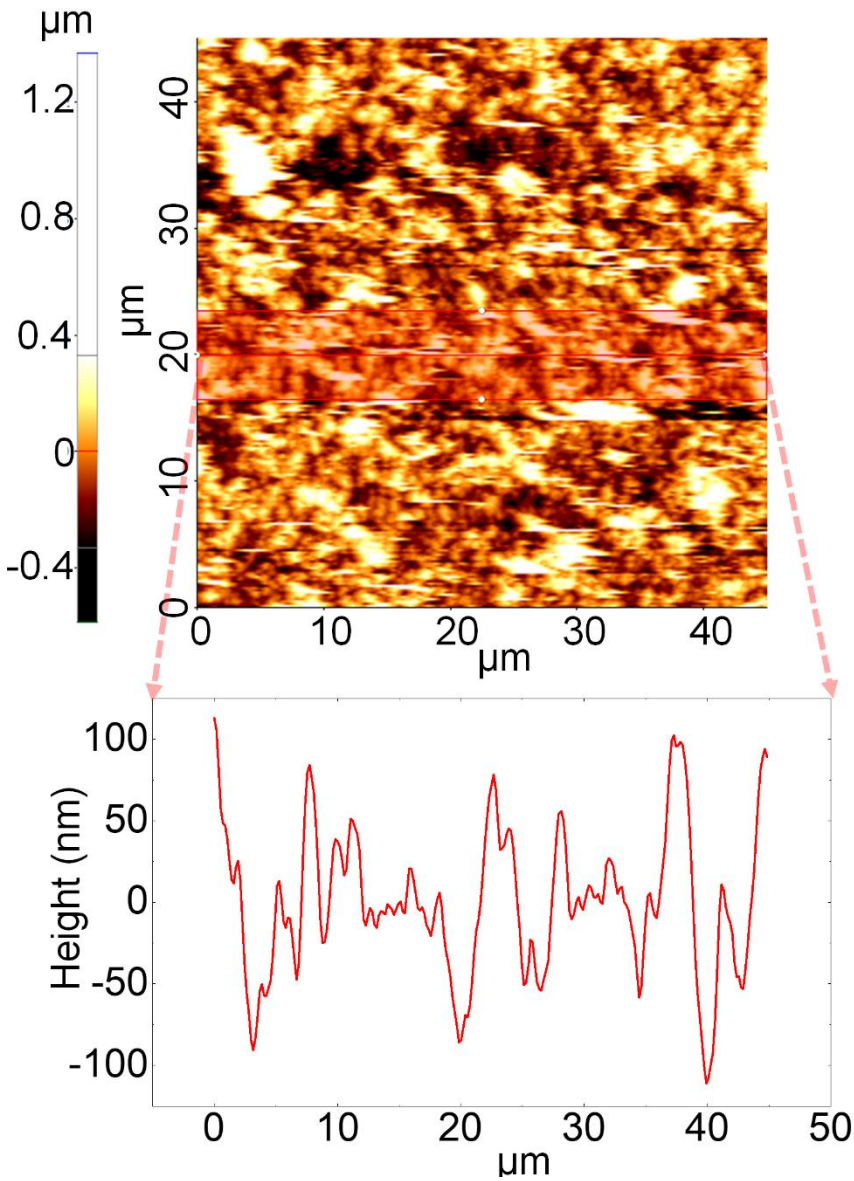

Figure 3.14 Line profile form AFM image of the transparent superhydrophobic layers by size 45 by 45 μm^2.

To prove that my transparent superhydrophobic layer could repel liquids with surface tensions lower than water, contact angles between liquids (0, 5, 10, 20 and 30% ethanol in water) and PFOTES-attached layers and their surface tensions were measured first. If contact angles between PFOTES-attached layers and the liquids were lower than 90°, the transparent superhydrophobic surfaces which were attached by PFOTES might lost its liquid repellency against the liquids by the equation of Cassie states.[31,38] For preparing PFOTES-attached layers, Ti layer was deposited onto a heavily *p*-doped Si substrate with SiO_2 (270 nm thick, 1.5 cm × 1.5 cm) by E-beam evaporator by 0.5 Å/s with pressure ~ 10^{-7} torr and then it was exposed to UV ozone cleaner for 30 min for better attachment of PFOTES. Next PFOTES of 0.5 g in HFE-7200 of 7 ml was spin coated onto the surface with 500 rpm for 30s. Then, the prepared liquids were dropped onto the surface and their contact angles and surface tensions were obtained by optical images (Figure 3.15). As a result, if liquids had ethanol more than 20%, contact angles with PFOTES-attached layers were less than 90°. Next, the prepared liquids were dropped onto the transparent superhydrophobic layers deposited onto the PDMS with tilted angle 10° and all the liquids were rolled off from the transparent superhydrophobic surfaces as soon as dropping it regardless of their surface tensions and contact angles with PFOTES-attached layers as shown in Figure 3.16. Even under 50% stretched PDMS substrates, the dropped liquids were rolled off from the transparent superhydrophobic layers on the substrates as shown in Figure 3.17. The reason for the excellent liquid repellency of the transparent superhydrophobic layers is that the surface having spherical nanoparticle clusters could act as re-entrant topologies as shown in Figure 3.10 and the re-entrant topologies of the transparent superhydrophobic layers did not break down by stretched conditions.[31,38]

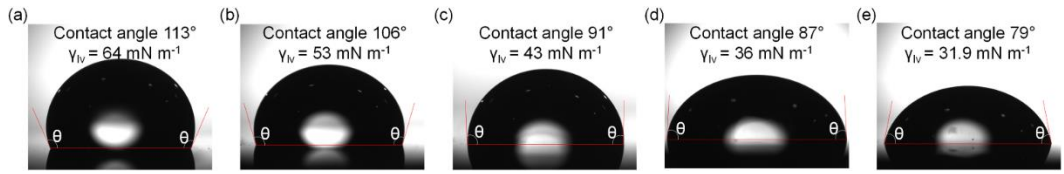

Figure 3.15 Surface tensions and contact angles for the water-based solution with different ethanol volume percentages (a) 0%, (b) 5%, (c) 10%, (d) 20% and (e) 30%.

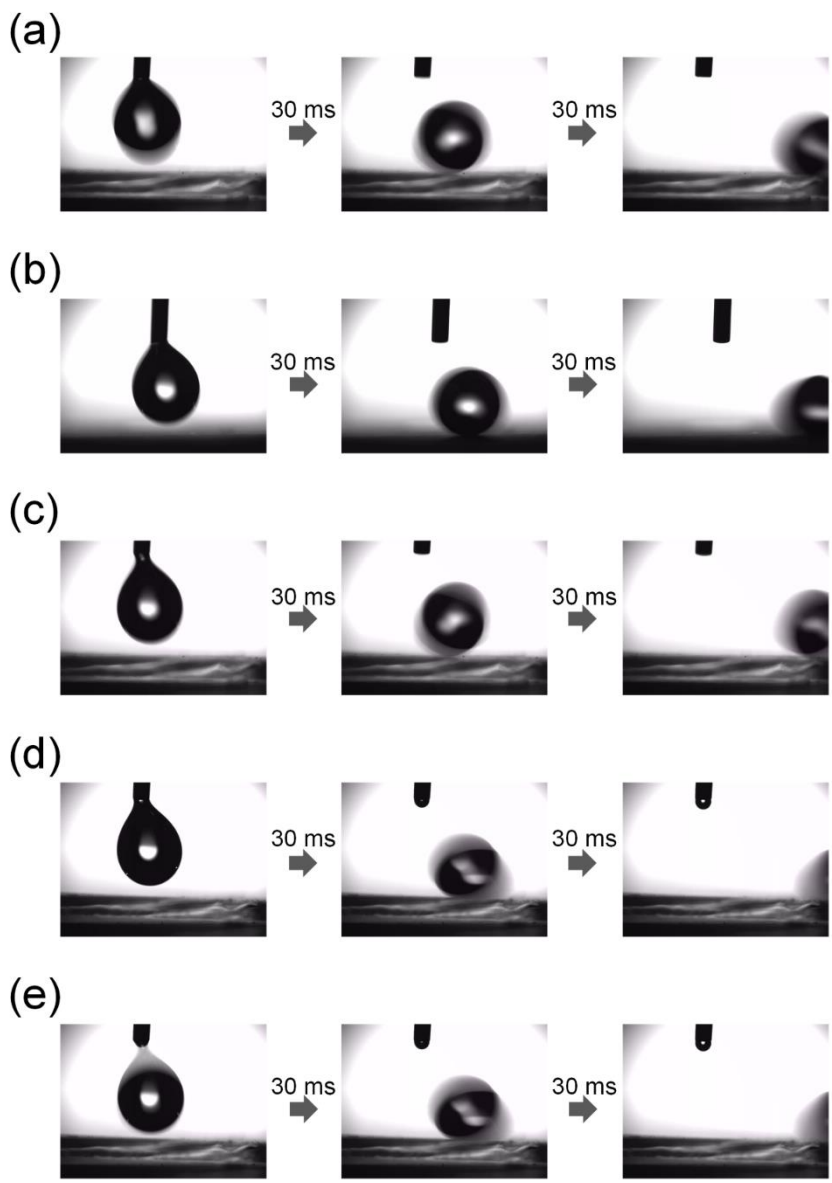

Figure 3.16 Optical images showed water-based solution with different ethanol volume percentages (a) 0%, (b) 5%, (c) 10%, (d) 20% and (e) 30% rolled off from the transparent superhydrophobic surface on PDMS substrate with tilted angle 10°.

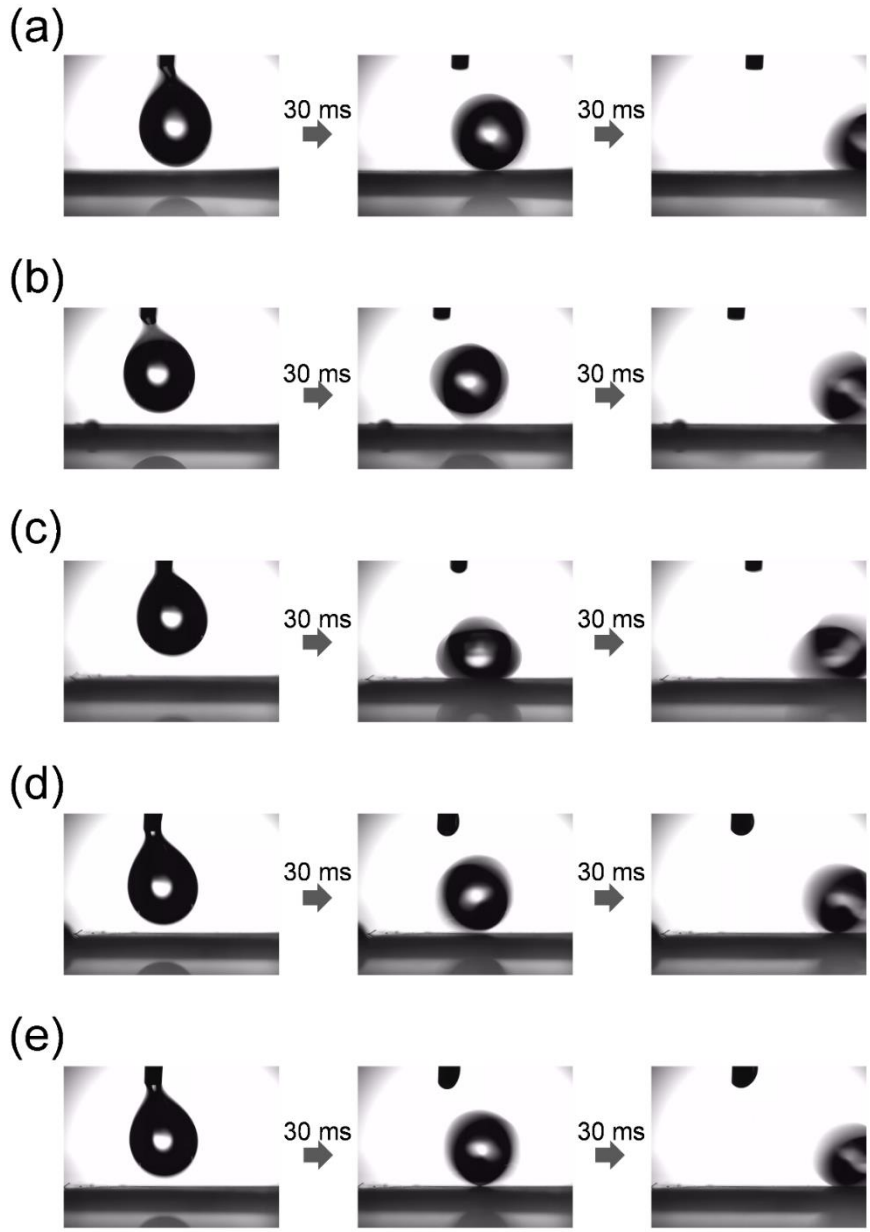

Figure 3.17 Optical images showed water-based solution with different ethanol volume percentages (a) 0%, (b) 5%, (c) 10%, (d) 20% and (e) 30% rolled off from the transparent superhydrophobic surface on 50% stretched PDMS substrate with tilted angle 10°.

3.3.4. Durability of transparent superhydrophobic layers against physical stresses

The high reliability of superhydrophobicity under light-, thermal- and mechanical stress is also one of the most desirable characteristics for the transparent superhydrophobic layers to be utilized in the open air. In particular, the durability against visible light exposure is necessary to bring the advantage of transparent organic optoelectronics. In this manner, various lasers with a wavelength ranging 405 nm and 780 nm were used to exposure high-intensity visible light on the proposed superhydrophobic layers. Note that light intensity power of 40 mW cm^{-2} with a spot size of 0.2 cm^2 was much higher than the experimental conditions which have been used in the previous results of organic phototransistors or other photosensors (less than 10 mW cm^{-2}).[3] Even high-intensity

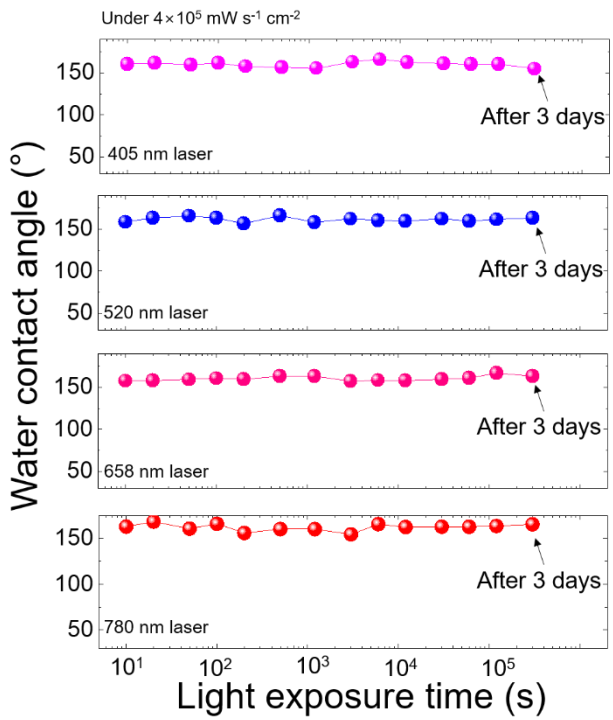

Figure 3.18 Water contact angles of the transparent superhydrophobic layer under light-stress using visible light laser with 405, 520, 658 and 720 nm-wavelength for 3 days.

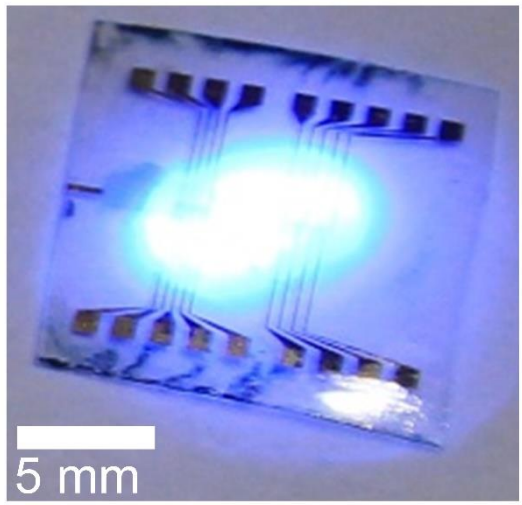

Figure 3.19 Optical images showed that blue light laser (450 nm) with light intensity 40 mW cm^{-2} was exposed to TIPS-pentacene phototransistor.

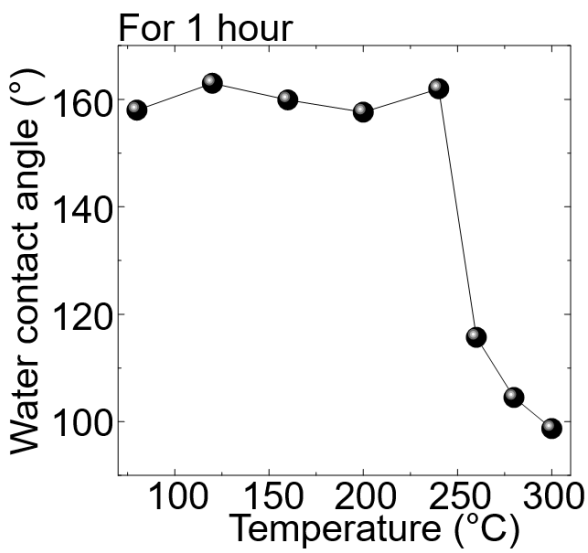

Figure 3.20 Water contact angles of the transparent superhydrophobic layer under thermal stress by changing temperature from 80 °C to 300 °C for 1 h.

visible light exposure for 3 days, they exhibited a contact angle over 150° regardless of a wavelength of lasers in visible light (Figure 3.18 and Figure 3.19).

Also, their superhydrophobicity was well-maintained on a hot-plate up to 240 °C for 1 h and degraded after 250 °C (Figure 3.20). This transition temperature was closed to the known desorption temperature of PFOETS which rendered low surface energy from TiO_2 nanoparticles.[7,39] My transparent superhydrophobic layers were also compatible to flexible organic optoelectronics fabricated on paper or polyethylene terephthalate (PET) substrates since the high contact angles over 150° were well-maintained under mechanical deformation, folding, bending with a radius of 3 mm for 10 k cycles (Figure 3.21 and 3.22). Even stretched conditions up to 50 % on PDMS substrates that indicates my strategy for offering the self-cleaning ability can be utilized in arbitrary-shaped objects or stretchable electronics (Figures 3.23 and 3.24) This outstanding mechanical durability was attributed to the well-preserved surface structures even after bending or stretching conditions without critical delamination issues. (Figures 3.25 and 3.26).

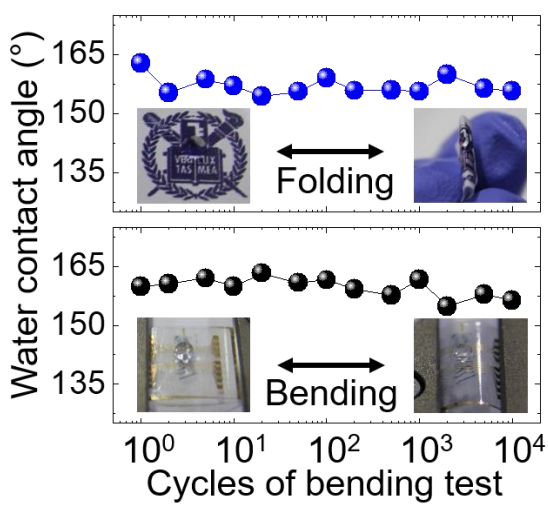

Figure 3.21 Water contact angles of the transparent superhydrophobic layer after folding and bending cycles.

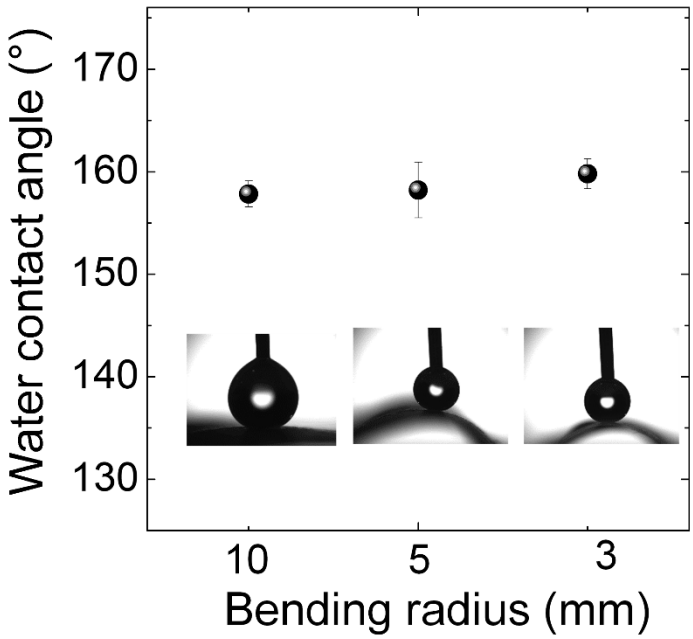

Figure 3.22 Water contact angles of the transparent superhydrophobic layers with bending radius 10, 5 and 3 mm.

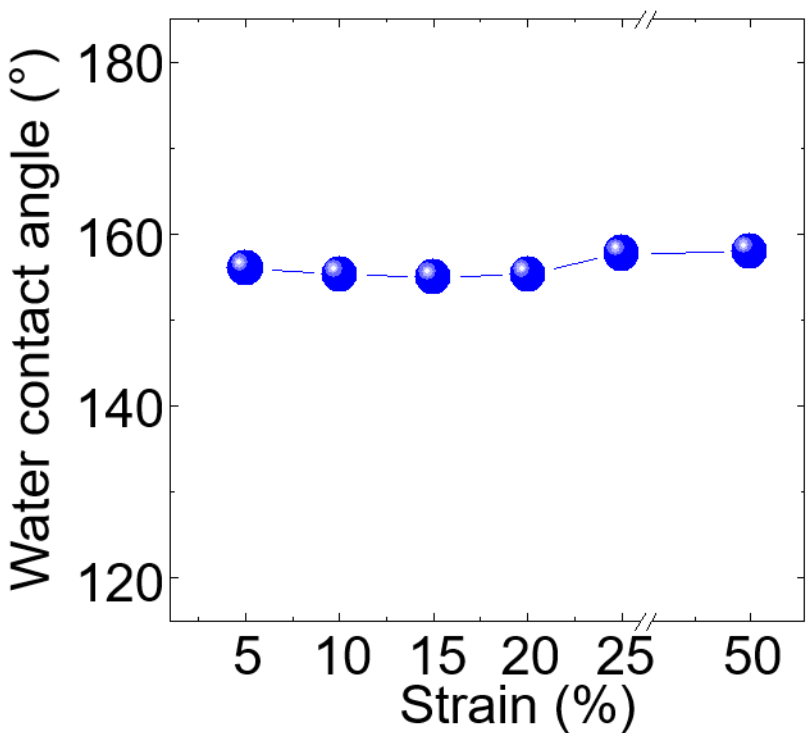

Figure 3.23 Water contact angles of the transparent superhydrophobic layers under stretched conditions.

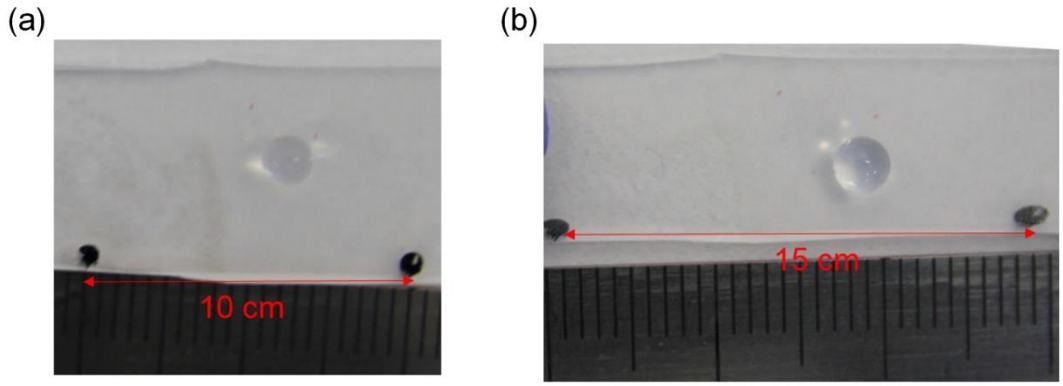

Figure 3.24 Optical images of the transparent superhydrophobic layers on PDMS substrate (a) before and (b) after stretching condition (50%), which exhibited superhydrophobicity.

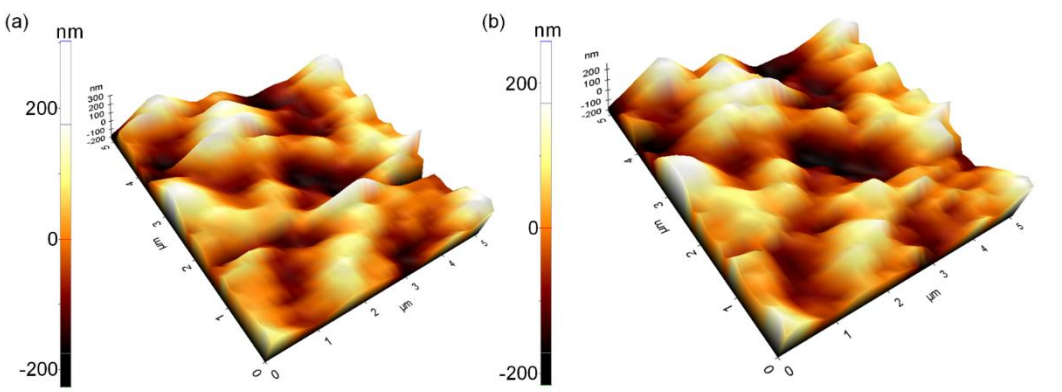

Figure 3.25 Water contact angles of the transparent superhydrophobic layers with bending radius 10, 5 and 3 mm.

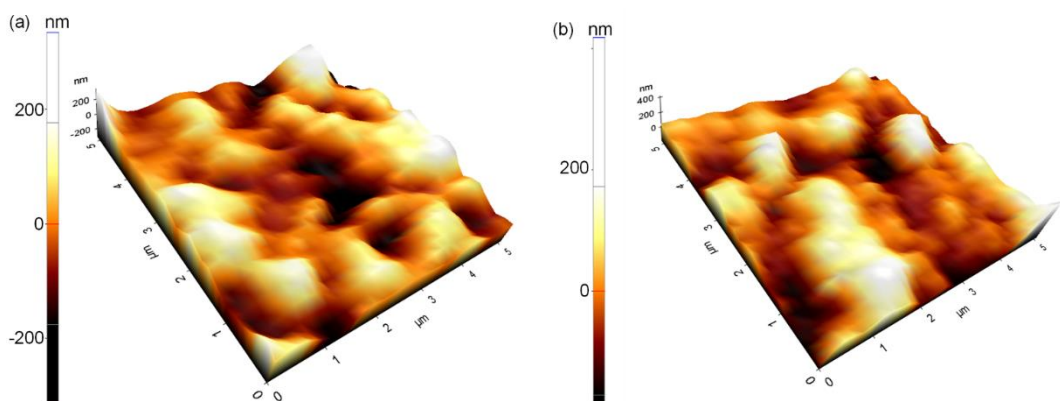

Figure 3.26 AFM images of transparent superhydrophobic layers on PDMS substrates (a) before and (b) after stretching ratio 50%.

3.3.5 Optoelectrical parameters about TIPS-pentacene phototransistor with and without transparent superhydrophobic layers

My transparent superhydrophobic layers also provided water-repellency and self-cleaning abilities to organic phototransistors, TIPS-pentacene phototransistors in this work, without degrading the optoelectronic properties of organic semiconductors under various light wavelengths and light intensities. Due to the use of fluorinated solvents and room temperature processing, the transparent superhydrophobic layers can be directly employed to organic phototransistors. All following transfer curves (drain-source current versus gate voltage, I_{DS}-V_{GS}) were obtained from V_{GS} ranging from 60 V to -60 V at a fixed drain-source voltage (V_{DS}) of -60 V. In a dark condition, there was no significant difference in the transfer curves of TIPS-pentacene phototransistors with and without transparent superhydrophobic layers, which is consistent with my previous result as shown in Figure 3.27 a and 4b.[7] Under light illumination with different wavelength 450, 520, 635 nm, which represent blue, green and red light, respectively, with light intensity as 1500 μW cm^{-2}, positively shifted transfer curves were obtained for both TIPS-pentacene phototransistors with and without the transparent superhydrophobic layers as shown in Figure 3.27a and d. As the wavelength was shorten, the shift of transfer curve increased the transfer curve to the positive direction for both organic phototransistors with and without the superhydrophobic layer. These behaviors were also observed with changing light intensities while the wavelength was fixed at 450 nm (Figure 3.27b and e). To prove that the transparent superhydrophobic layers did not degrade the light responsive characteristics of the TIPS-pentacene phototransistor, it was identified that threshold voltage shifts by varying the light intensity for each fixed light wavelength. As a result, threshold voltage shifts of TIPS-pentacene phototransistor after exposed to blue, green and red wavelength

of 450, 520 and 635 nm had not been changed even if light intensities were varied from ~ 10 μW to ~1000 μW (Figure 3.28). Also, optoelectronic parameters photoresponsivity, detectivity and external quantum efficiency (EQE) for light wavelength were also analyzed before and after depositing transparent superhydrophobic layers as shown in Figure 3.29 (Photo responsivity (R) , detectivity (D), and EQE were estimated by each following formulas, $R = I_{Ph}/P_{Light}$, $D = (RA_D^{1/2})/(2eI_{Dark})^{1/2}$ and $EQE = (I_{Ph}/e)/(P_{Light}/h\nu)$. Where I_{Ph}, P_{Light}, A_D, e, I_{dark} and hν denoted an illuminated current, an intensity of incident light, an effective detection area, the elementary charge and a photon energy.) The results showed that my transparent superhydrophobic layers did not degrade the optoelectronic properties of the TIPS-pentacene phototransistors regardless of light intensities with different wavelengths. In addition, my transparent superhydrophobic layers also bounced off water droplet, which could operate as a protective layer to prevent water-based threats from degrading phototransistor as shown in Figure 3.27c and f. With excellent water repellency, the self-cleaning ability of my superhydrophobic layers, could eliminate undesirable dusts, even heavily soils on the surface of TIPS-pentacene phototransistor by dropping water droplets. This strategy can maintain optoelectronic performances of environmentally sensitive organic phototransistors against external obstacles as shown in Figure 3.30.

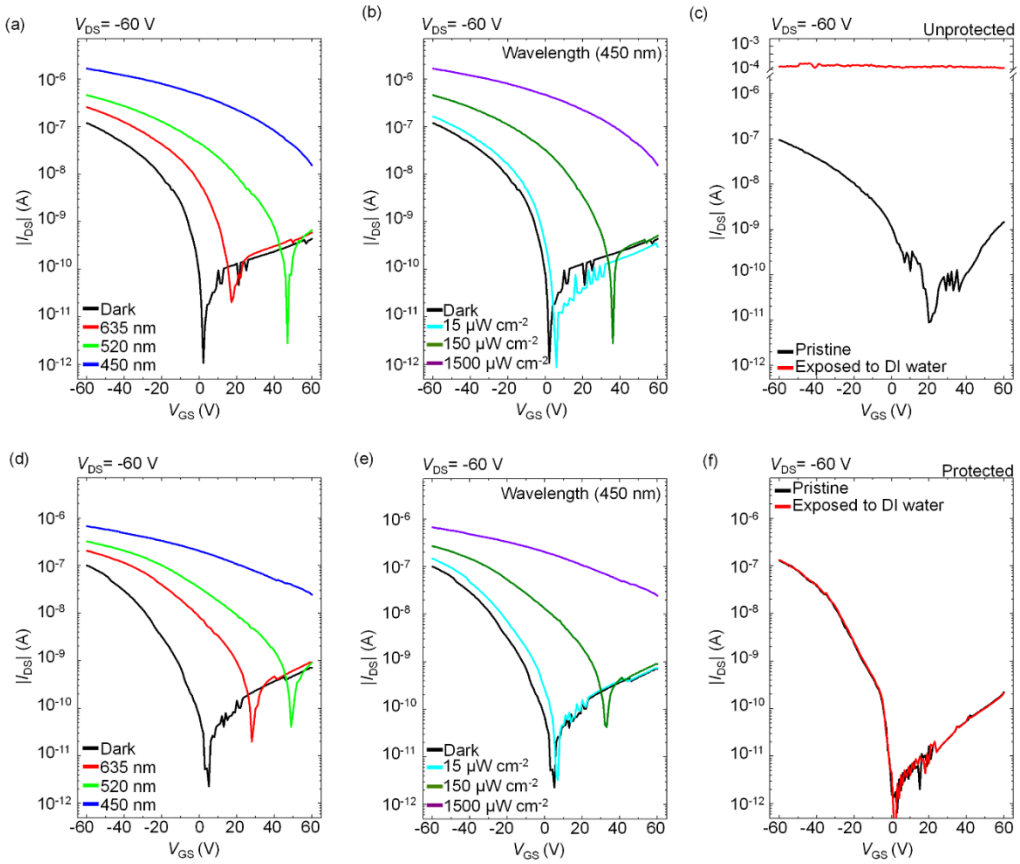

Figure 3.27 Representative transfer curves of TIPS-pentacene organic phototransistors with and without the superhydrophobic protection layer under light illumination. a,d) Transfer curves on the semilogarithmic scale for TIPS-pentacene organic phototransistors with and without transparent superhydrophobic layers under dark condition and light illumination with different wavelengths and fixed light intensity as 1500 μW cm^{-2} in ambient condition. b,e) Transfer curves on the semilogarithmic scale for TIPS-pentacene organic phototransistors with and without transparent superhydrophobic layers under dark and light illumination with fixed wavelengths 450 nm and different light intensity from 15 μW cm^{-2} to 1500 μW cm^{-2} in ambient condition. e,f) Transfer curves on the semilogarithmic scale for the TIPS-pentacene phototransistor with and without transparent superhydrophobic layer before after exposure to DI water in ambient condition.

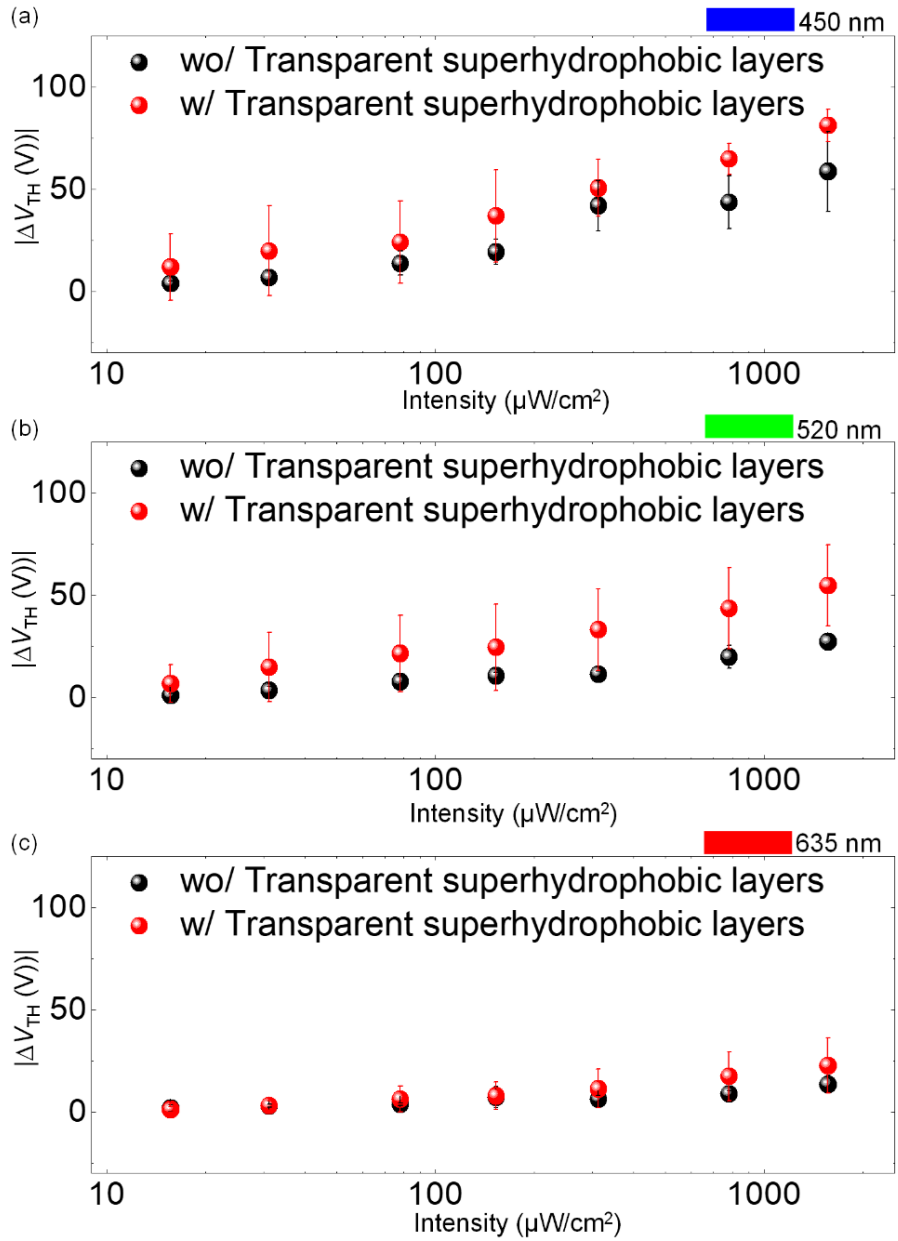

Figure 3.28 Threshold voltage shifts of TIPS-pentacene phototransistor with fixed wavelength of a) 450 nm, b) 520 nm and c) 635 nm while varying different light intensities from 10 to 1500 μW cm^{-2}.

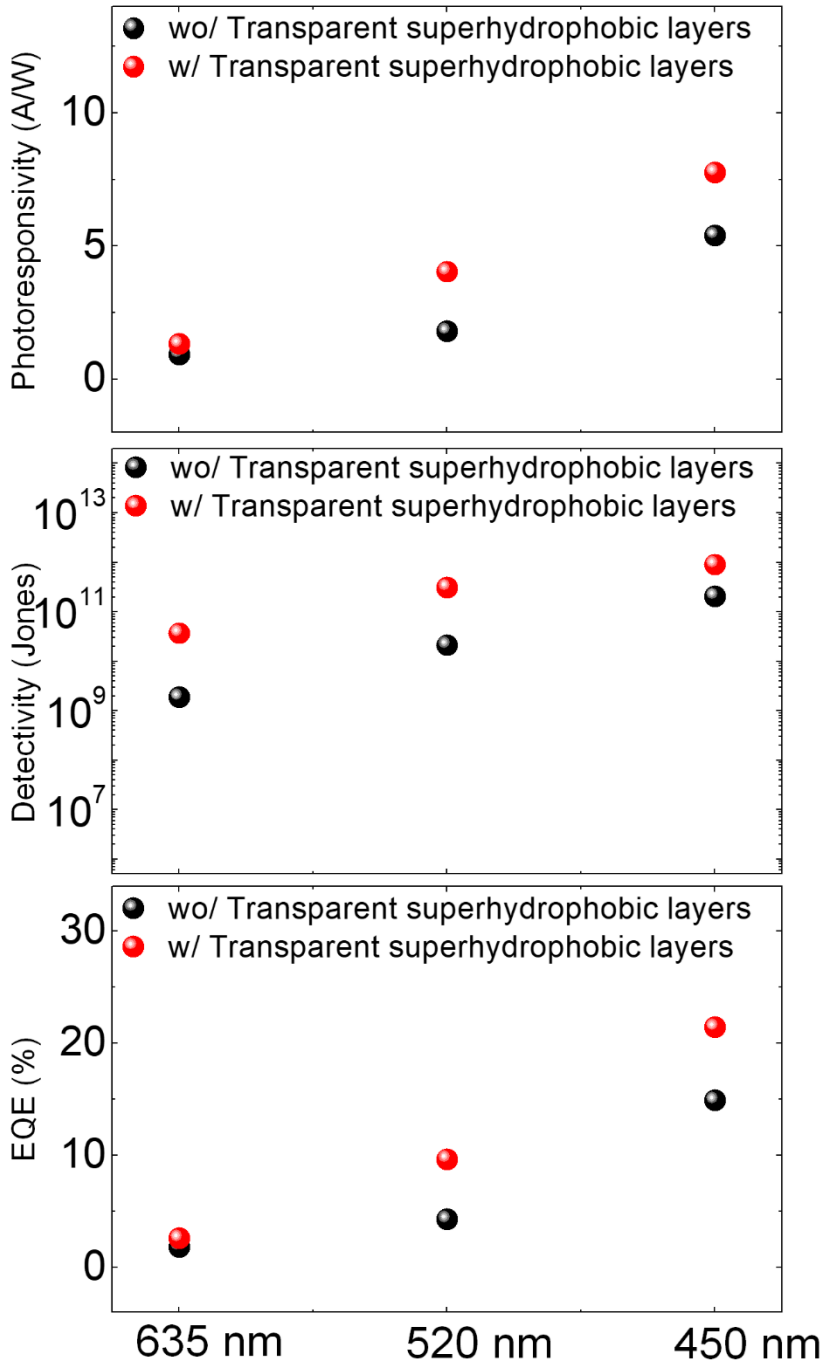

Figure 3.29 a) Photoresponsivity, detectivity and EQE of TIPS-pentacene phototransistor with different wavelength (450, 520 and 635 nm), fixed light intensities 1500 μW cm^{-2}, source-drain voltage of – 60V and gate-source voltage of - 60V with and without transparent superhydrophobic layers.

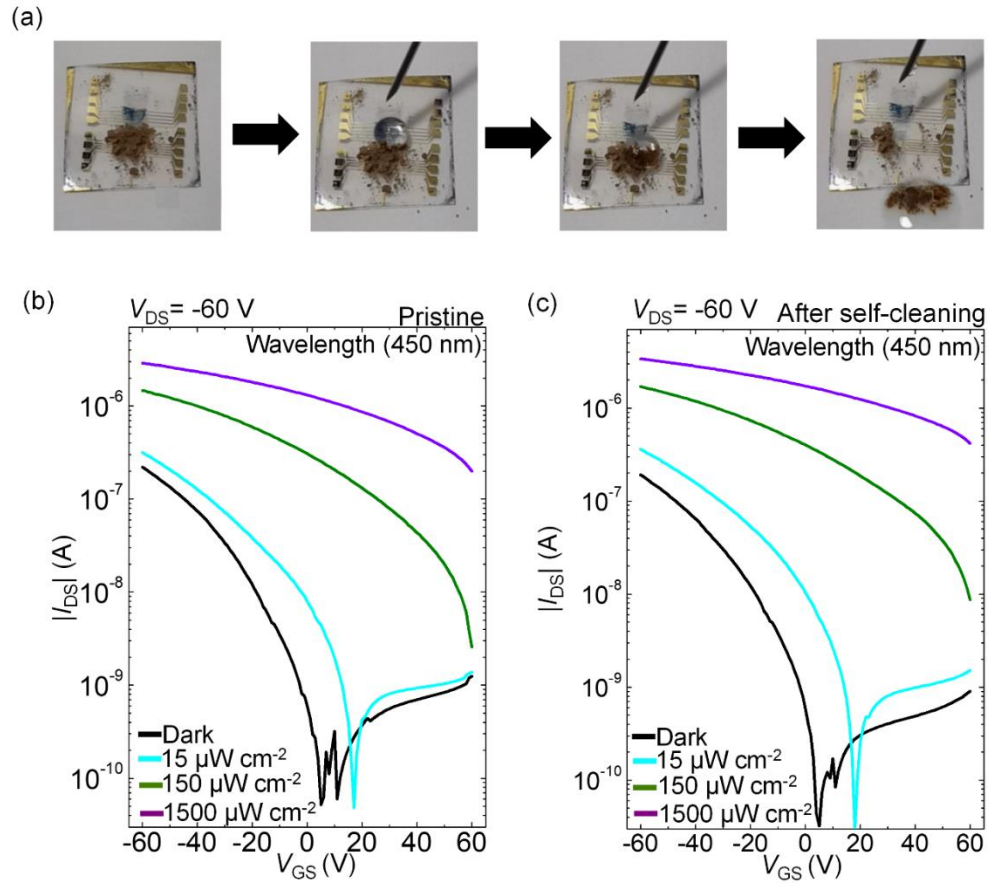

Figure 3.30 Self-cleaning ability of a TIPS-pentacene phototransistor by applying the transparent superhydrophobic layers. a) Removing soils on a TIPS-pentacene phototransistor with transparent superhydrophobic layers by simply dropping water droplets. b,c) Transfer curves on the semilogarithmic scale for TIPS-pentacene organic phototransistors with transparent superhydrophobic layers b) before and c) after self-cleaning process under dark and light illumination with fixed wavelengths 450 nm and different light intensity from 15 μW cm^{-2} to 1500 μW cm^{-2}.

3.4. Conclusion

In summary, I introduced organo-compatible transparent superhydrophobic layers on organic optoelectronics directly using facile solution processing. By rinsing process, I could control the surface roughness of TiO2 nanoparticle superhydrophobic layers which is a key approach to realize transparent layers minimizing Rayleigh and Mie scattering. In addition, superhydrophobicity was well preserved under accelerated light, thermal and mechanical stress. With these favorable properties of the transparent superhydrophobic layers, further reliable and self-cleanable TIPS-pentacene phototransistors against water-based threat and undesirable dusts were demonstrated maintaining their optoelectronic properties. This work can pave a key pathway for realizing further practical organic optoelectronics used in the open air.

References

[1] Forrest, S. R. *Nature* **2004**, *428*, 911-918.

[2] Sekitani, T.; Yokota, T.; Zschieschang, U.; Klauk, H.; Bauer, S.; Takeuchi, K.; Takamiya, M.; Sakurai, T.; Someya, T. *Science* **2009,** *326*, 1516-1519.

[3] Baeg, K. J.; Binda, M.; Natali, D.; Caironi, M.; Noh, Y. Y. *Adv. Mater*. **2013**, *25*, 4267-4295.

[4] Lucas, B.; Trigaud, T.; Videlot-Ackermann, C. *Polym. Int*. **2012,** *61*, 374-389.

[5] Pierre, A.; Gaikwad, A.; Arias, A. C. *Nat. Photonics* **2017**, 11, 193-199.

[6] Huang, J.; Du, J.; Cevher, Z.; Ren, Y.; Wu, X.; Chu, Y. *Adv. Funct. Mater*. **2017,** *27*, 1604163.

[7] Yoo, D.; Kim, Y.; Min, M.; Ahn, G. H.; Lien, D. H.; Jang, J.; Jeong, H.; Song, Y.; Chung, S.; Javey, A.; Lee, T. *ACS Nano* **2018**, *12*, 11062-11069.

[8] Kaltenbrunner, M.; Sekitani, T.; Reeder, J.; Yokota, T.; Kuribara, K.; Tokuhara, T.; Drack, M.; Schwödiauer, R.; Graz, I.; Bauer-Gogonea, S.; Bauer, S.; Someya, T. *Nature* **2013**, *499*, 458-463.

[9] Simon, D. T.; Kurup, S.; Larsson, K. C.; Hori, R.; Tybrandt, K.; Goiny, M.; Jager, E. W. H.; Berggren, M.; Canlon, B.; Richter-Dahlfors A. *Nat. Mater.* **2009**, *8*, 742-746.

[10] Sandström, A.; Dam, H. F.; Krebs, F. C.; Edman, L. *Nat. Commun.* **2012**, *10*, 1002.

[11] Lafuma, A.; Quéré, D. *Nat. Mater.* **2003**, *2*, 457-460.

[12] Lu, Y.; Sathasivam, S.; Song, J.; Crick, C. R.; Carmalt, C. J.; Parkin, I. P. *Science* **2015**, *347*, 1132-1135.

[13] Nakajima, A.; Fujishima, A.; Hashimoto, K.; Watanabe, T. *Adv. Mater.* **1999**, *11*, 1365-1368.

[14] Deng, X.; Deng, L X.; Mammen, L.; Butt, H.-J.; Vollmer, D. *Science* **2012**, 335, 67-70.

[15] Rahmawan, Y.; Xu, L.; Yang, S. *J. Mater. Chem. A* **2013**, *1*, 2955-2969.

[16] Wang, C. Y.; Groenzin, H.; Shultz, M. J. *Langmuir* **2003**, *19*, 7330-7334.

[17] Lai, Y.; Tang, Y.; Gong, J.; Gong, D.; Chi, L.; Lin, C.; Chen, Z. *J. Mater. Chem.* **2012**, *22*, 7420-7426.

[18] Feng, L.; Li, S.; Li, Y.; Li, H.; Zhang, L.; Zhai, J; Song, Y.; Liu, B.; Jiang, L.; Zhu, D. *Adv. Mater.* **2002**, *14*, 1857-1860.

[19] Nishino, T.; Meguro, M.; Nakamae, K.; Matsushita, M.; Ueda, Y. *Langmuir* **1999,**

15, 4321-4323

[20] Zakhidov, A. A.; Lee, J. K.; Fong, H. H.; DeFranco, J. A.; Chatzichristidi, M.; Taylor, P. G.; Ober, C. K.; Malliaras, G. G.; *Adv. Mater.* **2008**, *20*, 3481-3484.

[21] Rao, A.V.; Latthe, S. S.; Nadargi, D. Y.; Hirashima, H.; Ganesan, V.; *J. colloid Interface Sci.* **2009**, *332*, 484-490.

[22] Fresnais, J.; Chapel, J. P.; Poncin-Epaillard, F. *Surf. Coat. Technol.* **2006**, *200*, 5296-5305.

[23] Lee, M. Y.; Hong, J.; Lee, E. K.; Yu, H.; Kim, H.; Lee, J. U.; Lee, W.; Oh, J. H.; *Adv. Funct. Mater.* **2016**, *26*, 1445-1453.

[24] Xu, H.; Liu, J.; Zhang, J.; Zhou, G.; Luo, N.; Zhao, N. *Adv. Mater.* **2017**, *29*, 1700975.

[25] Fujisaki, Y.; Koga, H.; Nakajima, Y.; Nakata, M.; Tsuji, H.; Yamamoto, T.; Kurita, T.; Nogi, M.; Shimidzu, N.; *Adv. Funct. Mater.* **2014**, *24*, 1657-1663.

[26] Ganesh, V. A.; Raut, H. K.; Nair, A. S.; Ramakrishna, S. *J. Mater. Chem.* **2011**, *21*, 16304-16322.

[27] Patankar, N. A. *Langmuir* 2**003**, *19*, 1249-1253.

[28] Milne, A. J. B.; Amirfazli, A. *Adv. Colloid interface Sci.* **2012**, *170*, 48-55.

[29] Extrand, C. W.; *Langmuir* **2002**, *18*, 7991-7999.

[30] Nosonovsky, M. *Langmuir* **2007**, *23*, 3157-3161.

[31] Luo, C.; Xiang, M.; Liu, X.; Wang, H. *Microfluid. Nanofluid.* **2011**, *10*, 831-842.

[32] Gao, S.; Dong, X.; Huang, J.; Li, S.; Li, Y.; Chen Z.; Lai, Y. *Chem. Eng. J.* **2018**, *333*, 621-629.

[33] Bravo, J.; Zhai, L.; Wu, Z.; Cohen, R. E.; Rubner, M. F. *Langmuir* **2007**, *23*, 7293-7298.

[34] Carniglia, C. K.; Jensen, D. G.; *Appl. Opt.* **2002**, *41*, 3167-3171.

[35] Mor, G. K.; Varghese, O. K.; Paulose, M.; Grimes, C. A. *Adv. Funct. Mater*. **2005**, *15*, 1291-1296.

[36] Lechner, M. D. *J. Serb. Chem. Soc.* **2005**, *70,* 361-369.

[37] Wang, S.; Jiang, L *Adv. Mater.* **2007**, *19*, 3423-3424.

[38] Liu, T. L.; Kim, C. J. *Science* **2014**, *346*, 1096-1100.

[39] Nørgaard, A. W.; Jensen, K. A.; Janfelt, C.; Lauritsen, F. R.; Clausen, P. A.; Wolkoff, P. *Environ. Sci. Technol.* **2009**, *43*, 7824-7830.

Chapter 4. Summary

In this thesis, I researched about organo-compatible nanoparticle-based superhydrophobic layers to enhance environmental reliability of organic thin film devices. The main chapters were devoted to surface morphologies of the superhydrophobic layers and how they preserve electrical performances of organic transistors against water based hindrances and contaminants.

First, I reported a facile method to directly fabricate an organo-compatible superhydrophobic protection layer on organic devices under ambient conditions. The superhydrophobicity was achieved by simply dipping organic devices in a highly fluorinated solution dispersed with fluoroalkylsilane-coated titanium-dioxide nanoparticles. Furthermore, the uniform protection layer could be deposited using a simple dipping process without any physical damages by optimizing the solvent system to match surface energy with underlying organic semiconductors. The proposed superhydrophobic protection layer had good resistance against mechanical-stress, light-stress and water-based threats. Moreover, protected organic devices exhibited reliable electrical properties even exposed to strong solvents while maintaining self-cleaning properties from extreme water. This approach could be a good alternative solution to protect low-cost and flexible organic electronics working in the opened air.

And secondly, I reported a facile method to realize a transparent superhydrophobic layer onto organic phototransistors through an organo-compatible solution process. TiO2 nanoparticles coated with fluorinated silane molecules are dispersed in a highly fluorinated solvent, so I can introduce a superhydrophobic surface onto organic devices directly. The optimized transmittance over 90 % in the visible wavelength region is attributed to the

controlled roughness parameters of my superhydrophobic layer. The transparent superhydrophobic layers exhibit good water repellency without critical delamination issues even after or during bending and stretching tests. Moreover, flexible organic phototransistors with the transparent superhydrophobic layers show self-cleaning abilities from excellent water repellency, therefore harmful contaminants on the surface can be eliminated by dropping water droplets while preserving their optoelectronic characteristics. This work can provide a key pathway to implement a transparent self-cleaning layer for more reliable organic optoelectronic devices.

국문초록

이산화타이타늄 나노입자 기반의 초소수성 박막을 이용한 유기 트랜지스터의 소자 안정성 향상 연구

유대경

서울대학교 물리천문학부

지난 수십 년 동안 유기물 전자소자 재료는 저비용의 용액 공정을 사용하여 다양한 형태의 유연한 전자소자로 사용될 수 있는 가능성을 보여주었다. 이러한 유기 전자소자의 실용적인 활용을 위해서는, 무엇보다 소자 안정성을 갖는 유기 전자소자가 필요하다. 특히, 유기 전자소자 표면에 축적된 먼지나 물은 소자의 기능을 저하할 수 있기 때문에 이러한 외부 요인들에 대응할 수 있는 실용적인 해결책에 대한 요구가 있어 왔습니다. 이와 관련하여, 초소수성 박막을 유기 물질 위에 직접 증착하는 방식을 도입해서, 초소수성 표면에서 나타날 수 있는 물방울이 튕기는 현상(발수성)과 초소수성의 자가 세정 능력을 통해서 오염물질이나 물을 소자 표면에서 제거하는 방법이 바람직하다.

첫 번째 연구로, 일반적인 환경에서 유기 반도체에 유기친화적인 초소수성 보호층을 손쉽게 증착하는 방법을 연구하였다. 유기물 박막 시료를 플루오로 알킬 실란 유기물이 코팅된 이산화타이타늄 나노 입자가 포함한 불소화 용액 안에 집어넣는 간단한 공정을 사용하여 우수한 발수성 및 자가 세정 능력을 나타내는 보호 박막을 유기 반도체 표면에 증착하였다. 이 초소수성 박막은 유기 반도체를 손상하지 않았으며 특히 물에 의한 요인 및 기계적, 열적, 빛에 의한 요인에 대해서도 우수한 저항성을 보였다. 초소수성 박막으로 보호된 유기 전계효과 트랜지스터 소자는 초소수성으로 인해 강한 용매에 노출되는 경우에서도 신뢰성 있는 소자의 전기적 특성을 나타냈다.

두 번째 연구로, 투명한 유기 광전자 소자를 위한 초소수성 층을 연구

하였다. 플루오로 알킬 실란 유기물이 부착된 이산화 타이타늄 나노입자 박막의 표면 거칠기와 박막의 두께를 최적화 함으로써 투명하면서 초소수성을 가지는 박막을 만들 수 있었다. 이렇게 제작된 투명 초소수성 박막은 유기 광전자, 특히 광 트랜지스터 소자에 활용할 수 있는 가능성을 보여주었다. 유기 반도체에 직접 증착할 수 있는 투명 초소수성 박막은 굽히거나 늘리는 물리적인 변형에도 심각한 표면 구조의 손상 없이 일관된 초소수성을 나타냈다. 그 결과로, 투명 초소수성 박막을 가진 유연한 유기 광 트랜지스터 소자는 우수한 발수성과 자기 세정 능력으로 소자 표면의 물방울과 유해한 오염 물질에 대해 향상된 소자 안정성을 보여주었다.

Keywords: 유기 물질, 티타늄-이산화물 나노 입자, 초소수성, 트랜지스터, 광 트랜지스터, 불소 물질

Student Number: 2015-30093

감사의 글

대학원의 경우에는 학생으로서 면모와 종종 일을 하는 지적 노동을 하는 노동자로서의 모습 모두 겪을 수 있습니다. 그런 부분들이 즐거울 때도 있지만 때때로 힘들 때도 있습니다. 이런 대학원 과정을 잘 마칠 수 있게 해 주신 많은 분들께 감사드립니다.

먼저, 저의 대학원 생활 동안 저를 잘 지도해주시고 올바른 연구자로서 나아갈 수 있게끔 많이 가르쳐주신 지도교수 이탁희 교수님께 감사드립니다. 교수님께서 보여주신 인품과 연구에 있어서 큰 그림을 제시해주시는 방향성 덕분에 제가 무사히 대학원 박사과정을 마무리 지을 수 있었습니다. 교수님께서도 앞으로 건강히 행복하게 지내시기를 바라겠습니다.

그리고 대학원에서 연구를 진행하면서 연구 교수로서 도와 주시고 그 후에 KIST로 연구원으로 가신 후에도 제 연구 전반에 있어서 디테일적인 부분에 대해서 저를 많이 도와 주셨던 정승준 박사님께도 감사를 드립니다.

다음으로 저의 대학원 생활 동안 저를 응원해주신 부모님께 감사드리겠습니다. 7년 동안 다양한 방향에서 저를 응원해주시고 지원해주셨습니다. 그런 만큼 앞으로 박사과정을 마무리하고 보다 박사과정 전보다 보다 좋아진 모습을 보여질 수 있도록 노력하겠습니다.

그 다음으로 저희 실험실 분들께 감사의 말씀을 드리겠습니다. 처음 들어왔을 때 지금은 박사가 되신 장진곤 형, 송영걸 형에게 기초부터 많은 도움을 받았습니다. 그 다음에는 같은 팀으로 들어온 김영록 박사에게 장비 셋팅이나 실험에 대한 관점에 대해서 크게 도움을 받았습니다. 그리고 또 후배로 들어온 우철이가 실험실이나 장비의 전반적인 관리를 잘해주어서 제가 무사히 졸업할 수 있었습니다. 그리고 포닥으로 오신 강박사님께도 많은 도움을 받을 수 있었습니다.

그리고 이미 졸업한 박진수 박사에게는 같이 미국 생활을 하면서 많이 도움을 받을 수 있었습니다. 조경준 박사에게는 저의 연구실 생활을 재밌게 그리고 보다 잘 적응할 수 있도록 도움 받았습니다. 구정민 석사의 경우에는 의대를 갔는데 좋은 진로를 찾아간 것 같습니다. 김태영 박사님의 경우는 방장으로서 연구실 내 생활에 대해서 저를 잘 가이드 해주셨습니다. 그리고 왕택이도 연구실 방장을 하면서 실험실의 안전에 대해서 저에게 많은 교훈을 주었습니다. 그리고 장연식 박사에게는 스타크레프트에 대해서 즐거운 얘기를 나누면서 대학원 생활의 스트레스를 풀 수 있었습니다. 재근이도 옆에서 많은 얘기를 나누면서 실험실 생활을 같이 잘 진행할 수 있었습니다. 준우의 경우에는 뒤늦게 유기팀(=페로브스카이트)으로 들어와서 적응하느라 힘들었을 텐데 잘 적응하고 있어서 다행입니다. 지원이의 경우에는 항상 밝게 실험실의 분위기를 좋게 만들어주는 것 같습니다. 재영이의 경우에는 캐나다 출신 답게 연구실이 보다 프리한 분위기를 유지하는 데 도움을 주었습니다. 민우의 경우에도 실험실에서 어린 나이인데 형들에게 싹싹하게 잘해줘서 좋았습니다. 준태의 경우에는 친해질 기회가 별로 없었지만 남은 실험실 생활 잘 했으면 좋겠습니다. 종훈이형에게도 페로브스카이트/유기팀 미팅을 진행하면서 많은 도움을 받았던 것 같습니다. 행정실의 이고은 선생님도 일을 잘해 주셔서 저를 포함한 실험실 학생들이 연구에 보다 집중할 수 있었습니다.

이렇게 실험실 멤버들뿐만 아니라 제 주변의 친구들, 특히 학부 07들에게 많은 정서적 도움을 받을 수 있었습니다.

주변의 많은 도움을 받아서 박사를 받은 만큼 앞으로도 사회에 기여할 수 있는 연구자가 될 수 있도록 노력하겠습니다.